# A new habitability assessment and organic matter detection instrument for Mars

Peter Rory Gordon

Department of Earth Science and Engineering

Imperial College London

A thesis submitted for the degree of

*Doctor of Philosophy*

The copyright of this thesis rests with the author and is made available under a Creative Commons Attribution Non-Commercial No Derivatives licence. Researchers are free to copy, distribute or transmit the thesis on the condition that they attribute it, that they do not use it for commercial purposes and that they do not alter, transform or build upon it. For any reuse or redistribution, researchers must make clear to others the licence terms of this work.

All original data and results presented in this thesis are the outcome of my own work; any work by others has been appropriately credited. All passages of text have been authored by myself with the editorial assistance of my supervisor.



Peter Rory Gordon

Supervisor: Prof. Mark Sephton

# Abstract

Mars Sample Return is the next major step in the search for life beyond Earth. Mineralogical studies have revealed a wetter, more dynamic Mars than previously considered; the past environments of Mars could have hosted life and the search for its remains is a major scientific preoccupation. The return to Earth of the very best samples requires an effective prioritization and selection process, thus there is a requirement for a triage instrument which examines mineral phases in situ to determine the habitability potential of a region and to detect important biosignatures contained in any rock. This thesis demonstrates the viability of a pyrolysis-Fourier transform infrared spectroscopy (FTIR) instrument to fulfil these mission requirements. Thermal decomposition techniques have long been used on Mars to analyse solid samples, and FTIR instruments have been successfully deployed on the Martian surface. The combination of the two presents a resource efficient and robust analytical solution.

Investigations were conducted using pyrolysis-FTIR to show how habitability and the biosignature preservation potential of rocks can be assessed through the release of key gases, namely carbon dioxide, water and sulfur dioxide. The sensitivity limits for detecting organic matter and the effects of different mineral matrices on the organic compound signal were also investigated though measurement of methane and larger hydrocarbon compounds. Finally a field study was conducted using samples collected from a sulfate stream ecosystem which represents an analogue for the Hesperian of Mars. The investigations have shown that pyrolysis-FTIR, through utilisation of different temperature modes and the qualitative and quantitative feedback of resulting spectra, provides adequate information to determine mineral phases relating to habitability. Pyrolysis-FTIR detects organic compounds present in quantities as low as tens of parts-per-million. Sulphates and chlorinated mineral phases diminish organic compound signals, but combustion products offer another avenue for detection. The field study demonstrated that a phased pyrolysis-FTIR protocol will select the most valuable samples.

This thesis includes recommendations for the progress of pyrolysis-FTIR to the next design iteration.

# Acknowledgements

I first must recognise the privilege that has been afforded to me by Imperial College London and the Science and Technology Facilities Council. These past four years have been an arena for me to develop personally as well as academically; this has only been a material opportunity through the investment and support provided by these institutions.

Most of this development has been facilitated by the staff and colleagues throughout the college who have shared this experience with me (to whom I will find more appropriate displays of gratitude than a few lines in a thesis). Regarding the project, it is appropriate to give special recognition to Dr. Richard Court for laying the pyrolysis-FTIR groundwork and providing guidance and assistance, Dr. Jon Watson and Dr. Wren Montgomery for general lab assistance and administration, and Dr. James Lewis for his generosity in collaboration and ever-so-dependable Mars expertise. Dr. Caroline Smith of the Natural History Museum and Dr. Karen Olsson-Francis of the Open University are thanked for hosting me on sub-project work.

Of course my successes would not have been possible without the love and support of my family and friends. I am truly humbled by my parent's dedication and sacrifice and thank them dearly for their support.

However, the lion's share of gratitude is reserved for my supervisor, Prof. Mark Sephton. The academic and professional assistance and wisdom he has provided surpassed all expectations, only to be exalted by displays of personal support. His consolidation of experience, insight and academic prowess is a significant asset to this department, thus my blessings have been well and truly counted having landed myself as one of his students. Considering some of the challenges presented it's not far-fetched to envisage less desirable outcomes had it not been for the affable nature and patience so defining of Mark's character, and for that I will be eternally indebted. It is my sincere wish that this work brings returns that are well in excess of his investment.

# Publications by the author

## Published works

- Mark A. Sephton, Richard W. Court, James M. Lewis, Miriam C. Wright, Peter R. Gordon, Selecting samples for Mars sample return: Triage by pyrolysis–FTIR, *Planetary and Space Science*, Volume 78, April 2013, Pages 45-51, ISSN 0032-0633, http://dx.doi.org/10.1016/j.pss.2013.01.003.
- Peter R. Gordon, Mark A. Sephton, Rapid habitability assessment of Mars samples by pyrolysis-FTIR, *Planetary and Space Science*, Volume 121, February 2016, Pages 60-75, ISSN 0032-0633, http://dx.doi.org/10.1016/j.pss.2015.11.019.

## Accepted for publication

- Peter R. Gordon, Mark A. Sephton, Organic matter detection on Mars by pyrolysis-FTIR: an analysis of sensitivity and mineral matrix effects, *Astrobiology*.

## In preparation

- Peter R. Gordon, Mark A. Sephton, Pyrolysis-FTIR survey of an acid stream ecosystem and its implications for sample triage during Mars Sample Return.

# Contents

Abstract ..... 3

Acknowledgements ..... 4

Publications by the author ..... 5
Published works ..... 5
Accepted for publication ..... 5
In preparation ..... 5

Contents ..... 6

List of figures ..... 11

List of tables ..... 14

List of abbreviations ..... 17

Chapter 1 Review of sample return missions, life on Mars and instrument development ..... 19
1.1 Introduction to thesis ..... 20
1.2 Sample return ..... 21
1.3 Pyrolysis-FTIR ..... 24
1.3.1 FTIR in a triage application ..... 24
1.3.2 Pyrolysis in a triage application ..... 25
1.3.2.1 Thermal decomposition of minerals ..... 25
1.3.2.2 Extraction and thermal fission of organic matter ..... 26
1.3.3 Pyrolysis-FTIR as part of Mars Sample Return ..... 26
1.4 Life on Mars ..... 29
1.4.1 Mineralogical indicators of habitability ..... 29
1.4.2 Indicators of life ..... 31
1.4.2.1 Biosignatures in the atmosphere ..... 34
1.5 Instrument Design Process ..... 35
1.5.1 Instrument performance thresholds ..... 36
1.5.2 Instrument parameters ..... 37
1.6 Previous Instrument Development ..... 38
1.6.1 Mini-TES ..... 38
1.6.1.1 Miniaturization from MGS TES ..... 38

1.6.2 JPL DRIFTS FTIR instrument ..... 39
1.7 Summary ..... 41
1.8 Research aims ..... 41

Chapter 2 Methodology ..... 43
2.1 Introduction ..... 44
2.2 Background theory ..... 44
2.3 Sample acquisition ..... 46
2.3.1 Habitability samples ..... 47
2.3.2 Sensitivity and habitation samples ..... 47
2.3.3 Sulfate ecosystem samples ..... 48
2.4 Fourier transform infrared spectroscopy ..... 50
2.5 Attenuated total reflectance-FTIR ..... 52
2.5.1 Habitability ..... 53
2.5.2 Sensitivity and habitation ..... 54
2.5.3 Sulfate ecosystem ..... 54
2.6 Pyrolysis-FTIR ..... 54
2.6.1 Habitability ..... 58
2.6.1.1 Preliminary work ..... 59
2.6.1.2 Habitability investigation ..... 59
2.6.2 Sensitivity and habitation ..... 60
2.6.2.1 Preliminary work ..... 60
2.6.2.2 Sensitivity appraisal investigation ..... 60
2.6.2.3 Habitation investigation (assessment of mineral matrix effects) ..... 61
2.6.3 Sulfate ecosystem ..... 62

Chapter 3 Rapid habitability assessment of Mars samples by pyrolysis-FTIR ..... 65
Abstract ..... 66
3.1 Introduction ..... 67
3.2 Method ..... 69
3.2.1 Sample selection ..... 69
3.2.1.1 Phyllosilicates ..... 69
3.2.1.2 Carbonate minerals ..... 69
3.2.1.3 Sulfates and other salts ..... 70
3.2.1.4 Unaltered and altered igneous materials ..... 71
3.2.1.5 Organic matter bearing rocks ..... 71
3.2.2 Attenuated total reflectance-FTIR ..... 71

3.2.3 Pyrolysis-FTIR ..... 72
3.3 Results ..... 74
3.3.1 ATR-FTIR ..... 74
3.3.2 Single-step pyrolysis-FTIR ..... 74
3.3.3 Multi-step pyrolysis-FTIR ..... 75
3.4 Discussion ..... 83
3.4.1 ATR-FTIR ..... 83
3.4.2 Qualitative pyrolysis-FTIR analysis ..... 83
3.4.3 Quantitative pyrolysis-FTIR analysis ..... 84
3.4.4 Habitability assessment on Mars by pyrolysis-FTIR ..... 85
3.5 Conclusions ..... 88

Chapter 4 Organic matter detection on Mars by pyrolysis-FTIR: an analysis of sensitivity and mineral matrix effects ..... 89
Abstract ..... 90
4.1 Introduction ..... 91
4.2 Methods ..... 94
4.2.1 Sample selection ..... 94
4.2.2 Pyrolysis-FTIR ..... 95
4.2.3 Sensitivity appraisal ..... 96
4.2.4 Assessment of mineral matrix effects ..... 98
4.3 Results ..... 100
4.3.1 Sensitivity appraisal ..... 100
4.3.2 Mineral matrix effects ..... 105
4.3.2.1 Lycopodium spores (no minerals) ..... 112
4.3.2.2 Quartz ..... 112
4.3.2.3 Serpentinite ..... 113
4.3.2.4 Jarositic clay ..... 113
4.3.2.5 Palagonitic tuff ..... 115
4.3.2.6 JSC Mars-1 ..... 116
4.4 Discussion ..... 116
4.5 Conclusions ..... 118

Chapter 5 Pyrolysis-FTIR survey of an acid stream ecosystem and its implications for sample triage during Mars Sample Return ..... 120
Abstract ..... 121
5.1 Introduction ..... 122
5.2 Methods ..... 124

5.2.1 Sample selection ..... 124
5.2.2 Attenuated total reflectance-FTIR ..... 124
5.2.3 Pyrolysis-FTIR ..... 126
5.2.4 Triage operation ..... 127
5.2.4.1 Triage phase one (the habitability assessment phase) using single-step pyrolysis-FTIR (1000 °C) ..... 127
5.2.4.2 Triage phase two (the habitation assessment phase) using single-step pyrolysis-FTIR (700 °C) ..... 128
5.2.4.3 Triage phase three (the diagnostic phase) using multi-step pyrolysis-FTIR (500 °C, 750 °C and 1000 °C) ..... 128
5.2.5 Classifying and ranking sample potential ..... 128
5.3 Results ..... 131
5.3.1 Attenuated total reflectance-FTIR ..... 131
5.3.2 Single-step pyrolysis-FTIR (1000 °C) ..... 131
5.3.3 Single-step pyrolysis-FTIR (700 °C) ..... 134
5.3.4 Multi-step pyrolysis-FTIR ..... 135
5.4 Discussion ..... 137
5.4.1 Attenuated total reflectance-FTIR ..... 137
5.4.2 Triage phase one (the habitability assessment phase) using single-step pyrolysis-FTIR (1000 °C) ..... 138
5.4.3 Triage phase two (the habitation assessment phase) using single-step pyrolysis-FTIR (700 °C) ..... 140
5.4.4 Triage phase three (the diagnostic phase) using multi-step pyrolysis-FTIR (500 °C, 750 °C and 1000 °C) ..... 141
5.4.5 Assessment of the triage process ..... 143
5.5 Conclusions ..... 145

Chapter 6 Design considerations for a future Mars mission pyrolysis-FTIR spectrometer system ..... 146
6.1 Introduction ..... 147
6.2 Sampling gas cell design ..... 147
6.2.1 Multi-pass cell ..... 147
6.2.2 Cell windows ..... 156
6.3 Interferometer type ..... 157
6.3.1 Rotating refractor ..... 157
6.3.2 Non-moving parts spectrometry ..... 158
6.3.3 Tuned laser ..... 159
6.4 Mitigating consumables ..... 159
6.4.1 Purge gas for sampling cell ..... 160

6.4.2 Detector cooling ..... 161
6.4.3 Pyrolysis solution ..... 162
6.5 Volatiles trap & atmospheric sampling ..... 162
6.6 Other considerations ..... 166
6.6.1 Sampling time ..... 166
6.6.2 Resolution ..... 168
6.6.3 Pyrolysis temperature steps ..... 169
6.6.4 Beyond Mars Sample Return ..... 169

Chapter 7 Discussion & Conclusions ..... 170

Bibliography ..... 176

Appendix A ..... 184

Appendix B ..... 185

Appendix C ..... 191

# List of figures

Figure 1.1. Commemorative stamp for Luna 16 issued by the Soviet Union postal service to recognise the success of the mission. Luna 16 was remarkable in being the first fully automatic acquisition of rock samples from an extra-terrestrial body. Image credit: USSR Post (1970). ..... 23

Figure 1.2. Illustration of a hypothetical Mars Sample Return sample analysis workflow, highlighting the role and position of pyrolysis-FTIR. Image credit: NASA/JPL/Cornell/Canadian Light Source. ..... 28

Figure 1.3 - Diagram representing the mineralogical history of Mars as described by Bibring et al. (2006). The mineralogical history of Mars is defined by three main periods of alteration: the Phyllosian era, a nonacidic aqueous alteration, traced by phyllosilicates; the Theiikian era, an acidic aqueous alteration, traced by sulfates; and the Siderikian era, an atmospheric aqueous-free alteration, traced by ferric oxides. ..... 31

Figure 2.1. Sulfate rich stream environment in St. Oswald's Bay, Dorset, UK (above) and location map of St. Oswald's Bay and Stair Hole (below). On the map, the red circle marks the location within the UK of the Purbeck Heritage Coast along which the two sampling locations are found. ..... 49

Figure 2.2. Schematic diagram (top left) and photograph (top right) of a Michelson-Morley interferometer. A fast Fourier transform (FFT) is used to convert the output of the detector, an interferogram, into a frequency/wavelength spectrum of the multi-frequency source. ..... 51

Figure 2.3. Sampling interface for ATR-FTIR apparatus, showing the sampling crystal exposed before a sample is loaded (left) and showing the position of the compactor when pressing a sample against the sampling crystal surface (right). ..... 53

Figure 2.4. Schematic diagram of pyrolysis-FTIR (adapted from figure in (Sephton et al. 2013)). ..... 56

Figure 2.5. Pyrolysis-FTIR lab bench apparatus. ..... 57

Figure 3.1. The Phyllosian, Theiikian and Siderikian eras and the mineral types which define them, illustrated in chronological order. The eras defined by crater density and lava flows are included on the bottom for comparison (diagram adapted from that illustrated by Bibring et al. (2006)). ..... 68

Figure 3.2. A comparison of different Fourier transform infrared spectroscopy (FTIR) analytical techniques, by showing the relevant spectra of three different materials used in the survey; bastite, JSC Mars-1 analogue and the Blue Lias. The responses in the pyrolysis methods have been scaled to they show relative responses for when materials are all of the same mass. a) Attenuated total reflectance (ATR) FTIR. Spectral features which represent habitability indicators are labelled. b) Example spectra resulting from single-step pyrolysis-FTIR of the samples at 1000 °C. The positions of spectral features characteristic to two gases of interest, carbon dioxide and water, are labelled. c) Multi-step pyrolysis-FTIR. ..... 76

Figure 3.3. The temperatures at which gases are produced in pyrolysis-FTIR can be indicative of their source; trends observed in our survey for different mineral types allows us to construct an example framework of interpretation for multi-step pyrolysis-FTIR signals, illustrated here. During a pyrolysis-FTIR analysis program of ascending temperature steps, should any temperature step produce a gas (or combination of gases), a schema like this can be referenced to allow speculation on the source (given that adsorbed gases have been expunged at some lower temperature). The diagnostic capability of such an instrument allows a precursory determination of the scientific value of a sample, and this capability only

increases as such a framework for interpretation is expanded to include additional gases, temperature steps and quantitative measurements. ..... 86

Figure 4.1. Absorbance (measured by taking the total area under the combined peaks) in the hydrocarbon stretching region (3150 – 2740 $cm^{-1}$) plotted as a function of the quantity of Lycopodium spores present in the sample. All samples were subjected to 700 °C for 7.2 s before the evolved gases were measured by FTIR. For this study quartz was used to provide an inert substrate. Vertical error bars represent one standard deviation of the data produced by procedural blanks, while horizontal error bars arise from the uncertainty in mass measurements, with additional consideration made for Lycopodium spore loss during sample handling (10% of expected mass) on the lower uncertainty boundary. The dashed trend line represents a best-fit quadratic function for data points with Lycopodium spore mass < 200 µg, which is numerically represented as $A = 2\times10^{-5}m^2 + 0.0011m + 0.0008$ with a coefficient of determination of 0.9301, where $A$ is the relative absorbance and $m$ is the mass of Lycopodium spores (95% confidence bounds are illustrated by they area shaded grey). Three high concentration samples, with Lycopodium spore masses > 800 µg, do not adhere to this law and is likely due to saturation effects. It is interesting to note that the vertical intercept of 0.0008 is almost equal to the mean signal given by pure quartz samples of 0.0009 (i.e. when Lycopodium spore mass is zero). ..... 101

Figure 4.2. For a chosen detection threshold, there is a probability that pyrolysis-FTIR will make a detection given Lycopodium spores are present in sufficient quantities. This figure shows how this probability (sensitivity) varies as a function of the chosen detection limit (multiples of the standard deviation obtained from responses in blanks) for a range of concentrations of Lycopodium spores-quartz mixture. The solid lines represent best-fit cumulative probability functions, which have be superimposed upon data points calculated from measurements. ..... 104

Figure 4.3. Specificity (also known as the true negative rate) of pyrolysis-FTIR organic compound detection as a function of detection threshold. The plot suggests that false positives are unlikely when a detection threshold greater than approximately one standard deviation of the baseline fluctuation is chosen. ..... 105

Figure 4.4. Pyrolysis-FTIR spectrum of pure Lycopodium spore powder with prominent features of interest labelled (pyrolysed at 750 °C). ..... 106

Figure 4.5a. Representative pyrolysis-FTIR results from serpentinite and jarositic clay, where the results of using the unadulterated mineral have been overlain with spectra produced by a mixture containing 5% Lycopodium spores. Results have been scaled to represent a scenario where the quantity of mineral is equal in each case. The spectral features which are indicative of different gases are labelled. Colour coding highlights where the presence of Lycopodium produces a surplus of a gas (black) or a deficit (red) when compared to the mineral material alone, and where the two spectra overlap (yellow). ..... 107

Figure 5.1. Logic for scoring samples for the purpose of ranking them. ..... 130

Figure 5.2. Example triage operation. ..... 144

Figure 6.1. Comparison of absorption cross-section data sets for methane, demonstrating the success of the program written for this project (through the close resemblance of output to PNNL data). (a) These are images available on the VPL Molecular Spectroscopic Database made of PNNL data, which is not freely available. (b) and (c) are the resulting cross-section values calculated by the program written for this project, where the former calculated each value over the full specified frequency range at high resolution, while the latter only calculated at high resolution in regions where peaks had been identified by a low resolution calculation, saving significant computational time. Note the strong resemblance of calculated values to the

PNNL images. (b) and (c) were only calculated in the 4000 $cm^{-1}$ to 600 $cm^{-1}$, hence the feature at 4200 $cm^{-1}$ in the first PNNL image is missing. ..... 153

Figure 6.2 - The Designs & Prototypes 'Turbo FT' rotary refractor interferometer adopted by the JPL FTIR. The 'space frame' housing boasts excellent mechanical and thermal stability and weighs just over 0.55 kg (Wadsworth and Dybwad 2002, Mahaffy et al. 2009). ..... 158

# List of tables

Table 1.1 – Pyrolysis-FTIR could play a role in Mars Sample Return mission, using its ability to detect organic compounds and molecular habitability indicators such as water and carbon dioxide to select rocks of high scientific value. However, it is likely to come as part of a broader mission payload; listed are examples of instruments that could be included on a rover which would compliment pyrolysis-FTIR. ..... 27

Table 1.2 – List of biosignature types that MSL has been tasked with identifying. The table, originally in Summons et al. (2011), (Mahaffy et al. 2009), has been adapted to include descriptions of how these biomarkers should be treated in the MSR context. Any morphologies found on Mars are expected to be that of microorganism, thus are considered a low environmental indicator; it is accepted that morphologies of anything multicellular would give very high indication of environmental conditions. ..... 33

Table 1.3 - Upper limits on concentrations of certain gas species in the Martian atmosphere found through Earth based observations (Villanueva et al. 2013, Mahaffy et al. 2009). ..... 34

Table 1.4 - Specifications of MGS TES in comparison with those for Mini-TES (Christensen et al. 2001, Christensen et al. 2003). ..... 39

Table 2.1. Spectral locations of features characteristic to different functional groups. The third column describes the relative nature of the feature: s - strong, m - medium, ss - strong sharp, sb - string broad. .. 53

Table 2.2. Gases of interest for pyrolysis-FTIR experiments and the spectral features used for measurement. ..... 58

Table 2.3. Test plan for experimental work in this thesis. ..... 64

Table 3.1. Details of samples for the pyrolysis-FTIR study. ..... 70

Table 3.2. Results of ATR-FTIR analysis. A solid circle indicates the clear presence of spectral features linked to different mineralogical habitability indicators (hydroxyl and water of hydration for hydrated minerals, the carbonate ion for carbonate bearing materials and aliphatic hydrocarbons for organic bearing materials). A solid square represents cases where the features were clearly identifiable while an unfilled square represents tentative identification. ..... 77

Table 3.3. Qualitative results for the single-step pyrolysis-FTIR method. A solid square indicates a detection of high confidence, where the signal produced by that gas exceeded four standard deviations of the baseline noise. An empty square represents a tentative detection. ..... 78

Table 3.4. Quantitative results for the single-step pyrolysis-FTIR method. Values show the mass of pyrolysis products as a percentage of the initial sample mass, with associated uncertainty. The mass of the pyrolysis products was calculated by measuring the peak area of a chosen spectral feature (characteristic of the gas) and referencing a mass calibration curve. Values in parenthesis do not exceed the calculated uncertainty, and thus can effectively be considered absent. ..... 79

Table 3.5. Qualitative results for the multi-step pyrolysis-FTIR method. A solid circle indicates a detection of high confidence, where the signal produced by that gas exceeds four standard deviations of the baseline noise. An empty circle represents a detection of lower confidence. ..... 80

Table 3.6a. Quantitative results for the multi-step pyrolysis-FTIR method. Values show the mass of pyrolysis products as a percentage of the initial sample mass, with associated uncertainty. The mass of the pyrolysis products was calculated by measuring the peak area of a chosen spectral feature (characteristic of the gas) and referencing a mass calibration curve. Values in parenthesis do not exceed the calculated uncertainty, and thus can effectively be considered absent. ..... 81

Table 4.1. Materials used in study. ..... 95

Table 4.2. Spectral features analysed in pyrolysis-FTIR spectra to measure abundances of gas species of interest. ..... 99

Table 4.3. Parameters for cumulative logistic probability functions used to model the results of the sensitivity investigation. Using the relationship $S(t) = [1 + e^{s(t-t_{1/2})}]^{-1}$, the probability of making a positive organic compound detection (or sensitivity $S$) can be calculated for a given detection threshold $t$, where $t_{1/2}$ is the threshold value which gives $S = 0.5$ and $s$ is a scaling parameter. $n$ is the number of samples used to make each grouping. ..... 103

Table 4.4. Results from pyrolysis-FTIR survey at 700 °C, showing quantities of gases produced from pure minerals and the differences produced when Lycopodium spores are introduced. In bold are the results of the pure mineral forms with gas masses expressed as percentages of the initial sample mass. Listed below are the mass differences between the gases produced by the mineral-Lycopodium spore mixtures and the pure mineral form, expressed as percentages of the mass of the mineral component in the sample. Three concentrations (5.0%, 1.0% and 0.5%) of mineral-Lycopodium spore mixture were analysed for each mineral. ..... 109

Table 4.5. Results from pyrolysis-FTIR survey at 1000 °C, showing quantities of gases produced from pure minerals and the differences produced when Lycopodium spores are introduced. In bold are the results of the pure mineral forms with gas masses expressed as percentages of the initial sample mass. Listed below are the mass differences between the gases produced by the mineral-Lycopodium spore mixtures and the pure mineral form, expressed as a percentage of the mass of the mineral component in the sample. Three concentrations (5.0%, 1.0% and 0.5%) of mineral-Lycopodium spore mixture were analysed for each mineral. ..... 110

Table 4.6. Relative strengths of hydrocarbon responses for different concentrations of Lycopodium spore-mineral mixtures and mineral samples free of Lycopodium spores (highlighted in bold) from pyrolysis-FTIR analyses. In this case, the response due to hydrocarbons is semi-quantitatively represented by the height of the dominant peak at the 2933 $cm^{-1}$ wavenumber, found in the region strongly associated with the C-H stretches organic compounds. Two temperatures of pyrolysis are compared, 700 °C and 1000 °C. ..... 111

Table 4.7. Relative absorbance responses for hydrogen chloride produced from the pure palagonitic tuff and palagonitic tuff mixtures with Lycopodium spores. ..... 116

Table 5.1. Samples from flowing and dry acidic, ferrous sulfate-rich streams. ..... 125

Table 5.2. ATR results. Solid squares represent strong identification while an empty square represents a relatively weak signal. A question mark is used to denote samples which exhibit a spectral feature in the characteristic region yet cannot be conclusively assigned: a broad peak around 1400 $cm^{-1}$ in the case of carbonates and a shoulder at around 1090 $cm^{-1}$ in the case of sulfates. ..... 132

Table 5.3. 1000 °C pyrolysis-FTIR analysis. C – Confirmed detection (signal over double the associated uncertainty), T – tentative detection (signal greater than the associated uncertainty, but weaker than

double), N – null detection (signal less than uncertainty). Uncertainties reported are two standard deviations of the mean calculated from procedural blanks. ..... 133

Table 5.4. 700 °C single-step analysis. C – Confirmed detection (signal over double the associated uncertainty), T – tentative detection (signal greater than the associated uncertainty, but weaker than double), N – null detection (signal less than uncertainty). Uncertainties reported are two standard deviations of the mean calculated from procedural blanks. Scores based of 700 °C step results alone are displayed in grey, with final scores (i.e. scores after the 700 °C step after considering the results of the 1000 °C step) are in black. ..... 135

Table 5.5. Multi-step analysis, performed on the six highest priority samples identified through the preceding 'habitation sensitivity' triage phase (Table 5.4). Results are ordered by the total response of hydrocarbons for each sample across all three temperature steps. Two low priority samples, FlowMJ1b and FlowMG1c are included for comparison. ..... 136

Table 6.1. Cross-section data for molecules commonly measured in the project and other Mars relevant molecules. ..... 154

Table 6.2. Sensitivity limits calculated for a number of different cell designs: the single-pass Brill cell used currently in lab, the Brill cell modified to include a number of reflections (the number of reflections adopted from a comparable design) and three off-the-shelf multi-pass gas cells: an ultra-compact cell (designed for tuned lasers) with comparable volume to the Brill cell, a large volume cell for atmospheric sampling and a multi-pass cell designed for FTIR. Concentrations values displayed are mass fractions of a representative sample mass (based on sample quantities processed by MSL). These values were calculated by adopting a reflection co-efficient of 97.5%, a desired signal-to-noise ratio of 10 and a measured value for intrinsic noise in the lab bench pyrolysis-FTIR instrument. ..... 155

Table 6.3. Lower detection limits for molar concentrations of example organic compounds in the Martian atmosphere. These have been calculated for three designs of gas cell: the Brill cell used in this project, a FTIR multi-pass cell designed for atmospheric sampling (Specac Tornado) and a low volume multi-pass cell designed for FTIR (MKS MultiGas 2030). The values in bold represent the improved limits when a volatile trap (of similar design to that used for MSL) is utilised, maintained at 0 °C. Volumes are listed for the amount of Martian atmosphere that needs to be sampled to achieve the limits in bold. ..... 164

Table 6.4. Possible sensitivity limits for solid sample analyses with the addition of an MSL equivalent volatiles trap. Concentration values are mass fractions while the numbers in bold are the number of repeat analyses after which volatiles are lost from the trap (from which the minimum detectable concentration arises). These calculation assumed a carrier gas volume equivalent to three times the sampling cell volume is used in each analysis. Methane values for the Specac Tornado cannot be quoted as the large volume of the cell means that the breakthrough volume for methane is exceeded in just one analysis procedure.... 164

# List of abbreviations

| | |
|---|---|
| **ATR** | Attenuated total reflectance |
| **CCD** | Charge-coupled device |
| **CdTe** | Cadmium telluride |
| **DRIFTS** | Diffuse reflectance infrared Fourier transform spectroscopy |
| **DTGS** | Deuterated triglycine sulfate |
| **EGA** | Evolved gas analysis |
| **FTIR** | Fourier transform infrared spectroscopy |
| **GC-MS** | Gas chromatography–mass spectrometry |
| **HITRAN** | High-resolution transmission molecular absorption database |
| **HWHM** | Half width at half maximum |
| **IR** | Infrared |
| **JAXA** | Japan Aerospace Exploration Agency |
| **JPL** | Jet Propulsion Laboratory |
| **JSC** | Johnson Space Center |
| **KBr** | Potassium bromide |
| **MCT** | Mercury cadmium telluride |
| **MER** | Mars Exploration Rover Mission |
| **MGS** | Mars Global Surveyor |
| **Mini-TES** | Miniature Thermal Emission Spectrometer |
| **MS** | Mass spectrometry |
| **MSL** | Mars Science Laboratory |
| **MSR** | Mars Sample Return |
| **NASA** | National Aeronautics and Space Administration |
| **NIST** | National Institute of Standards and Technology |
| **OMEGA** | Observatoire pour la Minéralogie, l'Eau, les Glaces et l'Activité |
| **OPD** | Optical path difference |
| **PNNL** | Pacific Northwest National Laboratory |
| **ppb** | Parts per billion |

| | |
|---|---|
| **ppm** | Parts per million |
| **SAM** | Sample Analysis at Mars |
| **SNR** | Signal-to-noise ratio |
| **TEGA** | Thermal and Evolved Gas Analyzer |
| **TES** | Thermal Emission Spectrometer |
| **TLS** | Tunable Laser Spectrometer |
| **VOCs** | Volatile organic compounds |
| **VPL** | Virtual Planetary Laboratory |
| **XRD** | X-ray diffraction |
| **ZnSe** | Zinc selenide |

# Chapter 1 Review of sample return missions, life on Mars and instrument development

## 1.1 Introduction to thesis

Our current understanding of Mars places it as a worthy focus for life searches ahead of other Solar System bodies. As a result a number of missions are actively gathering science that build towards a picture of the history on Mars, with an additional number planned for the future.

To conclusively determine the presence of life, extinct or extant, will likely require careful, expansive and sensitive scientific analysis. Robotic missions to Mars are restricted in terms of analytical capacity when compared to what is achievable through Earth based laboratory tests. Thus Mars Sample Return (MSR), a mission returning a sample of the Martian surface to Earth, would greatly further our understanding of the Red Planet and beginning such a mission has been identified as a top priority for the coming decade (McLennan and Sephton 2011).

The highest priority scientific objectives to be addressed by returned samples have been defined by McLennan et al. (2012):

i. Finding evidence for past life or its precursors and its potential for preservation and past habitability.
ii. Constrain the age, context and processes of accretion; early differentiation; and magmatic and magnetic history of Mars.
iii. Revealing the history of surface and near-surface processes involving water.
iv. Building a picture of past climate change.
v. Identifying potential environmental hazards to future human exploration.
vi. Understanding the history and significance of surface modifying processes.
vii. Evaluate the origin and evolution of the Martian atmosphere.
viii. Identifying critical resources for future human explorers.

This complex task, being the first of its kind on such a scale, requires the engineering of a range of new vehicles and tools. Importantly, the mission stage tasked with collecting the sample for return needs to identify the best candidate by surveying numerous sampling opportunities on the planet's surface.

Once in the setting of a strategically chosen landing site, sample selection will be based on certain criteria - mainly the local geological context and constituents of the rock. Samples indicating previously habitable conditions, those containing potential biosignatures or those which demonstrate a high potential to preserve fossils are primary targets (McLennan et al. 2012).

Actual detection of definitive evidence of life will be tasked to Earth laboratory investigations, thus payload design and resources should be focused towards effective sample selection, i.e. the development of a robust 'triage' protocol is required. Regardless of the overall complexity of the sample selection procedure, first port-of-call for physical samples will be an initial screening instrument – an instrument which is multi-use, fast and energy efficient that gives adequate feedback on selection criteria for a large amount of samples.

It has been proposed that a Fourier transform infrared spectroscopy (FTIR) instrument can satisfy Mars Sample Return (MSR) triage requirements (Sephton et al. 2013). The purpose of this PhD project was to further develop this instrument concept – primarily in our understanding of its potential as a triage tool and secondly advise on its technical progression towards a mission ready form.

## 1.2 Sample return

Samples originating from solar system bodies have been studied in laboratories on Earth for decades. The majority of material studied has been meteoritic in origin. However, meteoric samples may have undergone some degree of alteration from their native form; for planetary meteorites, the shock processes during ejection from the parent body can alter the mineralogy of the rock (Bridges et al. 2001, El Goresy et al. 2013) and terrestrial weathering and contamination are a threat to all meteorites given sufficient time (Lee and Bland 2004). Although not affecting the interior of a meteorite, the interplanetary environment (Honda

and Arnold 1961, Fleischer et al. 1967, Saladino et al. 2015) and atmospheric entry can alter the condition of the surface of a meteorite (Genge and Grady 1999). These factors can mask useful information about the original environment. In addition samples returned by a mission can be considered in the context of the environment from which they were collected, which may be well characterised by other mission stages. For these reasons pristine samples returned via technological endeavour are of significantly greater scientific value than meteoric samples.

Previous sample return missions have demonstrated the potential for significant scientific return. Studies of Lunar samples collected by the NASA Apollo missions (380.96 kg in total) continue to yield valuable information about the history of the Moon and have been used to validate theories of its origin (Halliday 2012). The Russian Luna program returned a much lower quantity of Lunar samples, but did so entirely robotically (Balint 2002) - as is the proposed case for Mars Sample Return. The small quantities returned (0.326 kg) were still adequate for characterisation analysis and comparison with Apollo samples (Vinogradov 1971, Laul, Papike and Simon 1982). A postage stamp commemorating this achievement by depicting the launch of the sample capsule from the Lunar surface is shown in Figure 1.1.

The Genesis mission was the first mission to capture and return samples from beyond the orbit of the Moon. This mission used a collector array to passively collect particles from the solar wind (Burnett et al. 2003). Due to an unfortunate parachute deployment malfunction during the descent phase of its return to Earth, the Genesis sample return capsule suffered a hard landing. Despite damage and contamination breaches of the capsule due to impact, scientists were able to recover useful quantities of sample[1]. Similarly to Genesis, the Stardust mission passively collected material from beyond the Moon using a collector array. The mission focus was collecting dust from the coma of comet Wild 2 but the mission also exposed the collector during the cruise phase in the hope of collecting interstellar particles (Brownlee et al. 2003). The

[1] http://www.nasa.gov/home/hqnews/2005/apr/HQ_05102_genesis_collectors.html




Figure 1.1. Commemorative stamp for Luna 16 issued by the Soviet Union postal service to recognise the success of the mission. Luna 16 was remarkable in being the first fully automatic acquisition of rock samples from an extra-terrestrial body. Image credit: USSR Post (1970).

sample return capsule had a successful soft landing and the sample analyses furthered our understanding of solar system formation and astrobiology (Keller et al. 2006, Sandford et al. 2006). The JAXA Hayabusa mission opted for active sample selection; this mission touched down and collected samples from the asteroid Itokawa before returning them to Earth (Yano et al. 2006).

It should be noted the robotic missions mentioned above were not equipped with triage tools to identify priority samples in situ. NASA's planned Mars 2020, a rover deriving much of its design from Curiosity, is being equipped to cache samples for a subsequent sample return phase and will be equipped with a suite of instruments that will aid sample selection (Mustard et al. 2013). Although instrument payload has already been announced for Mars 2020[2], the need for new instruments remains because the Mars Sample Return effort is likely to involve multiple missions into the future.

[2] http://www.jpl.nasa.gov/news/news.php?release=2014-251

## 1.3 Pyrolysis-FTIR

Pyrolysis-FTIR involves rapidly heating a sample to produce gas phase products from its constituents which are subsequently measured by obtaining a spectrogram; this technique is explained in more detail in Chapter 2. It is fast, as scans can be made in only a matter of seconds. It is multi-use, as it does not rely on consumables for its fundamental operation. Pyrolysis tools and FTIR spectrometers have been successfully employed on previous missions to Mars. The Sample Analysis at Mars (SAM) instrument on NASA's Mars Science Laboratory (MSL) achieves thermal decomposition of solid samples using pyrolysis ovens (Mahaffy et al. 2009), however the downstream analysis has been performed by gas chromatography-mass spectrometry (GC-MS), which is a time consuming and complicated technique. The Miniature Thermal Emission Spectrometer (Mini-TES) on-board the Mars Exploration Rover (MER) missions is an example of a FTIR spectrometer successfully operated on the Martian surface (Silverman et al. 2006).

### 1.3.1 FTIR in a triage application

FTIR techniques are well suited to the triage application mainly because they are appropriate for detecting organic molecules and inorganic molecules related to habitability, such as water, carbon dioxide, sulfur dioxide and nitrates, as they have strong vibrational absorption bands in the infrared (IR) spectral range. Also, measurements only take a matter of seconds and the process is mechanically simple, involving only one moving part in most cases, or no moving parts at all. Spectra obtained by FTIR can be compared to gas phase libraries and computation screening for gases of interest is achievable.

However, it must be noted that good motion of the mirror is required for accurate results. This is not normally a problem under stable lab conditions where any motion irregularities can be compensated for using an additional reference laser. However, this system can be easily disturbed by harsh conditions in the field, not to mention having to withstand the extreme forces of space transit. Thus more stable types of interferometers have been developed that use rotating mirrors or refractors to achieve a varying optical path difference, including a design with no moving parts (Wagner, Dändliker and Spenner 2008).

### 1.3.2 Pyrolysis in a triage application

With FTIR some consideration has to be given to the sample delivery. Samples can be investigated in solid or liquid forms by analysing light reflected from their surfaces, or by passing the beam directly through a sample (either in a gaseous form or diffusely suspended in an IR transparent medium, commonly disks of KBr for solid samples). Some solid phase FTIR techniques, such as attenuated total reflection (ATR) and KBr disk transmission, would be difficult to implement in situ due to the complexity of sample loading (Anderson et al. 2005) and solid phase FTIR does not allow for rotational absorption, which can enhance the identification potential, thus investigating samples in the gas phase is an attractive option.

Pyrolysis, the decomposition of compounds when subjected to certain elevated temperatures, has been chosen as a way of producing gaseous products from solid or liquid samples. High degrees of control allow replicable results; commercially available pyrolysis probes allow controlled heating rates up to 20,000 °$Cs^{-1}$ with an accuracy of 10 °$Cs^{-1}$ and temperatures up to 1400 °C can be held with high precision (±1 °C)[3].

However, there are some drawbacks; pyrolysis is a destructive technique and secondary reactions can hide information about the original nature of the analysed samples.

#### *1.3.2.1 Thermal decomposition of minerals*

Rock samples are mostly composed of minerals and the temperatures at which different minerals decompose varies significantly. Hydroxide minerals generally begin to produce water when heated at relatively low temperatures (280 – 500 °C), while higher temperatures are required for water production from kaolinite-type phyllosilicates (530 – 600 °C) and serpentinite-type phyllosilicates (600 – 800 °C) (Földvári 2011). Dissociation of carbonates (to produce carbon dioxide) occurs at varied temperatures, for example, siderite at 540 – 555 °C, magnesite at 625 – 643 °C and calcite at 895 °C and similarly for dissociation of sulfates to produce sulfur dioxide, for example jarosite at 650 – 750 °C and gypsum at about 1200 °C (Földvári

[3] http://www.cdsanalytical.com/instruments/pyrolysis/pyroprobe_5000.html

2011). Certain rocks which are devoid of the previously described mineral phases will show little response to heating in these ranges, especially rocks which are mostly silicate, like olivine or volcanic rocks like basalt. Thus the release temperatures of specific gases should provide some diagnostic information on the specific mineral phases in a rock sample.

#### *1.3.2.2 Extraction and thermal fission of organic matter*

Thermal extraction techniques can be an effective way of present trace organic matter components of rock samples. The abundances of organic matter in rocks are normally very low, and can be trapped in microscopic pores or be present in insoluble high molecular weights, making solvent extraction less effective in an analytical procedure. Application of heat can desorb light weight organic matter and evacuate compounds trapped in pores. The high molecular weight compounds are called kerogens, from the Greek for wax-former, which represent assemblages of selectively preserved biopolymers and newly synthesised geopolymers, and these can be degraded by relatively high temperatures to produce smaller compounds, and these products can inform on the source of organic matter (Sephton et al. 2013).

### 1.3.3 Pyrolysis-FTIR as part of Mars Sample Return

Owing to its analytical strengths, resource efficiency and the successful use of its constituent technologies in previous missions, pyrolysis-FTIR has been identified a potential triage instrument for Mars Sample Return (Sephton et al. 2013). It is proposed that pyrolysis-FTIR would analyse drilled rock samples and select rocks worthy of return to Earth (based on their chemical constituents, targeting molecular species pertaining to habitability and habitation) but as with previous missions, it is likely to be deployed as part of a suite of instruments = Table 1.1 lists other technologies that could be included on a rover which would compliment pyrolysis-FTIR and the science requirements they address. Figure 1.2 illustrates where pyrolysis-FTIR would serve in an imagined Mars Sample Return sample acquisition procedure.

Table 1.1 – Pyrolysis-FTIR could play a role in Mars Sample Return mission, using its ability to detect organic compounds and molecular habitability indicators such as water and carbon dioxide to select rocks of high scientific value. However, it is likely to come as part of a broader mission payload; listed are examples of instruments that could be included on a rover which would compliment pyrolysis-FTIR.

| Technique | Existing instrument | Mission | Science requirement |
|---|---|---|---|
| Remote visual imaging | Mastcam-Z | Mars 2020 | Visually identify features at long ranges and assist navigation to sites for pyrolysis-FTIR analysis (Bell et al. 2016). |
| Remote spectroscopy | Miniature Thermal Emission Spectrometer (Mini-TES) | MER | Detect the mineral composition of rocks at a distance (Christensen et al. 2003). Could avail of shared FTIR optics should pyrolysis-FTIR be on board. Can provide solid state spectra for comparison with pyrolysis-FTIR results. |
| Atmospheric sampling | Tunable Laser Spectrometer (TLS) & Tenax traps | MSL | Perform precision measurements of gases in the Martian atmosphere where carbon isotope ratios are used to determine the origin of the gases (Mahaffy et al. 2009). Can also be used to trap and measure gases produced from rock samples with pyrolysis-FTIR. |
| Close proximity visual imaging | Mars Hand Lens Imager (MAHLI) | MSL | Take microscopic images of rocks and soil (Edgett et al. 2009). Could be used to identify structural biosignatures which cannot be detected by pyrolysis-FTIR. |
| Elemental analysis | Alpha Particle X-Ray Spectrometer (APXS) | MSL | Measure the abundance of chemical elements (including trace elements) in rocks and soils to compliment molecular techniques such as pyrolysis-FTIR (Gellert et al. 2009). |
| Subsurface radar | Radar Imager for Mars' Subsurface Experiment (RIMFAX) | Mars 2020 | Ascertain the geologic structure of the subsurface (Hamran et al. 2014). Could be used to identify drill targets and gives structural context to the results of pyrolysis-FTIR. |
| Molecular analysis | Sample Analysis at Mars (SAM) | MSL | Measure molecular composition and isotopic weights with high precision (Mahaffy et al. 2009). Covers much of the same ground as pyrolysis-FTIR in terms of detecting organic compounds and habitability indicators, but does so at a much higher resource cost. Could be used to further investigate pyrolysis-FTIR results for the improved sensitivity and diagnostic ability. |

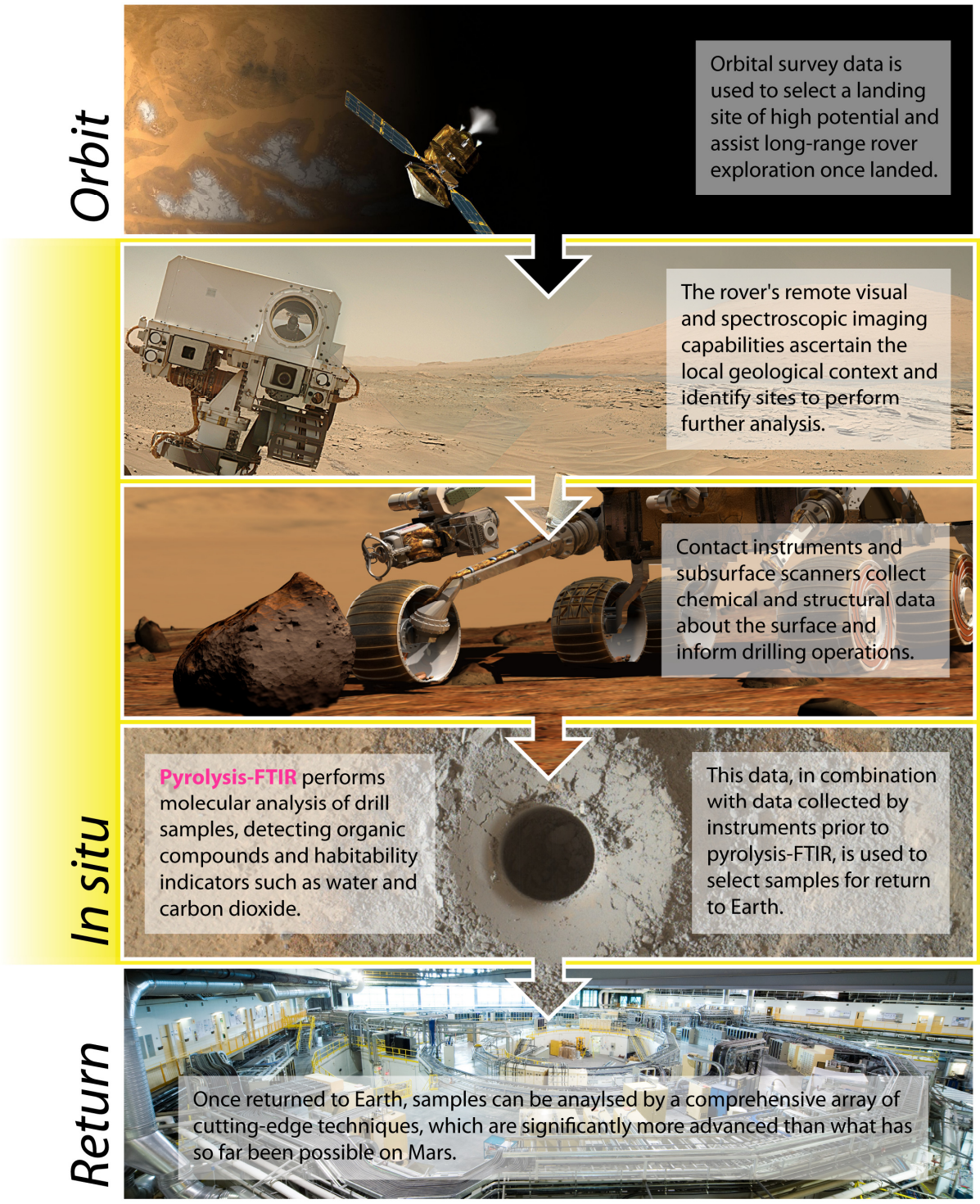



Figure 1.2. Illustration of a hypothetical Mars Sample Return sample analysis workflow, highlighting the role and position of pyrolysis-FTIR. Image credit: NASA/JPL/Cornell/Canadian Light Source.

## 1.4 Life on Mars

Can the search for life on Mars be justified? Well firstly, the possibility of extra-terrestrial life is one of humanity's most profound curiosities; the discovery of which would have far reaching implications in science and beyond. While life elsewhere in the universe is pretty much a statistical certainty, the scientific community remains uncertain that a discovery can be made within our own solar system – a discovery which would set limits on the richness of life in the universe. There has yet been conclusive evidence against the possibility. The following sections outline how Mars remains a candidate host for life and the important factors regarding life searches.

The search for life is led by the confirmation of habitable environments, the main criteria for which are:

- Sufficient quantities of liquid water
- An energy source
- And the necessary building blocks for life (see Section 1.4.2).

There is a promising body of evidence that liquid water flowed on the surface in the past and the hunt for organic compounds aims to discover if sufficient materials were available for building life forms.

### 1.4.1 Mineralogical indicators of habitability

Identification of hydrated or precipitated minerals indicates conditions in the past that have allowed the presence of liquid water. The type, association and abundance of water-associated minerals can reveal the nature of the habitable environment, i.e. how wet, when and for how long? A number of water-associated minerals have already been found by previous missions both in orbit and at the Martian surface.

In the context of a sample return mission, only those rocks that exhibit mineralogies consistent with habitable environments should be considered for return to Earth. Some classes of minerals which contain habitability information are discussed below.

Clay minerals generally form through the weathering of silicate bearing rocks, thus are composed mostly of hydrous-layer silicates. Results from the Observatoire pour la Minéralogie, l'Eau, les Glaces et l'Activité (OMEGA) mission show that ancient areas of the Martian surface are replete with phyllosilicates and, had these clay materials formed on the surface, early Mars would have seen abundant liquid surface water and a dense atmosphere (Bibring et al. 2006).

Carbonates provide a record of water chemistry in a region. They mostly form in regions which are pH neutral to slightly alkaline and aqueous; both favourable conditions for life. Some carbonate precipitation is strongly linked with microbial activity, and it has even been argued that carbonates found in unexpected regions on Mars could be explained by microbial activity (Fernández-Remolar et al. 2012).

The distribution of sulphate minerals on the Martian surface indicates a global shift from the habitable picture painted by the clay minerals to an acidic, inhospitable one (though sulfates can indicate the presence of water) (Bibring et al. 2006). On Earth life does not normally favour acidic conditions though some organisms have adapted to such extreme conditions.

Building on the findings mentioned above, Bibring et al. (2006) used the mapping data returned by OMEGA – in combination with surface information returned by the MERs – to derive a picture of the mineralogical and aqueous history of Mars. Their analysis led them to define three main eras 'characterized by the surface alteration products':

i. *a nonacidic aqueous alteration, traced by phyllosilicates (the "Phyllosian" era);*
ii. *an acidic aqueous alteration, traced by sulfates (the "Theiikian" era); and*
iii. *an atmospheric aqueous-free alteration, traced by ferric oxides (the "Siderikian" era)*

These mineralogical defined eras are shown in Figure 1.3 compared to eras defined by crater density and lava flows. They highlight the Phyllosian era as the most likely to host habitable conditions, thus sites indicative of this era should be the principal targets for life searches.

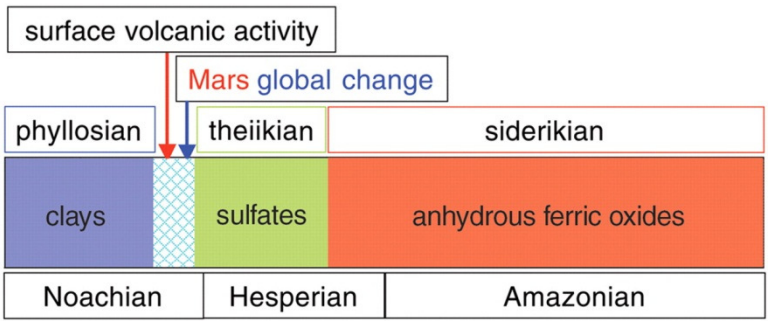



Figure 1.3 - Diagram representing the mineralogical history of Mars as described by Bibring et al. (2006). The mineralogical history of Mars is defined by three main periods of alteration: the Phyllosian era, a nonacidic aqueous alteration, traced by phyllosilicates; the Theiikian era, an acidic aqueous alteration, traced by sulfates; and the Siderikian era, an atmospheric aqueous-free alteration, traced by ferric oxides.

### 1.4.2 Indicators of life

While confirming habitable conditions keeps the possibility open, it will not serve as evidence of life – for this we will need to discover biosignatures. What these are, how indicative they are of life and their likelihood of survival should be well understood when conducting searches for life. Note that many biosignatures, even those found on Earth, present a challenge in their ambiguity (Summons et al. 2010) thus a picture of life is built up from many different elements understood in context with each other. Factors include chemical indicators, spatial structures and isotopic ratios.

Organic compounds are considered strong biomarkers, so a high detection capability is required of any triage instrument. FTIR can distinguish easily between functional groups as particular groups tend to be incorporated at particular wavelengths (Coates 2000), which is helpful when analysing complex organic mixtures.

Volatile organic compounds (VOCs) are considered as highly definitive biomarkers as on Earth they are largely of biogenic origin (Goldstein and Galbally 2007). Organic molecules of indefinite origin can be distinguished as biogenic or not through comparison with known abiological contexts (Sephton and Botta 2008).

Nitrogen compounds, such as ammonia, serve as biosignatures as they relate to compounds found in amino acids and proteins (Wagner and Musso 1983). Ammonia plays a role in the origin of life hypothesis demonstrated by Miller (1953).

The biosignature types MSL has been tasked with detecting are shown in Table 1.2 with added discussions contextualised for MSR. MSL serves as useful comparison for MSR, as it is currently the cutting edge of what can be identified through remote analysis.

Table 1.2 – List of biosignature types that MSL has been tasked with identifying. The table, originally in Summons et al. (2011), (Mahaffy et al. 2009), has been adapted to include descriptions of how these biomarkers should be treated in the MSR context. Any morphologies found on Mars are expected to be that of microorganism, thus are considered a low environmental indicator; it is accepted that morphologies of anything multicellular would give very high indication of environmental conditions.

| Biosignature type | Potential as a biosignature | Potential as an environmental indicator | MSL | MSR |
|---|---|---|---|---|
| Organism morphologies (cells, body fossils, casts) | Exceptionally high | Low | Minimum size would have to be greater than 100 mm and rock preparation techniques are not available to expose organisms within rock. Martian life is expected to be microbial, so the probability of detection is low. | Samples containing such biosignatures are the highest priority for return, thus triage platform must be able to index the likelihood of these being contained in subjected samples (through other indicators such as habitability) if actual identification is not possible. Retaining structural information is essential when processing for sample return. |
| Biofabrics (including microbial mats) | Moderate | Low | Accreted structures analogous to those on Earth are detectable; however, few bedding-plane surfaces are exposed, so potential surface biosignatures will be difficult to detect. | |
| Diagnostic organic molecules; organic carbon | Exceptionally high | High | Detection potential high including atmospheric gases | Triage instrument should make positive identification over a comprehensive range of such molecules. Quantitative information is key for candidate comparison. Detection of biogenic atmospheric gases would indicate that the source is nearby. |
| Biogenic gases (non-equilibrium) | High (e.g., $CH_4$) | Low | Excellent capacity to detect gases | |
| Isotopic signatures | Moderate | Low | Contextual knowledge is essential; results can be ambiguous and complex to interpret. | |
| Biomineralization and bioalteration | Low | Low | Detection of specific minerals is good; morphological pattern may be useful but needs very fine spatial resolution. | High triage requirement for assessing sample habitability and the likelihood of fossils, especially if the triage platform cannot do so directly. |
| Spatial patterns in chemistry | Low on its own | Low | C, N, S elemental distributions; detection potential on centimetre scale to facies scale. | Recognition should not be required from triage platform but would be learned consequentially in high detail Earth analysis. |

#### *1.4.2.1 Biosignatures in the atmosphere*

Methane has been detected in the Martian atmosphere but as its expected photochemical lifetime is many times shorter than Mars' lifetime, a source must be on the surface (Formisano et al. 2004). On Earth, atmospheric Methane is mainly a product of biogenic sources (Quay et al. 1999) which increases interest in its Martian origins, although abiotic processes cannot be over looked (Atreya, Mahaffy and Wong 2007).

Other organic molecules can have lifetimes ranging <1 year near the Martian surface (Summers et al. 2002), thus positive atmospheric detection by the triage platform (if capable) would be useful as it would indicate a source is nearby. Observed bulk releases of methane have been compared to hydrocarbon seep behaviour on Earth (Mumma et al. 2009). If atmospheric methane is coming from organic rich underground sources, there is a possibility for other organic molecules being released in tow.

Modern developments in ground based astronomy have allowed for sensitive searches for organics in the Martian atmosphere (Villanueva et al. 2013), giving upper limits for quantities of volatile organic species ($CH_4$, $CH_3OH$, $H_2CO$, $C_2H_6$, $C_2H_2$, $C_2H_4$), nitrogen compounds ($N_2O$, $NH_3$, HCN) and chlorine species (HCl, $CH_3Cl$); the results of which are presented in Table 1.3. Any atmospheric sampling capability incorporated in a triage instrument would need to significantly better these upper limits.

Table 1.3 - Upper limits on concentrations of certain gas species in the Martian atmosphere found through Earth based observations (Villanueva et al. 2013, Mahaffy et al. 2009).

| Molecule | Ppb |
|---|---|
| Methane ($CH_4$) | <6.6 |
| Ethane ($C_2H_6$) | <0.2 |
| Methanol ($CH_3OH$) | <6.9 |
| Formaldehyde ($H_2CO$) | <3.9 |
| Acetylene ($C_2H_2$) | <4.2 |
| Ethylene ($C_2H_4$) | <4.1 |
| Nitrous oxide ($N_2O$) | <65 |
| Ammonia ($NH_3$) | <45 |
| Hydrogen cyanide (HCN) | <2.1 |
| Methyl chloride ($CH_3Cl$) | <0.6 |
| Hydrogen chloride (HCl) | <0.6 |

## 1.5 Instrument Design Process

Wertz and Larson (1999) present guidelines for space mission design, however, they focus on low Earth-orbit space craft and they only give a detailed description for remote sensing instruments in their chapter on designing payloads. Below a summary of the basic steps for payload design is presented. Here, the terms 'payload' and 'instrument' are used interchangeably.

The first three requirements have already been identified for pyrolysis-FTIR.

1. Select Payload Objectives. This is a specific requirement which falls out of the broader mission objective. As outlined in the introduction Mars Sample Return requires a multi-use, fast and energy efficient instrument that provides adequate selection criteria feedback – pyrolysis-FTIR intends to fulfil this demand.
2. Conduct Subject Trades. The subject is what the payload interacts with or looks at. Primarily for the triage instrument this is solid material from the Martian surface, likely to be obtained from a short distance underground.
3. Develop the Payload Operations Concept. This is the end product of instrument operation. For pyrolysis-FTIR it will be an absorbance spectrum or series of spectra for a single sample, which allows operators to determine the sample's mineralogical and organic make-up.

The next three points are within the scope of this project (to varying extents).

4. Determine the Required Payload Capability. Determine what performance is required to meet the mission criteria. Here we will need to consider the spectral output, detector sensitivity, pyrolysis effectiveness and turnaround time.
5. Identify Candidate Payloads. The Mars Sample Return lander will involve multiple instruments. Possible other instruments and techniques should be considered on how they might work with or complement pyrolysis-FTIR.

6. Estimate Candidate Payload Characteristics. How instruments affect each other through resource demands, data output rates, processing requirements, input commands, size, orientation, thermal effects and weight needs to be considered. Detailed consideration is not required for this project.

The remaining steps will not be covered in this project.

7. Evaluate Candidates and Select a Baseline. Examine alternatives so that a preliminary combination of payloads can be decided upon and identify the monetary costs of different performance elements to obtain a baseline.
8. Assess Life-cycle Cost and Operability. 'Determine mission utility as a function of cost'.
9. Define Payload-derived Requirements. 'Provide a detailed definition of the impact of selected payloads on the requirements for the rest of the system (i.e. spacecraft bus, the ground segment, and mission operations)'.
10. Document and Iterate. The authors stress that all decisions are documented and importantly why they were taken, as this helps to makes trade-offs as the design progresses. This is also important because, as consequences of earlier decisions become apparent, the payload design process is revisited.

This list is considered helpful in providing areas that might have been overlooked however the list transitions from single payload guidelines towards an overall mission design list; an expanded breakdown of some of the earlier points would have been more useful. It is accepted that considering impacts on other spacecraft elements is needed in the design process, however at such early stages of development it is not possible to constrain these accurately.

### 1.5.1 Instrument performance thresholds

Wertz and Larson (1999) advise establishing the absolute minimum, desired and acceptable thresholds for the technical performance of space instruments - this list provides an initial framework for optimization.

For a Mars Sample Return triage instrument the minimum, desired and acceptable thresholds will need to be agreed for:

- Detection sensitivity / resolution
- Sample turnover time
- Number of uses / instrument lifetime
- Qualitative return from samples
- Quantitative return from samples

Specific requirements for a Mars Sample Return triage instrument have not currently been defined, however this project aims to make considerations for these properties for pyrolysis-FTIR by identifying their current state for the lab bench set up and where improvements can be made. This should allow useful comparison once the thresholds for a triage instrument are better defined.

### 1.5.2 Instrument parameters

An estimate of key instrument characteristics is needed before pursuing a detailed design. Wertz and Larson (1999) suggest three basic methods to estimating overall size and key parameters of an instrument:

- Analogy with existing systems
- Scaling from existing systems
- Budgeting by components

Section 1.6 presents a study of other instruments in order to address the first two points. Component budgeting would be of little value at this stage, as the resource costs of the current lab components are not representative of components which would be used in a stand-alone instrument.

## 1.6 Previous Instrument Development

The development and outcome of other instruments should be used to guide the development and final specifications of any new instrument and will provide additional understanding of the mission design process in general.

The instruments chosen are considered highly relevant to pyrolysis-FTIR; one of the instruments has been successfully deployed to Mars. Here the priority is to learn about the development processes (from lab to final flight instrument), but any design features that would benefit pyrolysis-FTIR design are noted.

### 1.6.1 Mini-TES

The Miniature Thermal Emission Spectrometer (Mini-TES) is a high resolution infrared Fourier transform spectrometer that has successfully been deployed on Mars as part of the NASA's Mars Exploration Rover Mission (MER) missions, thus is significantly relevant to pyrolysis-FTIR. It was designed to remotely identify the mineralogical composition and thermophysical properties of geological materials on the Martian surface, as well as study certain characteristics of the lower atmospheric boundary layer (Christensen et al. 2003).

Mini-TES is comparable with the current pyrolysis-FTIR set-up in that it employs a Michelson-Morley style interferometer with a moving mirror, just as in the spectrometer used in the lab. There are differences worthy of note - the most significant being that Mini-TES is a remote sensing instrument which produces spatially resolved images.

#### *1.6.1.1 Miniaturization from MGS TES*

Mini-TES was not developed from a lab bench starting point but from an orbit based predecessor Mars Global Surveyor (MGS) Thermal Emission Spectrometer (TES). As Table 1.4 shows, it was possible to make significant size and weight reductions in the design of Mini-TES although some of this can be attributed to changing instrument requirements.

Table 1.4 - Specifications of MGS TES in comparison with those for Mini-TES (Christensen et al. 2001, Christensen et al. 2003).

| | MGS TES | Mini-TES |
|---|---|---|
| Total weight (kg) | 14.47 | 2.40 |
| Dimensions (cm) | 23.6 x 35.5 x 40.0 | 23.5 x 16.3 x 15.5 |
| Spectral range (μm) | ~ 6 - 50 | ~ 5 - 29 |
| Operating power (W) | 10.6 | 5.6 |
| Launched | November 1996 | June 2003 |

The key areas of focus for the Mini-TES development were miniaturising electronics, reducing functional complexity and interferometer redesign. Approximately two-thirds of the weight reduction is attributed to optimisation of the electronics system. This was achieved by improving the electronic component packaging, replacing fixed digital logic components with programmable gate-arrays and using higher density memory components (Schueler et al. 1997).

I see this as a clear opportunity for reduction from our lab apparatus, which is designed to be versatile multi-purpose lab equipment thus would have electronics and systems surplus to that required for pyrolysis-FTIR on Mars. Further weight and power reductions were made by reducing the number of detector arrays to one, reducing the number of optical channels and altering the interferometer design. The surface application of Mini-TES allowed the designers to disregard certain orbit required components, such as the detector heaters.

### 1.6.2 JPL DRIFTS FTIR instrument

NASA's Jet Propulsion Laboratory have also identified active FTIR as a useful tool for Mars exploration and developed an instrument concept – a prototype for which has been field tested in Antarctica (Anderson et al. 2005). They argue that building on the success of remote sensing IR instruments sent in past (such as Mini-TES) with more sensitive in situ FTIR instruments is a logical next step. As highlighted earlier in the report, FTIR is favoured due to its aptitude for water, carbonate and organic molecule detection, in addition to accurately detect nitrogen compounds that have so far been elusive on Mars.

While finding much agreement in the suitability of FTIR there are a few differences between the JPL FTIR instrument and our bench top set-up. Firstly, the prototype employs a rotating refractor interferometer design rather than a Michelson–Morley style, to eliminate the need for a reference laser and overcome the mechanical instability of a linearly moving mirror. Their chosen interferometer was designed for rugged applications such as deployment on military aircraft, making it ideal for space missions. It is compact, lightweight and can achieve resolutions of 8 – 1 $cm^{-1}$ (Wadsworth and Dybwad 2002). For comparison, our measurements are generally taken with a resolution of 4 $cm^{-1}$.

This type of interferometer is worthy consideration for our instrument. Note that if a tuneable laser is implemented the argument for abandoning a mirror reference laser may be obsolete, at which point direct comparison of the two interferometers' other characteristics dictates which is chosen.

However, the fundamental contention in the instrument design is in the sampling method. At JPL, many sampling methods were assessed; Diffuse Reflection Infrared Fourier Transform Spectroscopy (DRIFTS) was chosen as the strongest candidate. However, pyrolysis was not considered in this comparison, which I argue holds certain advantages over DRIFTS.

Significantly, controllable pyrolysis temperatures allow for stepped analysis. This adds an extra layer of information to pyrolysis-FTIR's analysis. Investigations described within this thesis reinforce the benefits of this technique.

As pyrolysis products will be in the gas phase, rotational absorbance bands are possible allowing more absorption from the analytes and more certain identification. With a system adapted to detect gaseous products additional modes of operation, such as atmospheric sampling, become more tangible.

However, with pyrolysis, samples are destroyed while with DRIFTS they are available for further processing. Also, the energy demand of pyrolysis-FTIR is likely to be higher if we assume the sample delivery and

spectra capture energy demands are comparable for the two instrument types, i.e. the difference being the pyrolysis requirement (pyrolysis is achieved on MSL at about 35 – 45 watts (Mahaffy et al. 2012)).

Another advantage of the JPL instrument is that it can investigate inhomogeneity in samples by translocating them under a 1 mm focussing spot between measurements. However, if samples are delivered in a crushed form (as indicated in the report) they will likely be homogenised and lacking original structural information, making this an obsolete feature.

## 1.7 Summary

The growing evidence of potential habitable environments and the progresses made by modern in situ missions make a Mars Sample Return mission a sound scientific goal for the near future. However, if pyrolysis-FTIR is to be included on a mission in the coming decade, the instrument needs to be in a good working state so it can contend strongly with any other proposed instruments. Any instrument needs to be at the mature stage of its development and proven operationally before it can be considered for proposal. Thus, a working pyrolysis-FTIR prototype must be delivered in the next few years.

This underlines the urgency of this project. The aims of this work should adequately demonstrate the scientific viability of pyrolysis-FTIR and allow informed decisions on design choices. The capabilities, limits and resource demands of the final instrument should be well understood. Ultimately, satisfactory completion of this project should have the instrument developed sufficiently for the commencement of a 'bread-board' model, the precursor to a field-ready prototype.

## 1.8 Research aims

In this thesis, the application of pyrolysis-FTIR as a triage instrument for Mars Sample Return is assessed. The general aims were to assess the scientific capability of such an instrument and make considerations for its design. The five main areas of focus were:

1. The capability of pyrolysis-FTIR to identify regions of past or present habitability from the mineral record.
2. The sensitivity limits of pyrolysis-FTIR when detecting organic matter.
3. The effects of various mineral types on the detection of organic matter by pyrolysis-FTIR.
4. Demonstrate an effective pyrolysis-FTIR triage protocol in a simulated field test.
5. Make considerations for the design and optimisation of a pyrolysis-FTIR instrument.

# Chapter 2 Methodology

## 2.1 Introduction

The search for evidence of life on Mars seeks two key pieces of evidence. First that conditions were conducive to life, i.e. 'habitability', and second that life existed, i.e. 'habitation'. Habitability can be determined by examination of mineral phases while habitation can be assessed by the detection of organic matter.

Habitability is most commonly associated with liquid water and the thermal decomposition of minerals can reveal their past relationships with water containing environments. Habitation inevitably leads to the production of biomass and this type of organic matter, or its fossil remains, can also be accessed through thermal extraction or thermal decomposition (pyrolysis).

Detection of any gaseous mineral decomposition products can be achieved using spectroscopy. FTIR spectroscopy is particularly useful when analytes are in the gas phase owing to a number of diagnostic absorptions. Detection of thermal extraction or thermal degradation products of organic matter can also be achieved by gas phase FTIR. The variable functional group contents of organic matter lead to characteristic absorptions.

## 2.2 Background theory

Molecular vibrations arise from the periodic motions of the atoms (which are in stable bonds) within a molecule, in addition to the molecule as a whole being subject to periodic rotation (when in the gas phase). This periodic motion of atoms comes through the restorative action of competing attractive and repulsive interatomic forces, which are electromagnetic in nature, around an equilibrium position and can be thought of as a form of simple harmonic motion.

Due to the different degrees of freedom in three-dimensional space, molecule can have different vibrational modes which can take the form of: stretching (symmetric or anti-symmetric), which is a change in the linear distance between atoms; bending, which is a change in the angle between two bonds; rocking, which is the

change in the angle between groups of atoms which all lie in the same plane; wagging, which is the change in the angle of the plane of a group of atoms out of the plane of the rest of the molecule; twisting, which is the change in angle between two planes of atoms along a rotation axis; and 'out-of-plane' vibrations, which is a change in angle between a bond and the plane of the rest of the molecule (Wilson, Decius and Cross 2012).

Diatomic molecules can only have a stretching mode. Molecules with more atoms ($N > 2$) generally have $3N - 6$ vibrational modes, except for linear molecules which have $3N - 5$ modes (Landau and Lifshitz 1976).

Each mode is associated with a fundamental frequency. A quantum of energy, $E = hv$ where $h$ is the Plank constant and $v$ is the fundamental frequency of the vibrational mode, applied to the molecule in its ground state will excite the fundamental vibration. Successive photons of frequencies $v$ will excite the vibrational mode to higher overtones. In this way, the vibrational energies of molecules are quantised. An excited vibrational mode may cascade from an upper energy level down to the next lower energy level, causing the emission of a photon of the fundamental frequency (Eisberg and Resnick 1985).

For a given molecule, the interatomic forces can be influenced through the influence of conditions external to the molecule (e.g. increasing the pressure of a gas will 'squeeze' molecules together and shorten bond lengths, resulting in an increase in the interatomic repulsive force), thus fundamental frequencies of molecules can vary. In solids and liquids, such variations of the fundamental frequency are more prominent than for molecules in the gas phase, as in solids and liquids the influences of neighbouring molecules and bonds are more significant.

As transitions between energy levels of a given vibrational mode are closely related to a certain frequency, and result in absorption and emission of photons of that frequency, molecular vibrations can be utilised in spectroscopic methods. The fundamental frequencies of molecular vibrations lie in the mid-infrared region

(wavelengths 2.5–25 μm, or 4000–400 $cm^{-1}$). Should a vibrational mode be infrared active, infrared spectroscopy can be used to identify the presence of molecular species by the location of peaks in the frequency domain of a spectrogram. Increasing quantities of the molecule increases the probability of photons being absorbed or emitted, thus the intensity of peaks in the spectrogram gives information of the abundance of molecules. As mentioned above, the frequencies of vibrations (thus detected photons) are more subject to variance in solids and liquids than in the gas phase, thus gas phase spectroscopy offers more assured detection of compounds.

To reap the benefits of gas phase spectroscopy when targeting solid or liquid samples, conversion of samples to the gas phase can be achieved through the application of thermal energy. Through the same mechanism that gives us absorbance spectra in molecules, absorbance of a photon of the correct frequency will excite a molecular bond to a higher energy state. Should the bond be subjected to enough photons of the correct frequencies, the bond will eventually be excited to a dissociation energy level, breaking the bond. This mechanism causes macromolecules in solids to break into smaller constituent compounds (whose internal bond energies are higher i.e. more thermally stable). In many cases, the temperatures required to break these bonds are significantly higher than the critical temperature of the freed compounds, thus will be presented in the gas phase when released by the macromolecule. This can lead to a loss of information about the macromolecule, so the benefits of gas phase analysis must be weighed-up based on the desired application and outcomes.

This reaction, more generally known as thermolysis, is called pyrolysis when undergone by organic compounds under non-oxidising conditions. Pyrolysis is the adopted term in this project for consistency across all samples, regardless of their organic content levels.

## 2.3 Sample acquisition

Samples were obtained from the laboratory stockpile; either from commercially produced lab standards or natural samples obtained from field work for prior investigations. All samples had to be crushed into a fine

powder, done so in a ceramic pestle and mortar, before being processed by ATR-FTIR (Section 2.5) or pyrolysis-FTIR (Section 2.6) and were stored in screw capped vials.

### 2.3.1 Habitability samples

Samples were chosen such that the set covered a wide range of mineral types. This included samples with relevance to the mineralogically defined eras of Mars, identified by Bibring et al. (2006), and included terrestrially understood habitability indicators. The choice of minerals is detailed in Gordon and Sephton (2016b) which is presented in Chapter 3.

### 2.3.2 Sensitivity and habitation samples

As this investigation aimed to test the effects of Mars relevant minerals on organic constituents and also the sensitivity of pyrolysis-FTIR a characterised organic assemblage was needed that could be applied in controlled quantities. *Lycopodium* spores were chosen as they were available in industrially processed quantities, providing some guarantee of consistency, and their powdered form was conducive to mixing with other powdered materials. There is no specific biologically informed reason for their choice, i.e. another biological material / species with the same aforementioned practical qualities could have been chosen. For the sensitivity investigation of pyrolysis-FTIR different concentrations of a quartz and *Lycopodium* spore mixture were made: 0.50% to 0.05% in 0.05% steps, and 0.02%.

Of the laboratory stock pile minerals available in substantial quantities (to permit more accurate concentrations and high volume sampling where required) the best representative of each Martian era was chosen (a serpentinite for the Phyllosian, a jarositic clay for the Theiikian and a palagonitic tuff for the Siderikian). JSC Mars-1, of which stock was limited, was also included for being the established Mars analogue (Allen et al. 1998). Three concentrations, 5.0%, 1.0% and 0.5%, were made of each mineral and *Lycopodium* spore mixture. The choice of minerals and mixing procedure is detailed further in Gordon and Sephton (2016a) which is presented in Chapter 4.

### 2.3.3 Sulfate ecosystem samples

Cores were collected from a stream in St. Oswald's Bay, Dorset, UK and from a dry stream in a small cove known as Stair Hole, east of St. Oswald's Bay. This location had been identified from previous field work and was notable for being rich in sulfates and its high acidity (making it a suitable analogue for the Theiikian era on Mars). The St. Oswald's Bay steam is shown in Figure 2.1 with a location map for both sampling locations. Samples obtained from these cores were freeze-dried, crushed and characterised by X-ray diffraction (XRD) for work conducted prior to this investigation (Lewis et al. 2016), from which a representative subset was selected. These samples are discussed further in Chapter 5.

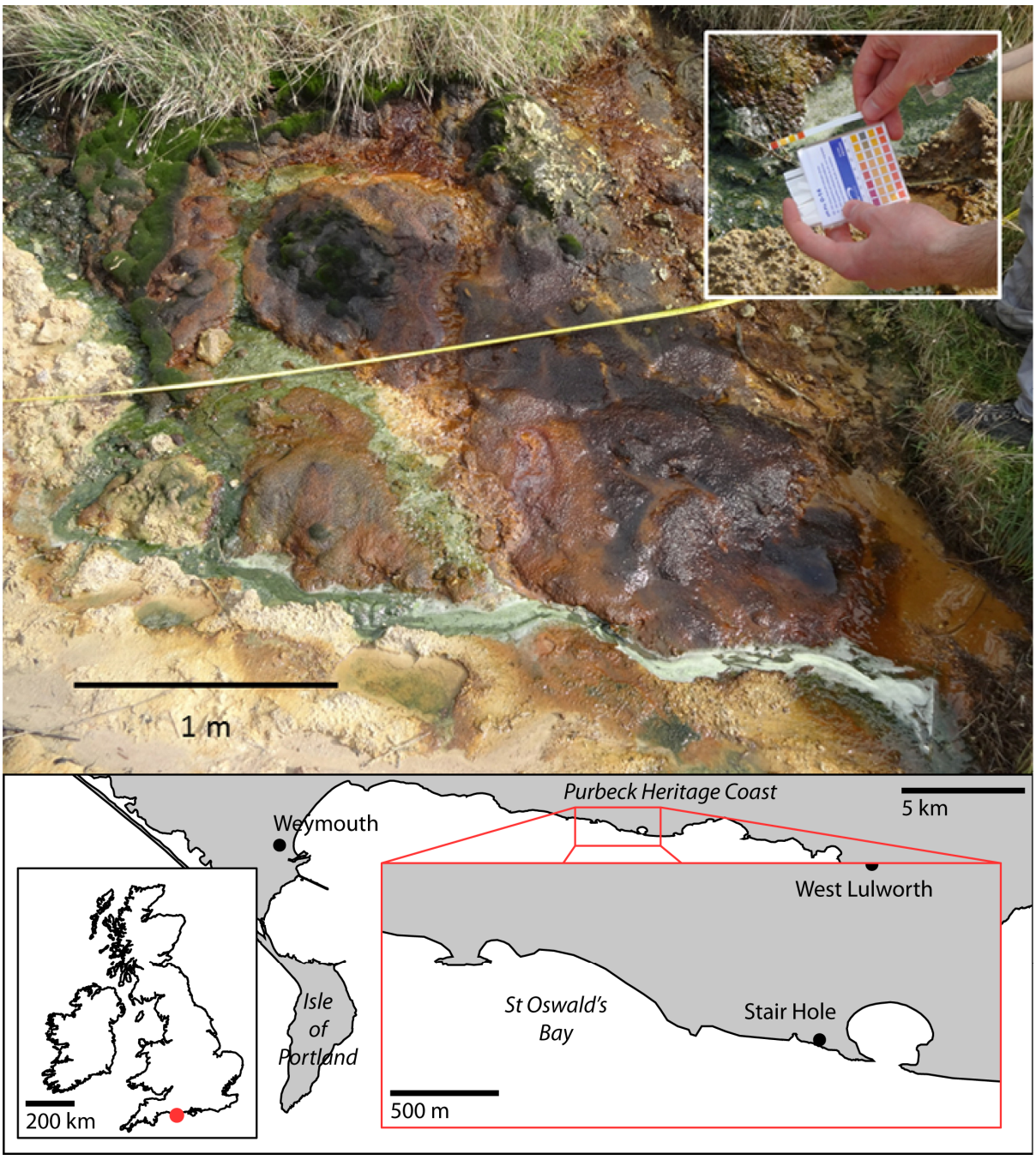



Figure 2.1. Sulfate rich stream environment in St. Oswald's Bay, Dorset, UK (above) and location map of St. Oswald's Bay and Stair Hole (below). On the map, the red circle marks the location within the UK of the Purbeck Heritage Coast along which the two sampling locations are found.

## 2.4 Fourier transform infrared spectroscopy

Fourier transform infrared spectrometry (FTIR), a technique which has found great use in analytical chemistry laboratories over recent decades due to its relative inexpensiveness and versatility (Griffiths and De Haseth 2007), can examine the molecular constituents of a sample by obtaining an absorption or emission profile (depending on the choice of analytical method, which is governed by the nature of the sample). Absorption or emission of a sample can be measured by comparing the frequency dependent light intensity profile of the sample with that resulting from background conditions.

To achieve an intensity spectrum in FTIR, a beam from a polychromatic source (covering wavelengths in the mid infrared) is passed through an interferometer, commonly a Michelson-Morley type where the beam is split into two beams of equal intensity. The optical path difference (OPD) between the split beams is varied periodically (by a linearly moving mirror in the case of the Michelson-Morley type) before having the beams recombine. Each frequency present in the source beam will undergo constructive and deconstructive interference as their split components' phase difference is shifted between 0 and $\pi$, which happens at different rates for each frequency. The interfered beam is ultimately passed onto a detector where the overall intensity of the beam is measured periodically. The interaction of the beam with the sample can occur either before or after it is passed through the interferometer, benefiting the versatility of FTIR configurations.

As the interference mechanism is controlled and well characterised, the OPD at any given time can be known, thus the pattern of intensity measured at the detector over time can be expressed as a function of the OPD. The resulting pattern is called an interferogram. The interferogram is a superposition of sinusoidal intensity patterns resulting from interference of each frequency (or frequency groupings, more accurately) within the beam, where the peak separation of each sine wave is unique for each frequency initially present in the infrared beam. Thus a Fourier transform of the interferogram results in a set of intensities for discrete frequencies, which gives the desired intensity spectrum. The interferometer operation is illustrated in Figure 2.2

Division of the sample intensity profile by the background intensity profile gives a transmission spectrum. In cases where the sample beam has encountered an absorbing medium, the transmission value will be <1 at and around the associated frequencies of the absorbing vibrational modes, resulting in peaks. The

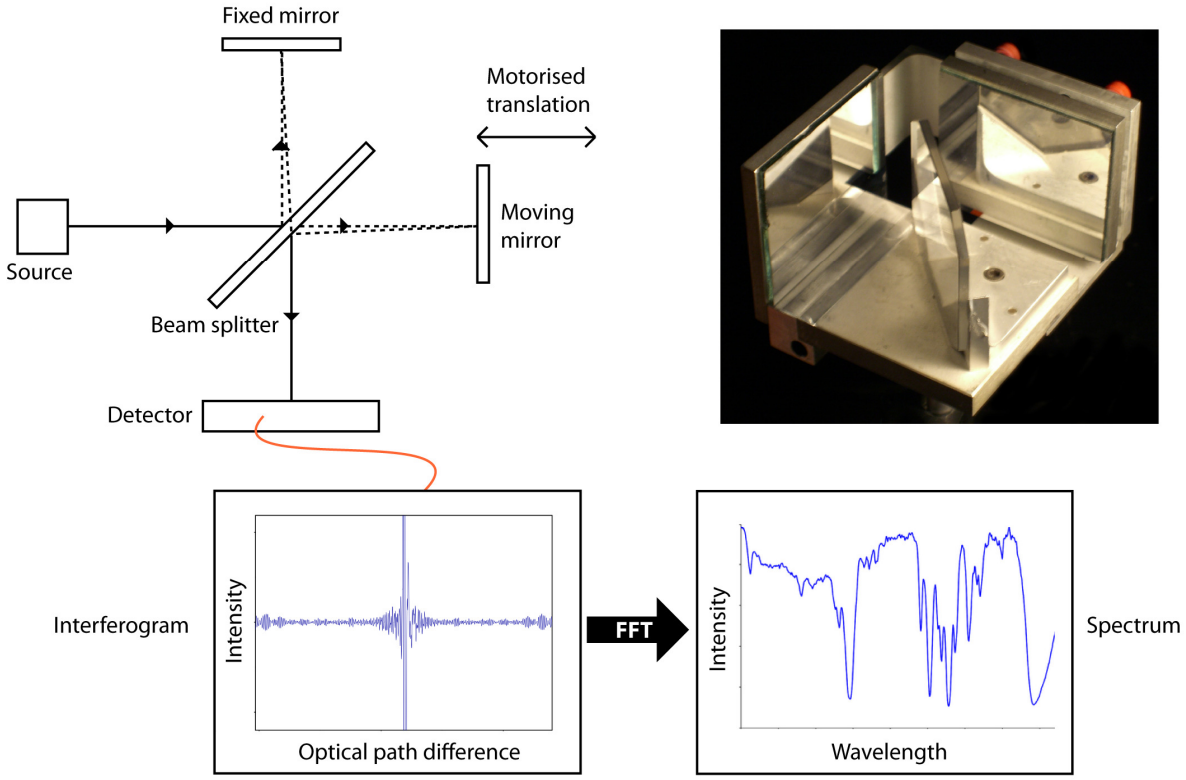



Figure 2.2. Schematic diagram (top left) and photograph (top right) of a Michelson-Morley interferometer. A fast Fourier transform (FFT) is used to convert the output of the detector, an interferogram, into a frequency/wavelength spectrum of the multi-frequency source.

presence and absence of peaks in the resulting spectrum at certain frequencies allows for qualitative identification of molecular species while the magnitude of peaks informs on the quantity present.

## 2.5 Attenuated total reflectance-FTIR

Attenuated total reflectance (ATR) FTIR is a relatively quick and simple method of obtaining information on the constituents of a liquid or solid sample. A sample is placed in surface contact with a sampling crystal. The infrared beam enters the crystal at an angle that causes total internal reflection at the sampling surface (provided the refractive index of the sample is low enough). For multiple reflections at the sample boundary, reflections can occur at a parallel surface of the crystal, opposite the sampling surface. Evanescent waves permeate into the sample beyond the contact boundary, which are subject to absorption, which results in attenuation of the beam each time it is reflected at the sampling boundary.

In this study, ATR-FTIR spectrometry was achieved using a Thermo-Nicolet 5700 FTIR spectrometer fitted with an attenuated total reflectance Thermo Orbit accessory which has a diamond sampling crystal. Measurements were made on a DTGS detector. Background spectra were obtained prior to sample collection by cleaning the compactor tip and crystal surface, then positioning the compactor tip snugly against the crystal and taking a spectrum. The sample spectra were achieved by loading the finely grained powdered sample onto the crystal surface and lowering the compactor, pressing the sample against the crystal, until the turning handle 'slips' (this ensures uniform pressure across samples) before taking the measurement. The sampling interface of the ATR-FTIR apparatus is shown in Figure 2.3.

The spectrometer was operated through the Thermo Scientific™ OMNIC™ Series Software which also recorded the spectra. Interpretation of samples was performed by reference to characteristic spectral features of different functional groups. Inorganic functional group identification was achieved by reference to absorption band tables provided in (Gadsden 1975). Identification of numerous organic functional groups can be achieved using a Colthup chart (Colthup 1950), although organic compounds can be broadly covered by identification of C-H stretching. Table 2.1 lists the identification features used in the project.

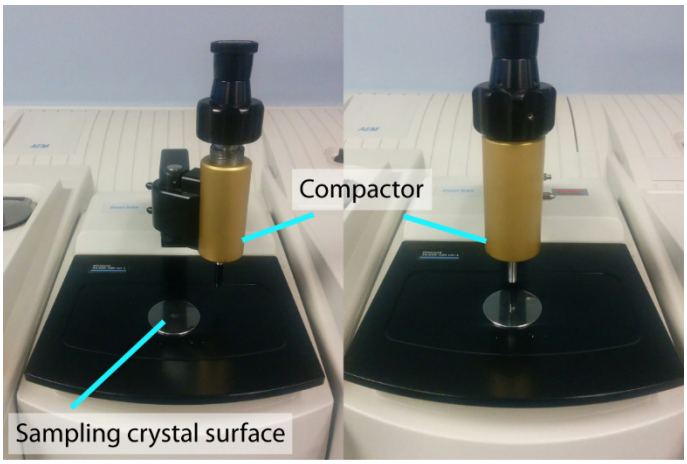



Figure 2.3. Sampling interface for ATR-FTIR apparatus, showing the sampling crystal exposed before a sample is loaded (left) and showing the position of the compactor when pressing a sample against the sampling crystal surface (right).

Table 2.1. Spectral locations of features characteristic to different functional groups. The third column describes the relative nature of the feature: s - strong, m - medium, ss - strong sharp, sb - string broad.

| Compound | Frequency range ($cm^{-1}$) | Strength |
|---|---|---|
| Hydroxyl | 3700-3500 | ss |
| Water of hydration | 3600-3200 | sb |
| Carbonate ion | 1450-1400 | s |
| | 890-800 | m |
| | 760-670 | m |
| Sulfate ion | 1210-1040 | s |
| | 1030-960 | m |
| C-H bearing | 3050-2650 | s |

The ATR method was used for two investigations to support results from gas phase FTIR analysis. These are described in Sections 2.5.1 and 2.5.3.

### 2.5.1 Habitability

In the habitability investigation (Chapter 3) ATR-FTIR was conducted to help characterise the pre-pyrolysis form of each sample. The data also allowed comparison between the information provided by solid phase and gas phase FTIR to explore the argument for choosing gas phase FTIR methods for Mars triage.

Samples were dried in a 110 °C oven before analysis to reduce the contribution of adsorbed species.

The FTIR collection method averaged 32 scans with a resolution of 4 $cm^{-1}$ in the 4000-525 $cm^{-1}$ infrared region; acquisition time was 39 seconds, a method established by previous investigations by the research group to give adequate gas phase spectra. Each analysis included a background scan obtained using the same method and conducted before the sample was loaded.

### 2.5.2 Sensitivity and habitation

No ATR-FTIR analyses were conducted for this investigation.

### 2.5.3 Sulfate ecosystem

ATR-FTIR measurements were made of the sulfate stream samples to accompany the XRD mineralogical characterisation data. Samples were not subjected to oven drying to match the conditions of the pyrolysis-FTIR experiment phase.

ATR-FTIR spectra were collected using a longer sampling scan than for the previous habitability investigation. 128 sample scans were taken over a 150 second period at a resolution of 4 $cm^{-1}$, from which a background scan (i.e. a spectrum taken of the crystal platform with no sample present) was subtracted. Only one background scan was taken at the beginning of each sampling session, and this background was used to form the transmission spectra of all samples taken in a session.

## 2.6 Pyrolysis-FTIR

Pyrolysis apparatus can apply thermal energy to solid samples in a controlled manner to release gaseous products. The heating rates can be rapid, up to 20 °C $ms^{-1}$, known as flash pyrolysis. Flash pyrolysis achieves thermal decomposition of samples at much lower energy costs than slower heating rates.

The expediency of thermal decomposition by flash pyrolysis compliments the short sampling times achievable by FTIR, thus pyrolysis-FTIR (where gas phase transmission FTIR is used to measure products of pyrolysis) is a convenient and versatile analytical technique.

The pyrolysis-FTIR apparatus used in the investigation combines a Thermo Nicolet 5700 FTIR spectrometer and a CDS 5200 pyrolysis unit. Pyrolysis products are contained within an air tight cell (called the Brill cell, manufactured by CDS Analytical). The Brill cell is windowed on two opposite sides by IR transparent ZnSe disks, which allows interfacing with the spectrometer. The spectrometer beam is passed through the Brill cell, which is carefully aligned so that the parallel set of windows are orthogonal to the propagation axis of the beam to reduce effects of refraction. A helium atmosphere is maintained in the Brill cell as it is infrared transparent and will reduce oxidation reactions. The Brill cell is equipped with an electronic heating element and is maintained at 250 °C to prevent condensation of pyrolysis products on the cell components.

The pyrolysis probe is a steel rod with the heating element (a platinum coil) at one end. Once inserted into the Brill cell, the heating element is located underneath the beam path. Powdered sample material (ranging from approximately 0.5 – 20 mg) is placed inside small quartz cylinders, capped at either end by quartz wool plugs, which fit neatly into the platinum coil. At each preparation step samples were weighed on a balance accurate to ±0.1 mg to ascertain the quantity of sample added to each quartz tube, to ultimately allow expression of pyrolysis yields as fractions of the initial sample mass. A simplified schematic diagram of the lab bench set-up is provided in Figure 2.4 and photographs of the pyrolysis-FTIR lab apparatus are shown in Figure 2.5.

Heating rates and temperatures are controlled using the CDS 5000 DCI software (provided with the pyrolysis unit). Spectrometer operations are conducted using the Thermo Scientific OMNIC Software Suite which also is used to record and process spectroscopic data. Band identification was achieved by searching through the spectral data available in the NIST Webbook (http://webbook.nist.gov/chemistry/) and use of the 'IR Spectral Analysis' function provided in the Thermo Scientific™ OMNIC™ Series software.

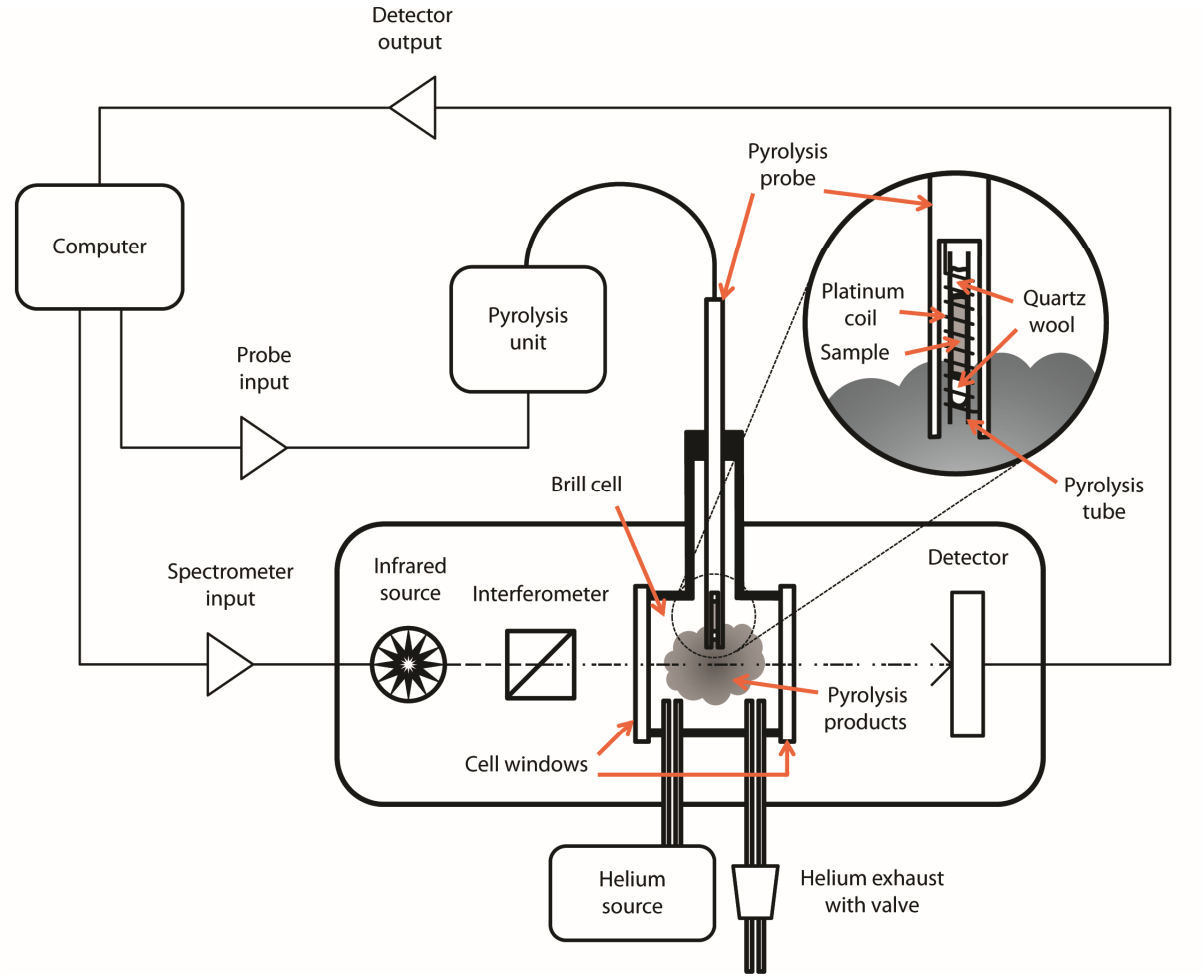



Figure 2.4. Schematic diagram of pyrolysis-FTIR (adapted from figure in (Sephton et al. 2013)).

The main gases of interest identified throughout the project are listed in Table 2.2, with details of the spectral features observed.

Mass calibration curves for the lab bench pyrolysis-FTIR setup were obtained for carbon dioxide, water, sulfur dioxide and methane by direct injection of known quantities of these gases into the Brill cell, which allowed quantification of results.

Before each sampling session liquid nitrogen had to be poured into the coolant well of the spectrometer. After allowing the detector to cool down (about 30 minutes after introducing the liquid nitrogen) a collection of three or more blank spectra were collected to observe that the spectrometer was properly

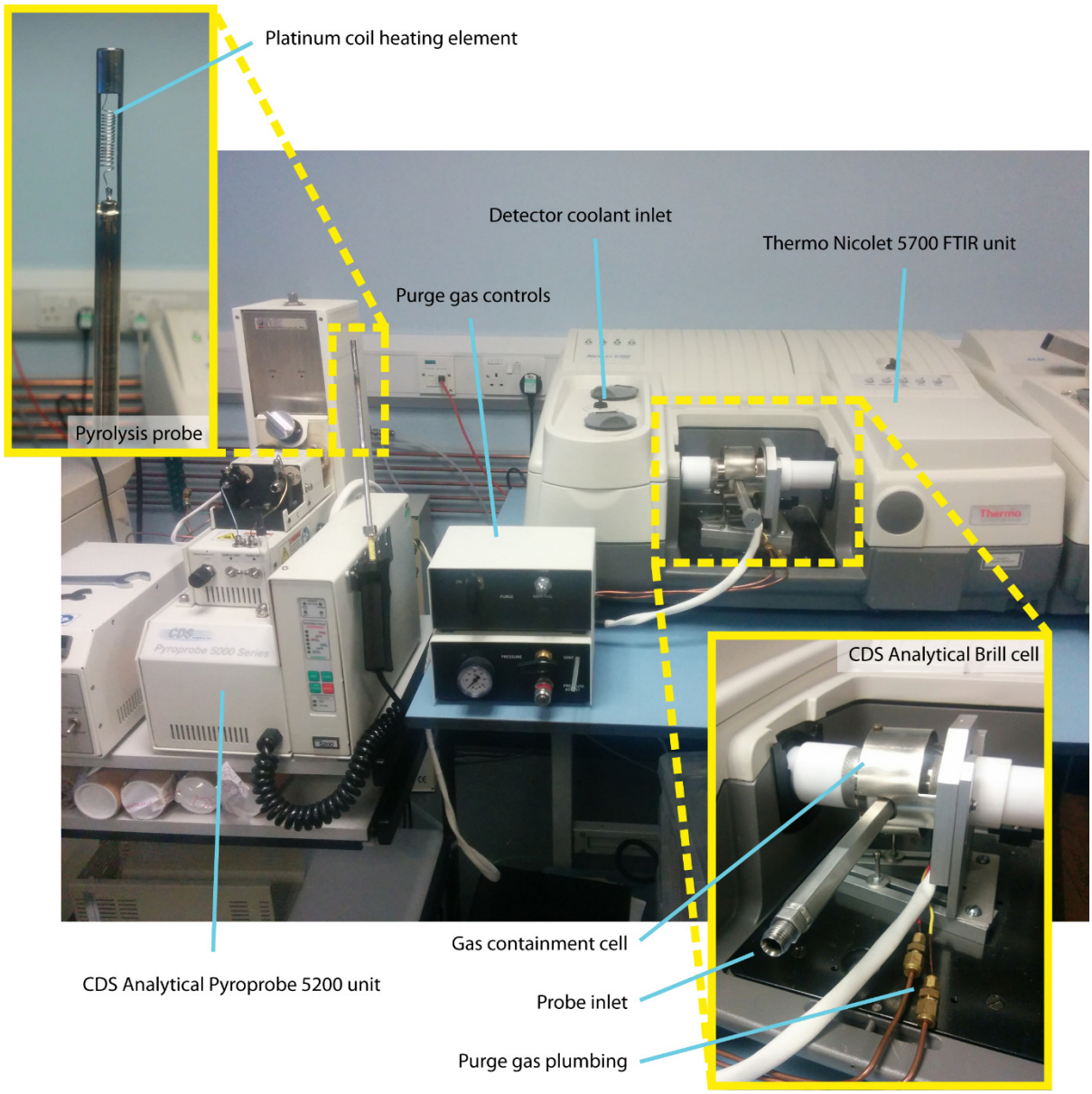



Figure 2.5. Pyrolysis-FTIR lab bench apparatus.

functioning and that the detector had reached an equilibrium state. Collecting a blank involved performing both the background and sample scans under the same condition, with no sample or probe present.

All background and sample spectra were a combination of 32 individual spectra with resolutions of 4 $cm^{-1}$ in the 4000-650 $cm^{-1}$ infrared region, collected over approximately 20 s, unless stated otherwise.

Over the course of the project, the exact procedure for pyrolysis-FTIR and data reduction was altered and improved upon. The specific details for each investigation; habitability, sensitivity, mineral matrix effects

and sulfate ecosystem, are included in Sections 2.6.1, 2.6.2, 2.6.2.3 and 2.6.3 respectively, and a test plan for the project is outlined in Table 2.3.

Table 2.2. Gases of interest for pyrolysis-FTIR experiments and the spectral features used for measurement.

| Gas | Relevance | Vibrational mode | Wavenumber |
|---|---|---|---|
| Carbon dioxide | Combustion product of organic compounds. Also released by carbonates which can serve as a habitability indicator. | Anti-symmetric stretching | 2349 $cm^{-1}$ |
| Water | Vital requirement of habitability and indicates aqueous alteration in rocks. | Stretching | 3853 $cm^{-1}$ |
| Sulfur dioxide | Produced by sulfates, which are known to aid preservation of organic compounds. | Anti-symmetric stretching | 1352 $cm^{-1}$ |
| Methane | Basic organic compound and can be a product of life processes. | Anti-symmetric stretching | 3016 $cm^{-1}$ |
| Hydrogen chloride | Has a fringe which occupies the same spectral position as the methane peak. | Stretching | 2798 $cm^{-1}$ |

### 2.6.1 Habitability

This investigation is discussed fully in Chapter 3.

To get an understanding of habitability indicators from minerals obtained from a dry environment, it was important to reduce the quantity of adsorbed species in each sample. Initially this was done by placing prepared samples (i.e. loaded in quartz tubes) for 2 hours or more in a 110 °C oven. For time efficiency, this method was replaced by subjecting the sample to a 120 °C pyrolysis burn for 15 s while under helium flow (using the pyrolysis-FTIR apparatus).

Initially, the mass of the sample was taken at each stage of preparation and of pyrolysis operation. This was done in order to ascertain the mass loss during the drying step, and the mass lost at each pyrolysis-FTIR analysis. It was found that this data was of little use; masses lost were often lower than the accuracy of the balance.

#### *2.6.1.1 Preliminary work*

A set of temperature steps had to be decided upon that would offer adequate information about unknown samples. A preliminary investigation was conducted on representative samples: calcium carbonate, gypsum, kaolinite, Kimmeridge Clay and siderite, to determine what the temperature steps should be. Each of these samples was subjected to a long, ramped temperature profile (250 to 1200 °C over 10 mins) by the pyrolysis probe, during which the levels of gases were continuously monitored by FTIR. This heating rate was considered gradual enough to provide ample resolution for identifying the temperatures at which pyrolysis effects occur. The resulting profiles (of relative gas response as a function of temperature) were compared, and three temperatures were identified which could be used to discern between these minerals 500 °C, 750 °C and 1000 °C. These steps were tested sequentially on the representative samples to confirm their diagnostic potential in a stepped heating profile (as opposed to a ramped heating profile).

#### *2.6.1.2 Habitability investigation*

Each mineral type was analysed by pyrolysis-FTIR using the sequentially stepped profile of the three temperatures determined by the preliminary investigation (500 °C, 750 °C and 1000 °C). They were also be subjected to a single-step pyrolysis-FTIR analysis for comparison. For single-step 1000 °C was used; in theory this should produce the same state of decomposition in samples ultimately experienced in multi-step analysis.

When performing pyrolysis-FTIR on samples in the habitability investigation, the background spectrum was taken before the probe was loaded into the Brill cell. Once loaded, samples were pyrolysed for 10 s at the required temperature immediately after which the sample spectrum was collected. Each combination of mineral type and pyrolysis mode was performed three times so that the resulting data accounted for experimental variability (via standard deviation).

In this investigation, the uncertainty calculated for each individual sample resulted from the error propagation of each measured quantity (sample mass & absorbance). The uncertainty in absorbance

values was obtained by taking the standard deviation of the planks performed before each sampling session.

### 2.6.2 Sensitivity and habitation

The results of these investigations are outlined and discussed in Chapter 4.

#### *2.6.2.1 Preliminary work*

The aim of the sensitivity investigation was to ascertain the sensitivity limit for quantities of organic matter, thus it was important to find the optimum temperature for organic detection. While this temperature may vary for different types of organic assemblages, it should be a constant for *Lycopodium* spores – the only organic matter being used in this investigation.

First, pure quantities of *Lycopodium* spores were subjected to various ramped heating profiles using the pyrolysis-FTIR apparatus, with the IR responses for organic structures and carbon dioxide recorded as a function of time. Stepped analysis on a pure *Lycopodium* sample (50 °C steps, increasing from 300 °C to 750 °C) was conducted to support the continuous temperature ramp data. Further investigations were conducted on *Lycopodium* spore and quartz mixtures to investigate any changes to the *Lycopodium* spore response to temperature once suspended in a mineral. Once the temperature of 700 °C was decided upon, samples of quartz and *Lycopodium* spores were subjected to 700 °C pyrolysis burns for extended periods (30 s) with the hydrocarbon response monitored over time from the start of the pyrolysis probe firing. It was found that the level of detected hydrocarbons does not increase after 7.2 s seconds, thus this is the most efficient burn time. Results representative of these preliminary investigations are displayed in Appendix A.1.

#### *2.6.2.2 Sensitivity appraisal investigation*

In the habitability investigation, the background spectrum was taken with the Brill cell empty of any sample. The method was changed for this investigation so that the background spectrum was taken with the probe inserted. After loading the probe with a new sample, a 90 s warm up time was allowed to achieve thermal

equilibrium within the Brill cell. In this time adsorbed gases would be desorbed from the sample, thus become part of the background signal. The method was changed like this to achieve increased time efficiency and to have background and sampling conditions matched as closely as possible.

Another change to the method was the addition of procedural blanks conducted at the beginning of each sampling session, for each pyrolysis temperature being used. These were collected in addition to the blanks obtained at the start of each session used to monitor the condition of the spectrometer and detector (described in Section 2.6). Procedural blanks involved loading the pyrolysis probe with an empty quartz tube and collecting the background and sample spectra as normal (i.e. firing the probe before collecting the sample spectrum).

A large number of data from the different concentrations of *Lycopodium* spores and quartz were required to build a reasonably accurate statistical picture: for 0.02%, 0.05% and 0.10% (30 data points); for 0.15%, 0.20% and 0.25% (15 data points); and for 0.30%, 0.35%, 0.40%, 0.45% and 0.50% (3 data points). These numbers were considered plenty for statistical analysis (with more data collected at lower concentrations as positive detection for these was less certain).

The spectra of procedural blanks from each data session were averaged (35 in total) and subtracted from the sample spectra. To ensure more consistent outcomes when using the automatic baseline correction function in the OMNIC Software Suite, spectra were truncated so that only the 3300 to 2650 $cm^{-1}$ wavenumber region remained (only the C-H stretching region was required, which occupies a subset of this wavenumber region). The area in the C-H stretching region (3150 – 2740 $cm^{-1}$) was then recorded and the errors reported in the results were taken from background fluctuation in blanks in the same spectral region (i.e. the instrumental error).

#### *2.6.2.3 Habitation investigation (assessment of mineral matrix effects)*

This investigation did not require any precursor investigation, as the two pyrolysis temperatures which would provide useful comparison had already been identified; most sensitive temperature for *Lycopodium*

spore detection, 700 °C, identified in the sensitivity investigation (Section 2.6.2, above) and the most sensitive temperature for mineralogical identifiers, 1000 °C, in the habitability investigation (Section 2.6.1, above).

The pyrolysis-FTIR procedure was identical to that of the sensitivity assessment, with the pyrolysis burn time being 7.2 s conducted immediately before FTIR measurement. Three repeat analyses were performed of each sample type and temperature combination.

Resulting spectra were truncated to a 4000 $cm^{-1}$ to 1250 $cm^{-1}$ wavenumber region before performing the OMNIC Software Suite automatic baseline correction. From the resulting spectra, peak intensities of the target gases were recorded. The responses for the target gases in the procedural blanks (averaged for the relevant collection session) were subtracted from the responses in the sample spectra. For each set of triplicate analyses, response values (with the blank values already subtracted) were averaged, from which the masses of pyrolysis products were ascertained using mass calibration curves. Error values stated in the results were obtained by taking standard deviation of the same triplicate response values and converting this to a mass value (giving the experimental error, accounting for variability in the sample construction and the instrument operation).

### 2.6.3 Sulfate ecosystem

The results of this investigation are outlined and discussed in Chapter 5.

There was no preliminary work required for this investigation, as procedure for sample selection using different modes of pyrolysis-FTIR could be informed by the previous investigations; a 'catch-all' phase using single-step 1000 °C pyrolysis-FTIR (sensitive to both mineral habitability indicators and the decomposition products of organic matter), as demonstrated in the habitability investigation (Section 2.6.1), followed by an organic content sensitive phase using single-step 700 °C pyrolysis-FTIR, as identified in the sensitivity

investigation (Section 2.6.2), of which the most worthy samples could be scrutinised by the diagnostic capability of the multi-step pyrolysis-FTIR mode.

Pyrolysis-FTIR was performed in the same procedure as for the sensitivity and mineral matrix effects investigations. To emulate true triage operation, samples were only subjected once at each of the triage steps (should they have been deemed worthy by the previous phase).

Prefacing each collection session, three procedural blanks were performed for each temperature mode used being used for analysis, in addition to the blanks which assessed the spectrometer and detector conditions.

For data reduction, the average spectrum of the procedural blanks (for the appropriate collection session and temperature) was subtracted from each sample spectrum. The responses were measured for the target gases and expressed as masses (where calibration curves were available). The uncertainties reported in the results are taken from the standard deviation of the responses in the procedural blanks.

Table 2.3. Test plan for experimental work in this thesis.

| Investigation | Aim | Method | Samples |
|---|---|---|---|
| Habitability investigation (Chapter 3) | Determine the capability of pyrolysis-FTIR to assess the habitability potential of rock samples. | Make pyrolysis-FTIR measurements of different rocks with habitability relevance and identify signatures. Compare single-step and multi-step modes of pyrolysis-FTIR for their diagnostic potential. Compare results with solid phase FTIR via ATR-FTIR. | A broad range of minerals exhibiting different habitability indicators including; phyllosilicates, carbonates, sulfates and other salts, igneous materials and organic matter bearing rocks (full list of samples in Section 3.2.1). |
| Sensitivity investigation (Chapter 4) | Assess the sensitivity limits of pyrolysis-FTIR when detecting biological materials. | Make pyrolysis-FTIR measurements of a reproducible biological substance in diminishing quantities. Make a high numbers of measurements in ranges where signal-to-noise is low to allow statistical analysis. | *Lycopodium* spores as a biological material and quartz as an inert mixing material. |
| Mineral matrix effects (Chapter 4) | Identify how key mineral types on Mars would influence the signals of organic matter when analysed by pyrolysis-FTIR. | Mix a reproducible organic assemblage with minerals representative of environments on Mars. Subject these mixtures to pyrolysis-FTIR analysis. Vary concentrations of organic material to isolate effects of the minerals and use different pyrolysis temperatures to highlight the effects of pyrolysis. | Quartz as an inert reference material, a serpentinite to represent the Phyllosian, a Jarositic clay for the Theiikian, a palagonite for the Siderikan and JSC Mars-1 as the standard Mars soil analogue (with *Lycopodium* spores as the organic assemblage). |
| Sulfate ecosystem study (Chapter 5) | Perform a pyrolysis-FTIR survey on samples from an analogue Mars environment and asses the capability to triage samples with pyrolysis-FTIR results. | Design a triage protocol using different modes of pyrolysis-FTIR. Subject samples to this protocol and rank samples based on the aims of Mars Sample Return and select those worthy of return. | A collection of samples obtained from a sulfate dominated ecosystem in St. Oswald's Bay, Dorset, UK and samples from a dried out sulfate stream in the nearby Stair Hole location (full sample details in Section 5.2.1). |

# Chapter 3 Rapid habitability assessment of Mars samples by pyrolysis-FTIR

Peter R. Gordon, Mark A. Sephton

*Published in Planetary and Space Science, Volume 121, February 2016, Pages 60-75, ISSN 0032-0633, http://dx.doi.org/10.1016/j.pss.2015.11.019.*

## Abstract

Pyrolysis Fourier transform infrared spectroscopy (pyrolysis-FTIR) is a potential sample selection method for Mars Sample Return missions. FTIR spectroscopy can be performed on solid and liquid samples but also on gases following preliminary thermal extraction, pyrolysis or gasification steps. The detection of hydrocarbon and non-hydrocarbon gases can reveal information on sample mineralogy and past habitability of the environment in which the sample was created. The absorption of IR radiation at specific wavenumbers by organic functional groups can indicate the presence and type of any organic matter present.

Here we assess the utility of pyrolysis-FTIR to release water, carbon dioxide, sulfur dioxide and organic matter from Mars relevant materials to enable a rapid habitability assessment of target rocks for sample return. For our assessment a range of minerals were analysed by attenuated total reflectance-FTIR. Subsequently, the mineral samples were subjected to single-step pyrolysis and multi-step pyrolysis and the products characterised by gas phase FTIR.

Data from both single-step and multi-step pyrolysis-FTIR provide the ability to identify minerals that reflect habitable environments through their water and carbon dioxide responses. Multi-step pyrolysis-FTIR can be used to gain more detailed information on the sources of the liberated water and carbon dioxide owing to the characteristic decomposition temperatures of different mineral phases. Habitation can be suggested when pyrolysis-FTIR indicates the presence of organic matter within the sample. Pyrolysis-FTIR, therefore, represents an effective method to assess whether Mars Sample Return target rocks represent habitable conditions and potential records of habitation and can play an important role in sample triage operations.

## 3.1 Introduction

Mars Sample Return (MSR) missions will allow samples from the red planet to be subjected to the full range of powerful analytical techniques available back on Earth (McLennan et al. 2012) and are believed to offer higher chances of success for life detection than in situ operation (Sephton and Carter 2015). The success of MSR will depend unavoidably on the selection of the correct samples for return. To maximise the probability of success, in situ instruments are needed to identify the most scientifically exciting samples, in particular those samples which can reveal the history of life on Mars. Constraining the past habitability reflected by Mars rocks and finding evidence for past life have been identified as the highest priority scientific objectives of MSR (McLennan et al. 2012).

When considering planetary habitability, areas of most interest are those where i) liquid water was prevalent, ii) where the building blocks of life were present and iii) where energetic conditions were favourable for life. If evidence suggests that habitable conditions persisted for long enough it is possible that life had originated and evolved. The initiation of life and its subsequent adaptation to its environments will lead to the continuous production of complex organic compounds, the remnants of which can become entombed in rocks. Thus assessing the presence of characteristic mineral phases that reflect habitability can reveal the likelihood of life existing contemporaneously with deposition of the rock. In addition, the detection of organic matter not only advocates habitability but raises the possibility of habitation.

The distribution of mineral types has led to a subdivision of Martian time into three mineralogically defined eras, illustrated in Figure 3.1 (Bibring et al. 2006). Each era represents a distinct planetary environment with very different associated habitabilities. The oldest era represents a period of non-acidic aqueous conditions that led to the production of widespread phyllosilicates (the Phyllosian Era), followed by an acidic aqueous environment reflected by sulfate deposits (the Theiikian Era) and finally water-free conditions that led to the generation of ferric oxides (the Siderikian Era). The changing global environmental conditions on Mars, as reflected in the rock record, indicate changing habitability with early

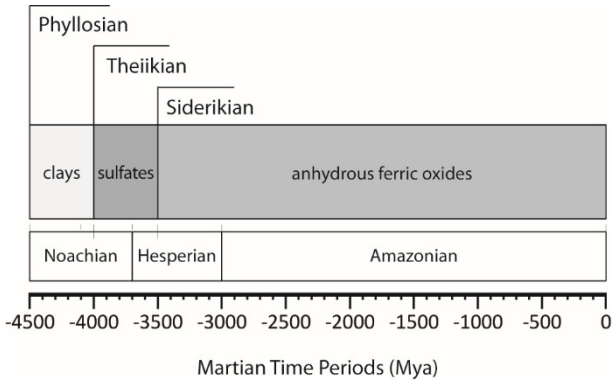



Figure 3.1. The Phyllosian, Theiikian and Siderikian eras and the mineral types which define them, illustrated in chronological order. The eras defined by crater density and lava flows are included on the bottom for comparison (diagram adapted from that illustrated by Bibring et al. (2006)).

Mars being much more conducive to life than at the present day. These widespread mineralogy-based divisions provide valuable guidance to the types of rock deposits within which Martian biosignatures may be contained.

Organic biosignatures from the habitable environments on early Mars need to be effectively preserved so they can be detected (Summons et al. 2011). The various Martian rock types have different propensities to preserve organic matter. Fortunately, those rock types that indicate habitable conditions such as phyllosilicate-rich rocks and sulfate deposits are also very good at preserving organic matter. For instance phyllosilicate-rich rocks are co-deposited with organic matter and have high surface areas that allow organic adsorption (Hedges 1977). Sulfates can host organic matter by promoting organic salt formation (Aubrey et al. 2006) and once organic matter is incorporated the low porosities and permeabilities will exclude agents of degradation, such as oxidants, and therefore assist preservation. By contrast, oxide rich rocks reflect oxidizing conditions which are generally incompatible with organic preservation.

Mars presents an overwhelming number of potential samples for return to Earth and some prioritisation is essential. Triage protocols, directed by detailed multidisciplinary scientific deliberations (Summons et al. 2011, McLennan et al. 2012) help to determine which samples are of highest priority. Triage methods must provide operational simplicity, wide applicability and should generate information-dense data sets.

One technique that may satisfy all these triage requirements is pyrolysis-Fourier transform infrared spectroscopy (FTIR) (Sephton et al. 2013). In this study we explore the capability of pyrolysis-FTIR for in-situ habitability assessment. Different modes of pyrolysis, namely single-step and multi-step, are compared. A simple approach was adopted for processing the resulting spectra; only a restricted set of spectral features were considered for determining habitability as reduced complexity is beneficial when rapid processing of samples is desired. Quantitative data sets were produced to assess their potential added analytical value. The data and interpretations provide guidance on the assessment of mineral decomposition products and their use in determining past habitability, biosignature preservation potential and even biosignature content for MSR target rocks.

## 3.2 Method

### 3.2.1 Sample selection

To assess the utility of pyrolysis-FTIR for recognising the habitability of depositional environments reflected by rock types that may be encountered on Mars we analysed a range of samples (Table 3.1).

#### *3.2.1.1 Phyllosilicates*

Phyllosilicates define the Phyllosian Era and generally form through the weathering of silicate bearing rocks. Thus detection of phyllosilicates on Mars indicates an area which experienced a period of abundant liquid water (Bibring et al. 2006). To assess the response of phyllosilicates and phyllosilicate-rich rocks to pyrolysis-FTIR we examined the standards montmorillonite and kaolinite. In addition to the phyllosilicate mineral standards we also analysed phyllosilicate mineral-containing natural sedimentary deposits, namely Upper Jurassic Kimmeridge Clay and a recent jarositic clay.

#### *3.2.1.2 Carbonate minerals*

Carbonate minerals also provide a record of water presence and chemistry. Carbonates mostly form in regions which are pH neutral to slightly alkaline and aqueous; both favourable conditions for life. Some carbonate precipitation is strongly linked with microbial activity, and it has even been argued that

Table 3.1. Details of samples for the pyrolysis-FTIR study.

| | Source | Age |
|---|---|---|
| Phyllosilicates | | |
| Kaolinite | Sigma-Aldrich | Not applicable |
| Montmorillonite | Sigma-Aldrich | Not applicable |
| Carbonate minerals | | |
| Calcium carbonate | Sigma-Aldrich | Not applicable |
| Siderite | Sigma-Aldrich | Not applicable |
| Magnesium carbonate | Sigma-Aldrich | Not applicable |
| Sulfates and other salts | | |
| Halite | Sigma-Aldrich | Not applicable |
| Iron(III) sulfate | Sigma-Aldrich | Not applicable |
| Gypsum | Sigma-Aldrich | Not applicable |
| Unaltered and altered igneous materials | | |
| Lherzolite | Ol Doinyo Lengai, Tanzania | Undefined |
| Olivine sand | Industrial source | Not applicable |
| Partially serpentinised peridotite | Kennack Sands, Cornwall, UK | Early-Mid Devonian |
| Bastite | Kynance Cove, Cornwall, UK | Early-Mid Devonian |
| JSC Mars-1 analogue | Pu'u Nene, Hawaii | Recent |
| Palagonitic tuff | Majorca, Spain | Recent |
| Sulfate-rich sediments | | |
| Jarositic clay | Brownsea Island, Dorset, UK | Eocene |
| Organic, clay and carbonate-rich rocks | | |
| Kimmeridge Clay | Kimmeridge Bay, Dorset, UK | Upper Jurassic |
| Blue Lias | Lyme Regis, Dorset, UK | Lower Jurassic |

carbonates found in unexpected regions on Mars could be explained by microbial activity (Fernández-Remolar et al. 2012). To assess the response of carbonates to pyrolysis-FTIR we examined calcium carbonate ($CaCO_3$), siderite ($FeCO_3$) and magnesium carbonate ($MgCO_3$). In addition to the carbonate standards we also analysed carbonate-containing natural sedimentary deposits, namely the Lower Jurassic Blue Lias and the aforementioned Upper Jurassic Kimmeridge Clay.

#### *3.2.1.3 Sulfates and other salts*

Sulfate minerals on the Martian surface indicate a global shift from the equable conditions reflected by the phyllosilicates to an acidic, less hospitable environment (Bibring et al. 2006). Life on Earth can adapt to acidic conditions and some organisms are capable of occupying such extreme conditions (Zettler et al.

2003). Salts can form through the evaporation of aqueous bodies. To assess the response of sulfates and other salts to pyrolysis-FTIR we examined halite (NaCl), iron(III) sulfate ($Fe_2(SO_4)_3$) and gypsum ($CaSO_4 \cdot 2H_2O$). A natural sulfate-containing sedimentary deposit was provided by the natural jarositic clay described above.

#### *3.2.1.4 Unaltered and altered igneous materials*

There are widespread igneous products or their alteration products on Mars. When igneous rocks are subjected to water they are partly or completely altered to rocks such as serpentinite. If the igneous rocks are fine grained or glassy then palagonite is a common alteration product. Weathering without the presence of water can produce ferric oxides. To reflect igneous rocks that may be encountered on Mars we have subjected a number of rock types to pyrolysis-FTIR that cover both unaltered and altered materials. For unaltered materials we chose lherzolite and olivine sand. For hydrothermally processed igneous rocks we analysed partially serpentinised peridotite and bastite serpentinite. For weathered igneous material we utilised the JSC Mars-1 Mars analogue and palagonitic tuff.

#### *3.2.1.5 Organic matter bearing rocks*

Natural rock samples provide examples of mineral mixtures that contain enclosed organic constituents and act as good test samples for the combined inorganic and organic complexity that may be encountered on Mars. The samples used in this study that represent organic containing matrices are the Lower Jurassic Blue Lias and the Upper Jurassic Kimmeridge Clay.

### 3.2.2 Attenuated total reflectance-FTIR

Spectra of solid phase samples were obtained using a Thermo-Nicolet 5700 FT-IR spectrometer fitted with an attenuated total reflectance (ATR) Thermo Orbit accessory. Powdered forms of each mineral (previously dried in a 110 °C oven to reduce the contribution of adsorbed species) were pressed against the ATR crystal and the FTIR spectra collection method was executed. The FTIR collection method averaged 32 scans with a resolution of 4 $cm^{-1}$ in the 4000-525 $cm^{-1}$ infrared region; acquisition time was 39 seconds. Each

analysis included a background scan obtained using the same method and conducted before the sample was loaded. Spectra were obtained and processed using the Thermo Scientific™ OMNIC™ Series software.

To identify hydrated minerals and carbonate bearing minerals as habitability indicators, the following spectral features were searched for: a strong sharp band in the 3700-3500 $cm^{-1}$ region arising from the stretching vibration from mineral bound hydroxyl; a single broad band arising from the two stretching bands of the water molecule, apparent in the 3600-3200 $cm^{-1}$ region for water of hydration and the 3400-3200 $cm^{-1}$ region for adsorbed water; and the carbonate ion spectral peaks, which include a strong band usually between 1450-1400 $cm^{-1}$ and medium strength bands at 890-800 $cm^{-1}$ and at 760-670 $cm^{-1}$. Data was also inspected for peaks arising from the sulfate ion in the 1210-1040 $cm^{-1}$ and 1030-960 $cm^{-1}$ regions and for the presence of C-H stretches in the 3050-2650 $cm^{-1}$ region as a test for the presence of organic matter. Quantitative analysis was not performed on the ATR-FTIR data set. Band identification was achieved by reference to published absorption band tables (Gadsden 1975).

### 3.2.3 Pyrolysis-FTIR

Pyrolysis was achieved using a CDS Analytical Pyroprobe 5200 and the FTIR spectra were obtained using the same Thermo-Nicolet 5700 FT-IR spectrometer as described above for ATR, using a nitrogen cooled MCT/A detector. Gas phase products were accumulated in a CDS Analytical Brill Cell™ containing IR transparent ZnSe windows. A helium atmosphere was maintained inside the cell, because helium is inert and IR transparent, and a helium flow allowed the cell to be purged between experiments. The Brill Cell was held constantly at 250 °C to prevent condensation of pyrolysis products on the cell components.

Solid samples, ground to a fine powder, were loaded in small amounts (approximately 0.4 – 18 mg) into quartz tubes and held in place by a quartz wool plug at each end of the tube. Before and after pyrolysis, samples were weighed on a balance accurate to ±0.1 mg to allow mass losses to be calculated and to express pyrolysis yields as fractions of the initial sample mass. The quartz tubes and wool were cleaned by progressive rinsing with water, methanol and dichloromethane before being baked at 500 °C. Before

pyrolysis, the probe was used for a final drying step by subjecting each prepared sample to 120 °C for 15 s to minimise the contribution of adsorbed species.

The spectral data was collected and processed using the Thermo Scientific™ OMNIC™ Series Software. Prior to firing the probe and collecting sample data, a background spectrum was taken for each analysis with the sample loaded in the cell. In each pyrolysis event, the desired temperature was attained at 20 °C ms-1 and held for 10 s before conducting FTIR data collection to allow adequate diffusion of pyrolysis products within the cell. The pyrolysis temperature was held for the duration of data collection to prevent gas products recombining with the sample residue. FTIR analyses were constructed by the combination of 32 individual spectra with resolutions of 4 $cm^{-1}$ in the 4000-650 $cm^{-1}$ infrared region, collected over approximately 20 s. Three spectra were collected for each sample at each temperature step. Before each experimental session, a series of blanks were obtained by replicating the full sample analysis procedure without any sample in place.

An automatic baseline correction was performed on each spectrum before recording the intensity of absorption peaks of four gases of interest; carbon dioxide, water, sulfur dioxide and methane. Band identification was achieved by searching through the spectral data available in the NIST Webbook (http://webbook.nist.gov/chemistry/) and use of the 'IR Spectral Analysis' function provided in the Thermo Scientific™ OMNIC™ Series software. For carbon dioxide and water the areas of characteristic peaks were recorded - one located at 2349 $cm^{-1}$ corresponding to the anti-symmetric stretch in carbon dioxide and one at 3853 $cm^{-1}$ arising from a stretching mode of water. For methane and sulfur dioxide the absorbance intensity was recorded at characteristic frequencies (at 3016 $cm^{-1}$ corresponding to the methane anti-symmetric stretching mode and at 1352 $cm^{-1}$ corresponding to the sulfur dioxide anti-symmetric stretching mode).

The measured responses of all gases were processed quantitatively. Carbon dioxide and water data sets were analysed further to evaluate the added value of a quantitative approach. Mass calibration curves were

constructed by direct injection of a known quantity of gas into the Brill Cell. Reference to the calibration curve allowed the masses of carbon dioxide and water yields from pyrolysis of samples to be calculated from the measured peak areas. Each value was expressed as a mass percentage of the initial sample mass.

## 3.3 Results

### 3.3.1 ATR-FTIR

A representative spectrum acquired by ATR-FTIR is displayed in Figure 3.2a, spectra for all samples are presented in Appendices A.1 to A.5 and qualitative results are presented in Table 3.2. A sharp hydroxyl band was seen in bastite serpentinite, kaolinite, jarositic clay and the Kimmeridge Clay, with less prominent bands being observed in montmorillonite and the Blue Lias. The broad spectral feature associated with water of hydration and adsorbed water is observed clearly in the partially serpentinised peridotite, iron(III) sulfate, jarositic clay and JSC Mars-1, and less obviously in magnesium carbonate, bastite serpentinite, montmorillonite, palagonitic tuff, Kimmeridge Clay, siderite and the Blue Lias. Only in the iron(III) sulfate sample is the band positioned at low enough frequency to identify it conclusively as adsorbed water. Whether the source of the water response is adsorbed water or water of hydration cannot be easily determined for the other samples. Presence of the carbonate ion was clearly identified in calcium carbonate, siderite, magnesium carbonate and the Blue Lias, with a weak response in the Kimmeridge Clay. Only the Kimmeridge Clay showed clearly identifiable absorption in the 3050-2650 $cm^{-1}$ region, indicating the presence of hydrocarbons. A response in the same spectral region can be reported for the Blue Lias but with less confidence.

### 3.3.2 Single-step pyrolysis-FTIR

A representative spectrum acquired by single-step pyrolysis-FTIR is displayed in Figure 3.2b and spectra for all samples are presented in Appendices A.1 to A.5. Carbon dioxide, water, sulfur dioxide and methane responses for single-step pyrolysis-FTIR are listed in Table 3.3. Only the Kimmeridge Clay produced an organic response, with a clearly pronounced methane band at 3014 $cm^{-1}$. Carbon dioxide and water mass

yields from single-step pyrolysis-FTIR, represented as fractions of the initial sample mass, are recorded in Table 3.4.

### 3.3.3 Multi-step pyrolysis-FTIR

A representative spectrum acquired by single-step-FTIR is displayed in Figure 3.2c and spectra for all samples are presented in Appendices A.1 to A.5. Carbon dioxide, water, sulfur dioxide and methane responses for multi-step pyrolysis-FTIR are recorded in Table 3.5. Again, only the Kimmeridge Clay produced identifiable organic responses, and only at 500 °C and 750 °C. A well pronounced methane peak is visible at 3014 $cm^{-1}$ at both temperatures, but at 500 °C there are also absorption peaks at 2966 $cm^{-1}$, 2933 $cm^{-1}$ and a double peak about 2875 $cm^{-1}$, arising from the C-H stretching modes of aliphatic hydrocarbons. Carbon dioxide and water mass yields from multi-step pyrolysis-FTIR, represented as fractions of the initial sample mass, are recorded in Table 3.6.

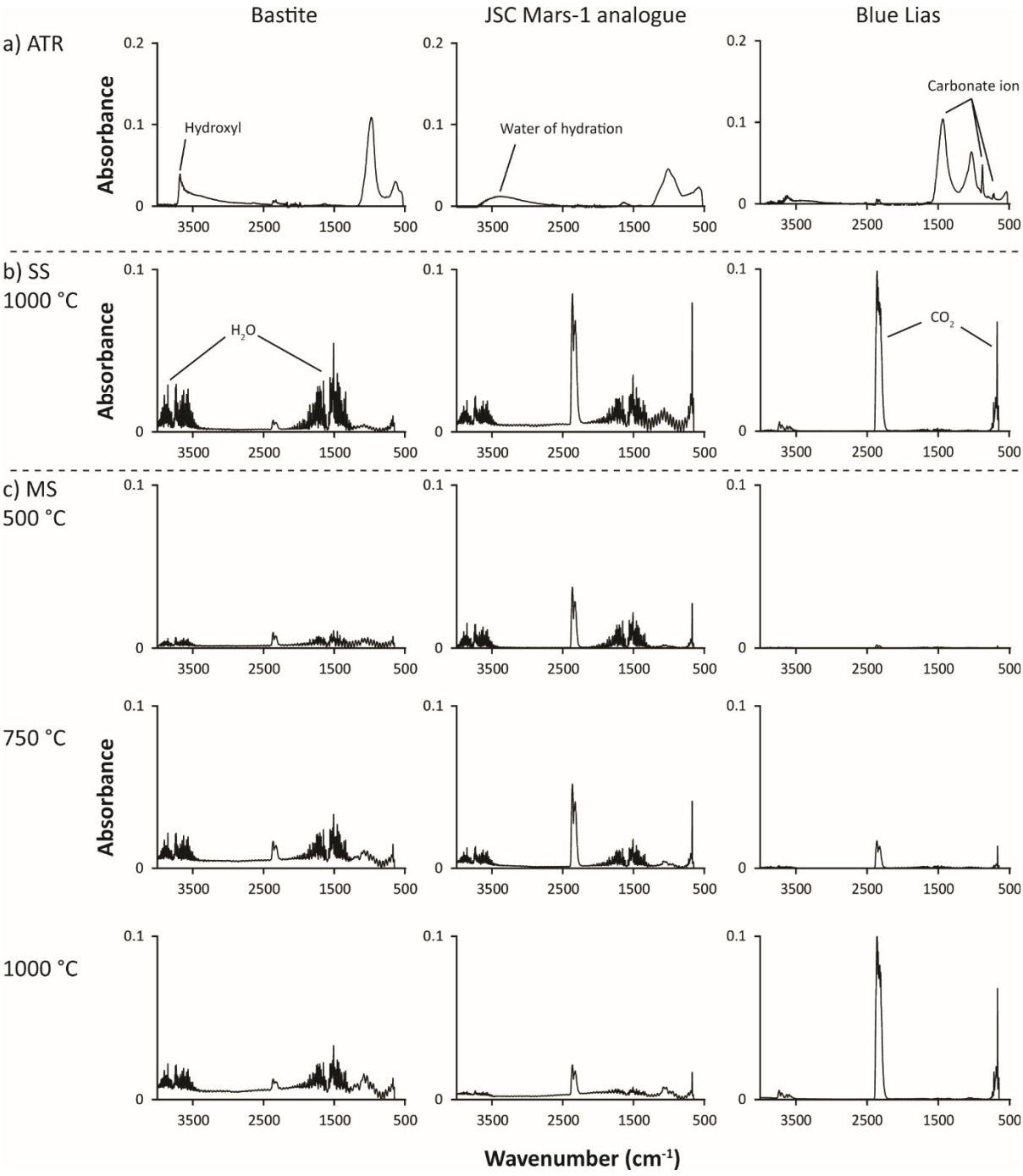



Figure 3.2. A comparison of different Fourier transform infrared spectroscopy (FTIR) analytical techniques, by showing the relevant spectra of three different materials used in the survey; bastite, JSC Mars-1 analogue and the Blue Lias. The responses in the pyrolysis methods have been scaled to they show relative responses for when materials are all of the same mass. a) Attenuated total reflectance (ATR) FTIR. Spectral features which represent habitability indicators are labelled. b) Example spectra resulting from single-step pyrolysis-FTIR of the samples at 1000 °C. The positions of spectral features characteristic to two gases of interest, carbon dioxide and water, are labelled. c) Multi-step pyrolysis-FTIR.

Table 3.2. Results of ATR-FTIR analysis. A solid circle indicates the clear presence of spectral features linked to different mineralogical habitability indicators (hydroxyl and water of hydration for hydrated minerals, the carbonate ion for carbonate bearing materials and aliphatic hydrocarbons for organic bearing materials). A solid square represents cases where the features were clearly identifiable while an unfilled square represents tentative identification.

| | Hydroxyl | Water of hydration/adsorbed water | Carbonate ion | Sulfate ion | Organic compounds |
|---|---|---|---|---|---|
| Phyllosilicates | | | | | |
| Kaolinite | ■ | | | | |
| Montmorillonite | □ | □ | | | |
| Carbonate minerals | | | | | |
| Calcium carbonate | | | ■ | | |
| Siderite | | □ | ■ | | |
| Magnesium carbonate | | □ | ■ | | |
| Sulfates and other salts | | | | | |
| Halite | | | | | |
| Iron(III) sulfate | | ■ | | ■ | |
| Gypsum | | | | ■ | |
| Unaltered and altered igneous materials | | | | | |
| Lherzolite | | | | | |
| Olivine sand | | | | | |
| Partially serpentinised peridotite | ■ | ■ | | | |
| Bastite | ■ | □ | | | |
| JSC Mars-1 analogue | | ■ | | | |
| Palagonitic tuff | | □ | | | |
| Sulfate-rich sediments | | | | | |
| Jarositic clay | ■ | ■ | | □ | |
| Organic, clay and carbonate-rich rocks | | | | | |
| Kimmeridge Clay | ■ | □ | □ | □ | ■ |
| Blue Lias | □ | □ | ■ | | □ |

Table 3.3. Qualitative results for the single-step pyrolysis-FTIR method. A solid square indicates a detection of high confidence, where the signal produced by that gas exceeded four standard deviations of the baseline noise. An empty square represents a tentative detection.

| | Carbon dioxide | Water | Sulfur dioxide | Methane |
|---|---|---|---|---|
| Phyllosilicates | | | | |
| Kaolinite | | □ | | |
| Montmorillonite | □ | □ | | |
| Carbonate minerals | | | | |
| Calcium carbonate | ■ | | | |
| Siderite | ■ | □ | | |
| Magnesium carbonate | ■ | | | |
| Sulfates and other salts | | | | |
| Halite | | | | |
| Iron(III) sulfate | □ | | ■ | |
| Gypsum | | | | |
| Unaltered and altered igneous materials | | | | |
| Lherzolite | □ | | | |
| Olivine sand | | | | |
| Partially serpentinised peridotite | | ■ | | |
| Bastite | | ■ | | |
| JSC Mars-1 analogue | ■ | ■ | | |
| Palagonitic tuff | | □ | □ | |
| Sulfate-rich sediments | | | | |
| Jarositic clay | ■ | ■ | ■ | |
| Organic, clay and carbonate-rich rocks | | | | |
| Kimmeridge Clay | ■ | ■ | □ | ■ |
| Blue Lias | ■ | ■ | | |

Table 3.4. Quantitative results for the single-step pyrolysis-FTIR method. Values show the mass of pyrolysis products as a percentage of the initial sample mass, with associated uncertainty. The mass of the pyrolysis products was calculated by measuring the peak area of a chosen spectral feature (characteristic of the gas) and referencing a mass calibration curve. Values in parenthesis do not exceed the calculated uncertainty, and thus can effectively be considered absent.

| | Carbon dioxide | Water | Sulfur Dioxide | Methane |
|---|---|---|---|---|
| Phyllosilicates | | | | |
| Kaolinite | [0.0 ± 1.0] | 12 ± 9 | [0 ± 5] | [0.0 ± 1.8] |
| Montmorillonite | [0.7 ± 0.7] | 5 ± 3 | [0 ± 2] | [0.0 ± 0.9] |
| Carbonate minerals | | | | |
| Calcium carbonate | 59 ± 14 | [1 ± 3] | [0 ± 3] | [-0.1 ± 1.1] |
| Siderite | 39 ± 3 | 1.7 ± 1.1 | [0 ± 1] | [0.0 ± 0.4] |
| Magnesium carbonate | 19 ± 3 | 3 ± 2 | [0.2 ± 1.7] | [0.1 ± 0.7] |
| Sulfates and other salts | | | | |
| Halite | [0.03 ± 0.11] | [0.2 ± 0.5] | [0.0 ± 0.4] | [-0.01 ± 0.18] |
| Iron(III) sulfate | 1.0 ± 0.7 | [3 ± 3] | 24 ± 6 | [0.3 ± 0.9] |
| Gypsum | [0.4 ± 0.5] | [0 ± 2] | [0.0 ± 1.8] | [-0.1 ± 0.8] |
| Unaltered and altered igneous materials | | | | |
| Lherzolite | 0.19 ± 0.07 | [0.1 ± 0.3] | [0.1 ± 0.3] | [0.00 ± 0.12] |
| Olivine sand | [0.07 ± 0.15] | [0.5 ± 0.7] | [0.0 ± 0.6] | [0.0 ± 0.2] |
| Partially serpentinised peridotite | [0.07 ± 0.18] | 9.7 ± 1.3 | [0.2 ± 0.7] | [0.1 ± 0.3] |
| Bastite | [0.10 ± 0.16] | 8.5 ± 1.1 | [0.1 ± 0.6] | [0.1 ± 0.3] |
| JSC Mars-1 analogue | 3.0 ± 0.7 | 4.4 ± 1.9 | [0.1 ± 1.4] | [0.1 ± 0.6] |
| Palagonitic tuff | [0.2 ± 0.2] | 2.0 ± 1.0 | [0.6 ± 0.8] | [0.1 ± 0.3] |
| Sulfate-rich sediments | | | | |
| Jarositic clay | 2.4 ± 0.3 | 6.2 ± 1.2 | 5.2 ± 1.0 | [0.1 ± 0.3] |
| Organic, clay and carbonate-rich rocks | | | | |
| Kimmeridge Clay | 2.5 ± 0.3 | 5.7 ± 1.0 | [0.6 ± 0.7] | 2.1 ± 0.4 |
| Blue Lias | 44.4 ± 1.9 | 1.3 ± 0.6 | [0.2 ± 0.5] | [0.07 ± 0.17] |

Table 3.5. Qualitative results for the multi-step pyrolysis-FTIR method. A solid circle indicates a detection of high confidence, where the signal produced by that gas exceeds four standard deviations of the baseline noise. An empty circle represents a detection of lower confidence.

| | Carbon dioxide | | | Water | | | Sulfur dioxide | | | Methane | | |
|---|---|---|---|---|---|---|---|---|---|---|---|---|
| | 500 °C | 750 °C | 1000 °C | 500 °C | 750 °C | 1000 °C | 500 °C | 750 °C | 1000 °C | 500 °C | 750 °C | 1000 °C |
| Phyllosilicates | | | | | | | | | | | | |
| Kaolinite | | | | | ■ | | | | | | | |
| Montmorillonite | | | | | | | | | | | | |
| Carbonate minerals | | | | | | | | | | | | |
| Calcium carbonate | | | ■ | | | | | | | | | |
| Siderite | ■ | ■ | | ■ | | | | | | | | |
| Magnesium carbonate | ■ | | | □ | | | | | | | | |
| Sulfates and other salts | | | | | | | | | | | | |
| Halite | | | | | | | | | | | | |
| Iron(III) sulfate | | | | ■ | | | □ | ■ | ■ | | | |
| Gypsum | | | | | | | | | | | | |
| Unaltered and altered igneous materials | | | | | | | | | | | | |
| Lherzolite | | | | | | | | | | | | |
| Olivine sand | | | | | | | | | | | | |
| Partially serpentinised peridotite | | | | □ | ■ | ■ | | | | | | |
| Bastite | | | | | ■ | ■ | | | | | | |
| JSC Mars-1 analogue | ■ | ■ | □ | ■ | ■ | | | | | | | |
| Palagonitic tuff | | □ | | □ | | | | | □ | | | |
| Sulfate-rich sediments | | | | | | | | | | | | |
| Jarositic clay | ■ | ■ | | ■ | □ | | ■ | ■ | □ | | | |
| Organic, clay and carbonate-rich rocks | | | | | | | | | | | | |
| Kimmeridge Clay | ■ | ■ | ■ | ■ | ■ | □ | | ■ | □ | ■ | ■ | |
| Blue Lias | ■ | ■ | ■ | | | | | | | | | |

Table 3.6a. Quantitative results for the multi-step pyrolysis-FTIR method. Values show the mass of pyrolysis products as a percentage of the initial sample mass, with associated uncertainty. The mass of the pyrolysis products was calculated by measuring the peak area of a chosen spectral feature (characteristic of the gas) and referencing a mass calibration curve. Values in parenthesis do not exceed the calculated uncertainty, and thus can effectively be considered absent.

| | Carbon dioxide | | | Water | | |
|---|---|---|---|---|---|---|
| | 500 °C | 750 °C | 1000 °C | 500 °C | 750 °C | 1000 °C |
| Phyllosilicates | | | | | | |
| Kaolinite | [0.2 ± 0.3] | [0.0 ± 0.3] | [-0.2 ± 0.5] | [1 ± 2] | 10 ± 5 | [2 ± 3] |
| Montmorillonite | [0.2 ± 0.3] | [0.2 ± 0.5] | [0.1 ± 0.7] | [2 ± 3] | [3 ± 4] | [2 ± 4] |
| Carbonate minerals | | | | | | |
| Calcium carbonate | [0.0 ± 0.3] | [0.5 ± 0.6] | 50 ± 13 | [0 ± 2] | [1 ± 4] | [0 ± 3] |
| Siderite | 21.9 ± 1.6 | 8.1 ± 0.8 | [0.0 ± 0.2] | 1.9 ± 0.8 | [0.2 ± 1.0] | [0.3 ± 0.9] |
| Magnesium carbonate | 16 ± 4 | [0.2 ± 0.4] | [-0.1 ± 0.6] | 4 ± 3 | [1 ± 3] | [0 ± 3] |
| Sulfates and other salts | | | | | | |
| Halite | [0.02 ± 0.03] | [0.01 ± 0.04] | [-0.02 ± 0.06] | [0.1 ± 0.2] | [0.2 ± 0.3] | [0.1 ± 0.3] |
| Iron(III) sulfate | [0.1 ± 0.2] | [0.2 ± 0.3] | [0.0 ± 0.5] | 8 ± 3 | [1 ± 2] | [0 ± 2] |
| Gypsum | [0.0 ± 0.3] | [0.2 ± 0.4] | [-0.1 ± 0.6] | [1 ± 2] | [1 ± 3] | [1 ± 3] |
| Unaltered and altered igneous materials | | | | | | |
| Lherzolite | [0.05 ± 0.10] | 0.20 ± 0.15 | [0.0 ± 0.2] | [0.0 ± 0.7] | [0.1 ± 1.1] | [0.4 ± 1.0] |
| Olivine sand | [0.02 ± 0.05] | [0.06 ± 0.08] | [-0.03 ± 0.13] | [0.0 ± 0.4] | [0.3 ± 0.6] | [0.3 ± 0.6] |
| Partially serpentinised peridotite | [0.06 ± 0.08] | 0.12 ± 0.11 | [-0.01 ± 0.18] | 0.9 ± 0.6 | 5.5 ± 1.2 | 3.6 ± 1.0 |
| Bastite | [0.06 ± 0.13] | [0.2 ± 0.2] | [0.0 ± 0.3] | [0.8 ± 1.1] | 4.5 ± 1.9 | 3.8 ± 1.8 |
| JSC Mars-1 analogue | 1.07 ± 0.16 | 1.7 ± 0.2 | 0.4 ± 0.2 | 3.6 ± 0.9 | 2.6 ± 1.1 | [0.6 ± 0.9] |
| Palagonitic tuff | [0.07 ± 0.11] | 0.21 ± 0.16 | [0.0 ± 0.2] | 1.8 ± 0.9 | [1.0 ± 1.2] | [0.4 ± 1.1] |
| Sulfate-rich sediments | | | | | | |
| Jarositic clay | 0.9 ± 0.2 | 0.9 ± 0.3 | [0.0 ± 0.3] | 4.2 ± 1.4 | 3.3 ± 1.8 | [0.5 ± 1.4] |
| Organic, clay and carbonate-rich rocks | | | | | | |
| Kimmeridge Clay | 0.66 ± 0.11 | 1.21 ± 0.17 | 2.3 ± 0.3 | 2.0 ± 0.7 | 3.9 ± 1.0 | 1.2 ± 0.8 |
| Blue Lias | 0.27 ± 0.08 | 3.3 ± 0.3 | 41 ± 2 | [0.5 ± 0.5] | 0.9 ± 0.8 | 1.7 ± 0.8 |

Table 3.6b. Quantitative results for the multi-step pyrolysis-FTIR method. Values show the mass of pyrolysis products as a percentage of the initial sample mass, with associated uncertainty. The mass of the pyrolysis products was calculated by measuring the peak area of a chosen spectral feature (characteristic of the gas) and referencing a mass calibration curve. Values in parenthesis do not exceed the calculated uncertainty, and thus can effectively be considered absent.

| | Sulfur dioxide | | | Methane | | |
|---|---|---|---|---|---|---|
| | 500 °C | 750 °C | 1000 °C | 500 °C | 750 °C | 1000 °C |
| Phyllosilicates | | | | | | |
| Kaolinite | [0.2 ± 1.3] | [-0.1 ± 0.8] | [0 ± 2] | [0.1 ± 0.3] | [0.3 ± 0.5] | [0.7 ± 1.0] |
| Montmorillonite | [0.2 ± 1.7] | [-0.1 ± 1.0] | [0 ± 3] | [0.2 ± 0.5] | [0.3 ± 0.6] | [0.9 ± 1.4] |
| Carbonate minerals | | | | | | |
| Calcium carbonate | [0.9 ± 1.8] | [0.9 ± 1.1] | [1 ± 3] | [-0.1 ± 0.4] | [0.0 ± 0.6] | [0.4 ± 1.3] |
| Siderite | [0.0 ± 0.5] | [0.0 ± 0.3] | [0.0 ± 0.8] | [0.06 ± 0.12] | [0.1 ± 0.2] | 0.3 ± 0.3 |
| Magnesium carbonate | [0.6 ± 1.5] | [0.1 ± 0.9] | [0 ± 3] | [0.1 ± 0.4] | [0.2 ± 0.5] | [0.6 ± 1.1] |
| Sulfates and other salts | | | | | | |
| Halite | [0.01 ± 0.14] | [0.00 ± 0.09] | [0.0 ± 0.3] | [0.02 ± 0.04] | [0.03 ± 0.05] | [0.08 ± 0.10] |
| Iron(III) sulfate | [1.1 ± 1.3] | 2.1 ± 1.0 | 23 ± 4 | [0.1 ± 0.3] | [-0.1 ± 0.4] | [0.4 ± 0.9] |
| Gypsum | [0.7 ± 1.5] | [0.6 ± 0.9] | [1 ± 3] | [0.0 ± 0.4] | [0.02 ± 0.52] | [0.4 ± 1.1] |
| Unaltered and altered igneous materials | | | | | | |
| Lherzolite | [0.0 ± 0.5] | [0.2 ± 0.3] | [0.5 ± 0.9] | [-0.02 ± 0.13] | [-0.05 ± 0.18] | [0.1 ± 0.4] |
| Olivine sand | [0.0 ± 0.3] | [-0.01 ± 0.18] | [0.0 ± 0.5] | [0.04 ± 0.07] | [0.1 ± 0.1] | [0.2 ± 0.2] |
| Partially serpentinised peridotite | [0.0 ± 0.4] | [0.1 ± 0.3] | [0.3 ± 0.7] | [-0.01 ± 0.10] | [0.00 ± 0.15] | [0.1 ± 0.3] |
| Bastite | [0.1 ± 0.7] | [0.3 ± 0.5] | [0.5 ± 1.3] | [-0.01 ± 0.18] | [0.0 ± 0.3] | [0.1 ± 0.5] |
| JSC Mars-1 analogue | [0.2 ± 0.5] | [0.2 ± 0.3] | [0.2 ± 0.8] | [0.01 ± 0.11] | [0.02 ± 0.16] | [0.1 ± 0.3] |
| Palagonitic tuff | [0.0 ± 0.5] | [0.3 ± 0.3] | [0.7 ± 1.0] | [0.08 ± 0.14] | 0.4 ± 0.2 | [0.3 ± 0.4] |
| Sulfate-rich sediments | | | | | | |
| Jarositic clay | 1.0 ± 0.7 | 2.9 ± 0.6 | [0.9 ± 1.3] | [-0.02 ± 0.17] | [0.1 ± 0.3] | [0.3 ± 0.5] |
| Organic, clay and carbonate-rich rocks | | | | | | |
| Kimmeridge Clay | [0.2 ± 0.4] | 0.4 ± 0.3 | [0.5 ± 0.7] | [0.09 ± 0.10] | 0.63 ± 0.15 | [0.1 ± 0.3] |
| Blue Lias | [0.2 ± 0.4] | [0.0 ± 0.2] | [0.3 ± 0.6] | [-0.01 ± 0.09] | [0.07 ± 0.12] | [0.1 ± 0.3] |

## 3.4 Discussion

### 3.4.1 ATR-FTIR

Trends can be identified in the ATR-FTIR results, such as hydroxyl being a common feature of phyllosilicate materials and the carbonate ion being easily identified in the majority of the carbonate bearing materials. Water of hydration appears in altered igneous materials while it is lacking in the unaltered examples. Organic matter is usually at least an order of magnitude lower in natural abundances than the mineral matrix, making detection by ATR-FTIR relatively difficult. However, detection of organic matter in the Kimmeridge Clay was possible.

### 3.4.2 Qualitative pyrolysis-FTIR analysis

Results show that the water signal in the single-step method discriminates between hydrated and non-hydrated mineral types. Single-step pyrolysis also produces a strong carbon dioxide signal for all carbonate materials tested. A concurrent release of water and carbon dioxide is observed for all materials bearing organic matter. Consistent with previously published work on the thermal decomposition of sulfates (Lewis et al. 2015), gypsum is the only sulfate rich material which does not produce a sulfur dioxide signal; decomposition of calcium sulfate only becomes appreciable around temperatures of 1200 °C and above (Newman 1941). The detection of methane for the Kimmeridge Clay sample shows that our single-step pyrolysis-FTIR method has the capability to detect organic matter when present in sufficient amounts.

Detection limits for gas phase FTIR equipment, when adjusted to parameters expected of a pyrolysis-FTIR instrument, are a few parts per million (Griffith 1996). Gas phase FTIR is substantially less sensitive than gas chromatography-mass spectrometer instruments, such as the Sample Analysis at Mars (SAM) instrument used on the Mars Science Laboratory (MSL) mission (Mahaffy et al. 2012), which have sensitivities at the parts per billion level. The most abundant organic compounds detected by the Mars Science Laboratory mission are chlorinated hydrocarbons which are found at levels up to several hundred parts per billion (Freissinet et al. 2015). If these data reflect indigenous organic matter, it is reasonable to

suggest that when other potential classes of organic compound are considered and when the confounding effects of perchlorate induced oxidation of organic matter (Glavin et al. 2013) are discounted, that organic matter at the level of parts per million in Mars mudstones becomes a realistic expectation.

Multi-step pyrolysis produces results that are in good agreement with those from single-step pyrolysis. Again, all carbonate materials produce a strong carbon dioxide signal. However, multi-step pyrolysis provides more diagnostic information; specific carbonates break down at different temperatures, showing that multi-step pyrolysis can discriminate between the various cations involved. The water responses of hydrated minerals from multi-step pyrolysis also provide detailed diagnostic information about mineral types, reflecting their formation conditions. Weathered materials such as JSC Mars-1 and jarositic clay produce water at low temperatures, phyllosilicates (with the exception of montmorillonite, which releases quantities of water below our chosen detection limits) produce water at the medium temperature step, while serpentinite minerals exhibit strong medium and high temperature water signals. The sulfate rich materials that were seen to produce sulfur dioxide signals in the single-step analysis are observed to produce sulfur dioxide across all temperature steps.

Although multi-step pyrolysis provides more diagnostic information than single-step pyrolysis it is associated with lower sensitivity. Whereas single-step pyrolysis combines all pyrolysis products into a single measurement multi-step pyrolysis products are spread over several analyses. The lower sensitivity of multi-step analyses is particularly evident for the Blue Lias where water is detected in the single-step method but is below the level of detection when spread across the multistep analyses. During triage operations on Mars, decisions must be made to prioritise sensitivity (single-step methods) over the acquisition of more diagnostic information (multi-step methods).

### 3.4.3 Quantitative pyrolysis-FTIR analysis

The quantitative findings for single-step pyrolysis-FTIR are in general harmony with those from qualitative analysis. Yet quantitative analysis does provide greater diagnostic potential. For example, materials from

similar origins such as the Blue Lias and the Kimmeridge Clay sedimentary rocks can be separated by the relative amounts of carbon dioxide (44 ± 2 wt% and 2.5 ± 0.3 wt% respectively). The Blue Lias contains a more substantial carbonate concentration than the Kimmeridge Clay. However, it can be the case that materials of different origins are indistinguishable through single-step quantitative analysis when only considering a small number of gases, for example jarositic clay (2.4 ± 0.4 wt% carbon dioxide, 6.2 ± 1.2 wt% water) and the Kimmeridge Clay (2.5 ± 0.3 wt% carbon dioxide, 5.7 ± 1.1 wt% water). The difficulty of discriminating between samples inevitably diminishes as more gases are examined, and an attractive feature of pyrolysis-FTIR is that information on multiple gases is provided in the same analysis, but even without additional information both samples could be considered representative of habitable conditions and are suitable for collection during a sample return mission.

The quantitative findings for multi-step pyrolysis-FTIR are concordant with those from qualitative analysis. It has been shown, in the qualitative analyses, that multi-step pyrolysis allows discrimination between rocks of generally similar types; the diagnostic potential of pyrolysis-FTIR is further enhanced when quantitative values are available. The differences between the Blue Lias and the Kimmeridge Clay that were observed in the single-step analysis are still apparent, however it is now clear that both samples release the bulk of their carbon dioxide at the higher temperature step, indicating the presence of calcium carbonate (see Table 3.6). Also as previously stated, it would be difficult to identify whether a sample is jarositic clay or Kimmeridge Clay if only single-step quantitative data was available for water and carbon dioxide. However, owing to the characteristic high temperature release of carbon dioxide from Kimmeridge Clay and low temperature release of water for jarositic clay, we are able to discern between the two samples by using the multi-step method (see Table 3.6).

### 3.4.4 Habitability assessment on Mars by pyrolysis-FTIR

Our results allow us to identify trends amongst mineral types and to construct a framework of interpretation for a pyrolysis-FTIR instrument conducting sample selection on the Martian surface. An example schema

for interpreting qualitative carbon dioxide and water signals in multi-step pyrolysis-FTIR operation is illustrated in Figure 3.3. Expanding this mechanism of analysis to incorporate quantitative analysis and additional gases enhances the identification potential of pyrolysis-FTIR.

During the early stages of any triage process the recognition of habitability (hydrated or precipitated mineral) or potential habitation (organic matter) could proceed with the relatively high sensitivity of single-step pyrolysis-FTIR. Once rocks are identified then more detailed analysis can occur by the multi-step pyrolysis-FTIR method. For habitability assessment water is produced from weathered rocks at low

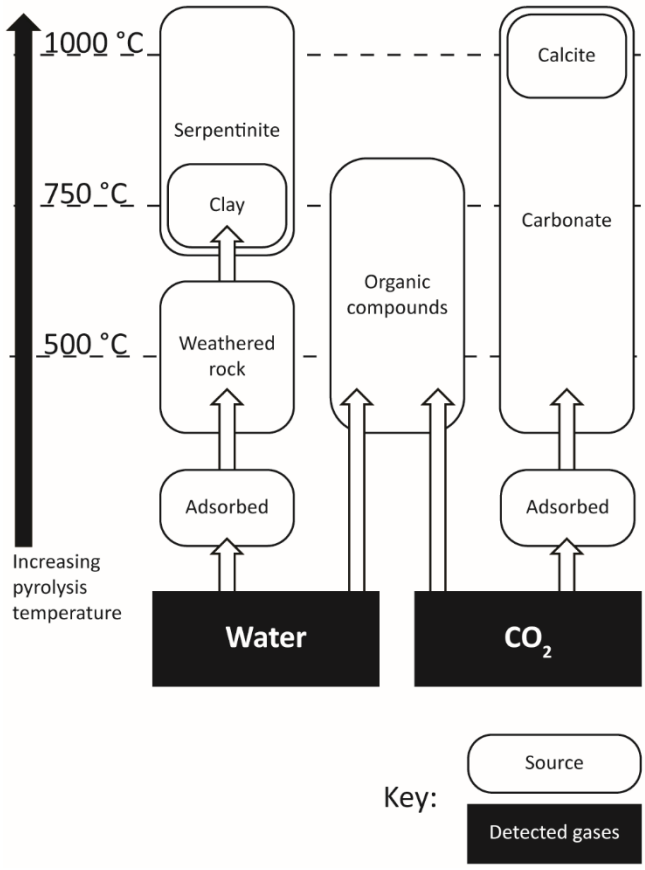



Figure 3.3. The temperatures at which gases are produced in pyrolysis-FTIR can be indicative of their source; trends observed in our survey for different mineral types allows us to construct an example framework of interpretation for multi-step pyrolysis-FTIR signals, illustrated here. During a pyrolysis-FTIR analysis program of ascending temperature steps, should any temperature step produce a gas (or combination of gases), a schema like this can be referenced to allow speculation on the source (given that adsorbed gases have been expunged at some lower temperature). The diagnostic capability of such an instrument allows a precursory determination of the scientific value of a sample, and this capability only increases as such a framework for interpretation is expanded to include additional gases, temperature steps and quantitative measurements.

temperatures, from clay minerals at medium temperatures and from serpentinites at medium and high temperatures. Carbon dioxide is produced from carbonate bearing samples across a range of temperatures (but at high temperatures for all materials containing calcium carbonate). For potential past or present habitation assessment, methane is detectable at the low and medium temperature steps and more complex organic compounds are detectable at the lower temperature step.

While our lab based version of the instrument has shown how pyrolysis-FTIR can aid sample selection, its consideration for application on Mars will be dependent on meeting the required technical limitations of a robotic surface mission instrument; specifically the weight, power and volume constraints. Encouragingly, the case for pyrolysis-FTIR is supported by previous missions where thermal extraction techniques, comparable with that used here, have been incorporated successfully.

The Viking landers, the first spacecraft to successfully land on the surface of Mars, both contained ceramic ovens which performed experiments on samples from the Chryse Planitia Region of Mars by heating them up to temperatures of 500 °C, primarily in the search for organic compounds (Biemann et al. 1976). The Phoenix lander, which reached the surface of Mars in May 2008, utilised ovens as part of the Thermal and Evolved Gas Analyzer (TEGA) instrument which could heat samples up to 1000 °C (Hoffman, Chaney and Hammack 2008). The SAM instrument on board the MSL mission employs ovens for evolved gas analysis, and can heat samples up to 1100 °C to liberate volatiles associated with mineral break-down, particularity water, carbon dioxide, sulfur dioxide (Mahaffy et al. 2012).

For the products of previous thermal extraction experiments on Mars, detection (in general) was achieved through mass spectrometer configurations. With mass spectrometry, water, carbon dioxide, sulfur dioxide and organic compounds (or the products of perchlorate oxidation and chlorination of organic compounds) have all been detected during investigations of the Martian surface. As all these gases have vibrational modes in the infrared, FTIR could be used to replace mass spectrometry for detecting thermally evolved gases as part of future instruments. Potential strategies to improve the FTIR sensitivity to levels comparable with

mass spectrometry include increasing the path length traversed through pyrolysis products in the gas cell, increasing the quantity of sample analysed, and the cumulative capture of volatiles on trapping materials from recurrent analyses followed by complete thermal desorption.

In the context of sample selection for a sample return, it is not important to perform an in-depth scientific analysis of a sample, but to survey a large number samples to identify those of greatest promise and provide high confidence in the scientific value of final candidates chosen for return to Earth. The expedience of pyrolysis-FTIR suggest that it could play a key role in sample triage on the red planet.

## 3.5 Conclusions

A pyrolysis-FTIR instrument can be used to assess the past habitability reflected by a Mars sample through the analysis of gas release. Gas release profiles of Mars samples are characteristic for certain mineral types. Important gases related to habitability that have been the target of previous space missions are detectable by FTIR, namely water, carbon dioxide and sulfur dioxide and their source materials have been shown here to have distinguishable temperature release profiles. FTIR also has a propensity for the detection of organic compounds, which could reveal potential cases of past or present habitation. The successful deployment of in situ instruments using thermal extraction technology on previous missions asserts the applicability of using pyrolysis-FTIR on Mars. Its operational attributes make it well suited for the triage phase of a Mars Sample Return mission.

# Chapter 4 Organic matter detection on Mars by pyrolysis-FTIR: an analysis of sensitivity and mineral matrix effects

Peter R. Gordon, Mark A. Sephton

*Accepted for publication in Astrobiology.*

## Abstract

Returning samples from Mars requires an effective method to assess and select the highest priority geological materials. The ideal instrument for sample triage would be simple in operation, limited in its demand for resources and rich in produced diagnostic information. Pyrolysis-FTIR is a potentially attractive triage instrument that considers both the past habitability of the sample depositional environment and the presence of organic matter which may reflect actual habitation. An important consideration for triage protocols is the sensitivity of the instrumental method. Experimental data indicate pyrolysis-FTIR sensitivities for organic matter at the tens of parts per million level. The mineral matrix in which the organic matter is hosted also has an influence on organic detection and here to provide an insight to matrix effects we simply mix well characterised organic matter with dry minerals prior to analysis. During pyrolysis-FTIR, serpentinites that may be encountered in the Phyllosian Era lead to no negative effects on organic matter detection, sulfates that may be recovered from the Theiikian Era can lead to the combustion of organic matter, and palagonites that may represent samples from the Siderikian Era can lead to the chlorination of organic matter. Any negative consequences brought about by mineral effects can be mitigated by the correct choice of thermal extraction temperature. Our results offer an improved understanding of how pyrolysis-FTIR can perform during sample triage on Mars.

## 4.1 Introduction

The search for extra-terrestrial life within our solar system, extant or otherwise, represents a major goal of astrobiology. Mars presents itself as the best candidate for contemporary life search-missions because it is the most Earth-like planet and is relatively accessible by spacecraft on reasonable timescales. Previous missions to Mars have been unable to detect evidence of past life, but their results have bolstered the case for further investigation. Evidence has accumulated which suggest that Mars was warm and wet enough during parts of its history to be habitable by life (Squyres and Kasting 1994). Remote (Mumma et al. 2009) and satellite (Formisano et al. 2004) observations have detected the presence of methane in the Martian atmosphere and results from atmospheric sampling by the Curiosity rover imply an irregular plume of methane (Webster et al. 2015). Although an abiogenic source of methane on Mars requires serious consideration, its origin from presently active biology is a remaining possibility (Court and Sephton 2009).

A future Mars Sample Return (MSR) mission would aim to utilise the unrestricted investigative potential of Earth based instrument suites to provide further insight into the question of Martian life (McLennan et al. 2012). The requirements of the MSR in situ mission phase would differ from those on previous Mars missions. MSR in situ operations would attempt to identify and cache samples that exhibit high scientific potential, rather than seeking maximum scientific return while on the Martian surface.

For the analysis of rock samples in situ on Mars, previous missions have generally employed mass spectroscopy (MS) or gas chromatography-mass spectrometry (GC-MS) instrument concepts (Viking, Beagle 2, Phoenix and Curiosity) (Hoffman et al. 2008, Klein et al. 1976, Mahaffy et al. 2009, Sims et al. 2000). GC-MS provides characterisation and quantification of molecular species and can be sensitive to low organic contents. If similar results to those provided by GC-MS can be achieved but at lower operational costs (mass, power, materials), then sample triage for MSR is facilitated and assessment of a higher number of samples is possible.

Fourier infrared spectroscopy (FTIR), which has been used on a number of space missions, provides a significant investigative return at low operational costs. FTIR is a relatively rapid and simple technique that delivers a large amount of information about the chemical nature of the analytes. To date FTIR instruments have been used on-board robotic Mars landers for remote sensing of rocks, but it has been proposed that use of FTIR could be extended to drilled samples (Anderson et al. 2005). FTIR instruments have generally lower sensitivities, when compared to GC-MS, but the fewer resource and analytical requirements make FTIR attractive for screening and caching samples for future return to Earth.

A pyrolysis-FTIR instrument has been proposed to fulfil the role of triage for a Mars Sample Return mission (Sephton et al. 2013). Pyrolysis-FTIR involves heating solid samples rapidly (up to 20,000 °C $s^{-1}$) to liberate gaseous products which are subsequently characterised and quantified though infrared transmission spectra. A pyrolysis-FTIR instrument can comfortably meet the weight, power and structural requirements of a mission landed on the Martian surface, as the primary components involved have all been successfully used on a number of in situ missions. For example, pyrolysis ovens were used on the Mars Science Laboratory (MSL) mission (Mahaffy 2008) and remote scanning FTIR spectrometers were employed on the Mars Exploration Rover (MER) mission (Christensen et al. 2003).

A sample should only be considered high priority for biosignature detection if it is known to come from a habitable environment. It has been demonstrated that pyrolysis-FTIR can provide diagnostic insight into the mineralogy of samples through which past habitability can be assessed (Gordon and Sephton 2016b). Hydrated and evaporite minerals reveal past aqueous conditions which are vital for habitability, and these can be identified by the temperature release profiles of gases in pyrolysis-FTIR analyses. The temperature at which water is liberated from a sample indicates the nature of the rock, with higher temperatures required to liberate the mineral bound hydroxyl of serpentinites than the temperatures required for the release of adsorbed water from weathered materials. Carbonates, which mostly form in regions chemically and

energetically favourable for life, are generally detectable through strong carbon dioxide signals from pyrolysis-FTIR analysis.

Once past habitability is established, the preservation potential for biosignatures must be considered. The stability of any biosignature is dependent on its initial form, the matrix in which it is hosted and the chemical and physical processes it is subjected to over time. Some of the most favourable host rocks are those rich in clay minerals and carbonates. It has been shown that pyrolysis-FTIR can be successful in detecting clay rich sediments and carbonates (Gordon and Sephton 2016b), which based on evidence from Earth's geological record can maintain fossils for up to $3.5 \times 10^8$ years. Sulfates, also detectable by pyrolysis-FTIR through the production of sulfur dioxide, can offer fossil stabilities for timescales of up $1 \times 10^6$ years (Farmer and Des Marais 1999). Thus the preservation potential of biosignatures can be inferred through pyrolysis-FTIR results.

Because entirely abiotic mechanisms are able to form morphologies similar to the biosynthetic structures of early Earth organisms organic compound detection is required before a case for life can be conclusively made (Cady et al. 2003). Organic compounds produce distinctive signals in the infrared region and gas phase FTIR currently offers sensitivities on the order of a few parts per million (ppm). To-date, the detection of organic compounds on the surface of Mars has proven difficult. The most abundant organic compounds detected were found at a few parts per billion (ppb) in the Sheepbed Mudstone at Gale Crater by MSL (Freissinet et al. 2015). The detection of organic molecules by a pyrolysis-FTIR instrument at concentrations of a few ppm or above would indicate conditions conducive to the creation and preservation of organic matter. Any sample rich in organic matter would be of high scientific value thus such a discovery during triage would be enough to select it for return to Earth.

This study aims to characterise the ability of a pyrolysis-FTIR instrument to detect organic matter in Mars samples. An assessment of various concentrations of organic matter in a mineral matrix provides information on the sensitivity limits of the instrument, while a survey of comparable concentrations across

a number of Mars relevant minerals aims to provide information on the effects of mineral matrices on the detection of organic matter.

## 4.2 Methods

### 4.2.1 Sample selection

This study required a suitable test biomaterial and a range of appropriate mineral matrices. *Lycopodium* spores powder, made from the dry spores of clubmosses, is manageable for mixing with powdered minerals and is available in commercially processed quantities, providing some guarantee of reproducibility. Although the spores are the product of organisms more highly evolved than anything likely to have existed on Mars, they represent a well-characterised organic assemblage.

Characterisation of the response of this biomaterial allows comparison between modes of pyrolysis-FTIR operation and serves as a reference point for mineral effects. To achieve this, a mixture of quartz sand (U.S. Silica F-110) and high purity silica powder (Sigma Aldrich) was produced at a ratio of 3:1, hereafter just referred to as 'quartz', which allowed effective mixing and suspension of the *Lycopodium* spores.

The choice of other mineral matrices was informed by the predominant eras of mineral alteration on Mars, as identified by (Bibring et al. 2006); a serpentinite was chosen to represent the Phyllosian, a jarositic clay was selected for the Theiikian and two palagonites (altered basaltic glass) were chosen for the Siderikian. Details of the materials used in this study are listed in Table 4.1.

All minerals were powdered and *Lycopodium* spores were then added and the total weight monitored through iterative mass measurements on a balance accurate to 0.1 mg, to produce a 5% mixture by mass (an organic matter concentration typical of topsoils on Earth, thus chosen as a 'best case' scenario starting point). Subsequent lower concentrations of 1% and 0.5% were produced, each made from a dilution of the former mixture. In the case of quartz, further mixtures were made for the purpose of sensitivity appraisal, from 0.45% to 0.05% (in 0.05% steps) and one at 0.02%. Each mixture was stored in a screw

Table 4.1. Materials used in study.

| Role | Name | Source | Details |
|---|---|---|---|
| Biomaterial | *Lycopodium* | Sigma Aldrich | |
| Inert substrate | Quartz | Sigma Aldrich/U.S. Silica | A mixture of three parts F-110 U.S. Silica quartz sand and one part high purity silicon oxide powder from Sigma Aldrich. |
| Phyllosian analogue | Serpentinite | Partially serpentinised peridotite, Kennack Sands, Cornwall, UK | *Lower-Mid Devonian*<br>Regions on Mars which exhibit the minerals that characterise the Phyllosian era serve as the best candidates for past habitation. |
| Theiikian analogue | Jarositic clay | Parkstone Clay Member, Brownsea Island, Dorset, UK | *Eocene*<br>Pyrite exposed to present day atmosphere oxidises to jarosite, a sulfur rich mineral. Similar hydrated sulphates present on Mars are used to define the Theiikian era. |
| Siderikian analogue | Palagonitic tuff | Madeira, Portugal | *Pleistocene*<br>Contains chlorinated phases. Chlorinated compounds influence the production of organic species during pyrolysis. |
| | JSC Mars-1 | Pu'u Nene, Hawaii | *Holocene*<br>Well documented Martian regolith simulant developed by NASA's Johnson Space Center (Allen and others 1998). |

capped vial and mixed manually for 5 minutes, to ensure homogeneity. It is recognised that the simple mixing process is not wholly representative of the juxtaposition and chemical bonding of organic matter and minerals that have undergone co-deposition and diagenesis but it is hoped that the *Lycopodium* spores-mineral mixtures adequately reflect the thermally-induced processes experienced during the analysis of natural samples. Using powdered samples emulates the form of drilled samples delivered to pyrolysis chambers on current and past Mars rovers.

### 4.2.2 Pyrolysis-FTIR

Samples were loaded in quantities of approximately 15 mg into quartz tubes and held in place by quartz wool plugs at either end. Pyrolysis was achieved using a CDS Analytical Pyroprobe 5200 and the FTIR spectra were collected using a Thermo Scientific Nicolet 5700 FTIR spectrometer. Gases resulting from pyrolysis were contained within a CDS Brill Cell fitted with IR transparent ZnSe windows. This gastight

chamber was supplied with a controllable helium flow, used to maintain an oxygen free atmosphere during analysis and to purge the cell of any spent analytes. Both pyrolysis and FTIR operations were controlled by CDS 5000 DCI software and Thermo Scientific OMNIC Series software respectively, the latter also being used to record and process spectra. Each session of sample analysis was preceded by collection of three or more spectra from procedural blanks. Unless otherwise stated, sample spectra are composed of 32 scans taken over 19.5 s at a resolution of 4 $cm^{-1}$, collected immediately after the pyrolysis probe had ceased firing.

### 4.2.3 Sensitivity appraisal

To conduct the sensitivity appraisal, the optimal pyrolysis temperature for maximum signal response from *Lycopodium* spores was identified. First, pure quantities of *Lycopodium* spores were subjected to various heating rates and the IR responses for organic structures were recorded as a function of time. These initial investigations were then corroborated with data from a stepped analysis. The acquired data indicated that most *Lycopodium* spores break down below or at 700 °C. To test *Lycopodium* spore performance in a mixture and to examine the influence of continued probe heating on the pyrolysis products, samples of 5% *Lycopodium* spores in quartz were subjected to a range of static temperatures and the IR responses of the products measured over a 30 s period. The data showed that an analysis at 700 °C and for 7.2 s produced the greatest yield of organic products and this pyrolysis mode was used for all samples unless stated otherwise.

For a statistical investigation of sensitivity of pyrolysis-FTIR, a large number of data were required. A different number of data points were obtained for the various concentrations of *Lycopodium* spores studied: for 0.02%, 0.05% and 0.10% (30 data points); for 0.15%, 0.20% and 0.25% (15 data points); and for 0.30%, 0.35%, 0.40%, 0.45% and 0.50% (3 data points).

Using the OMNIC Software Suite, each sample spectrum was reduced by subtracting the average spectrum of procedural blanks conducted during the relevant data collection session. Spectra were then truncated, leaving the 3300 to 2650 $cm^{-1}$ wavenumber region, and the baseline corrected to provide a baseline against

which the total area under peaks in the C-H stretching region (3150 – 2740 $cm^{-1}$) was recorded. Taking the total area in a relatively wide section of the frequency domain, rather than targeting specific peaks, allows for blanket detection of molecular structures containing C-H bonds. The signal produced by this method is hereafter referred to as the 'hydrocarbon response'.

From sample mass measurements, the quantity of *Lycopodium* spores in each sample was ascertained and plotted against the associated hydrocarbon response. A sensitivity analysis was performed using the hydrocarbon responses. Results were grouped based on the mass of *Lycopodium* spores present in the sample ($m$), with limits chosen so that there was an adequate number of samples ($n$) in each grouping. The following limits were used: 1 µg ≤ $m$ but < 5 µg ($n$ = 30), 5 µg ≤ $m$ but < 10 µg ($n$ = 29), 10 µg ≤ $m$ but < 15 µg ($n$ = 23), 15 µg ≤ $m$ but < 25 µg ($n$ = 29), $m$ ≥ 25 µg ($n$ = 39).

Sensitivity of the instrument (i.e. the ability for the instrument to make a correct detection of organic matter) was investigated by calculating the rate of true positive detections as the detection threshold varies, defined as follows:

$$sensitivity = \frac{number\ of\ true\ positives}{number\ of\ true\ positives + number\ of\ false\ negatives}$$

A result was deemed positive if the hydrocarbon response equalled or exceeded a chosen detection threshold, which in this case was multiples of the baseline fluctuation of the instrument (measured by taking the standard deviation of signals, in the same hydrocarbon response region, obtained from 35 procedural blanks).

Measurements of the hydrocarbon response from 15 pure quartz samples was used to investigate the specificity of the instrument, defined as:

$$specificity = \frac{number\ of\ true\ negatives}{number\ of\ true\ negatives + number\ of\ false\ positives}$$

Where a true negative would be a pure quartz sample producing a signal in the hydrocarbon region lower than the detection threshold (as described for sensitivity).

Values from both sensitivity and specificity investigations were plotted as a function of multiples of the same measure of the baseline fluctuation.

### 4.2.4 Assessment of mineral matrix effects

To assess the effects of minerals on pyrolysis-FTIR organic matter responses, two temperatures were used: 700 °C which recorded the optimal yield of hydrocarbons established by experimentation, and 1000 °C which was determined to be a temperature that leads to high sensitivity detection for mineral indicators of habitability (Gordon and Sephton 2016b). Three concentrations of the mineral-*Lycopodium* spore mixture were analysed for each mineral type (5%, 1% and 0.5%) in addition to the pure mineral (i.e. 0%). Each sample type was subjected to three repeat analyses.

Using the OMNIC Software Suite, spectra were truncated to a 4000 $cm^{-1}$ to 1250 $cm^{-1}$ wavenumber region, then baseline corrected. Peak intensities were then measured and recorded; one located at 2349 $cm^{-1}$ corresponding to the anti-symmetric stretch in carbon dioxide, one at 3853 $cm^{-1}$ arising from a stretching mode of water, one at 1352 $cm^{-1}$ corresponding to the sulfur dioxide anti-symmetric stretching mode, one at 3016 $cm^{-1}$ corresponding to the methane anti-symmetric stretching mode and the height of a peak at 2933 $cm^{-1}$, present and dominant when pure *Lycopodium* spore samples are pyrolysed, to account for the broad hydrocarbon signal in the 3150 $cm^{-1}$ to 2740 $cm^{-1}$ region.

Note that, if present, hydrogen chloride produces a fringe which overlaps the 3016 $cm^{-1}$ peak used to measure the methane response. To overcome this overlapping issue, a reference spectrum for hydrogen chloride was obtained from the NIST database and subtracted from the sample spectra found to contain a hydrogen chloride signal, thereby allowing measurement of any methane peak. When applicable, the relative intensity of the 2798 $cm^{-1}$ peak of hydrogen chloride was measured to account semi-quantitatively

for the amount of hydrogen chloride produced. Table 4.2 lists the spectral features utilised in this study and their wavenumbers.

Table 4.2. Spectral features analysed in pyrolysis-FTIR spectra to measure abundances of gas species of interest.

| Species | Vibrational mode | Wavenumber ($cm^{-1}$) |
|---|---|---|
| Carbon dioxide | Antisymmetric stretching | 2349 |
| Water | Stretching | 3853 |
| Sulfur dioxide | Antisymmetric stretching | 1361 |
| Methane | Antisymmetric stretching | 3015 |
| Organic compounds | C-H stretching | 3150 - 2740 |
| Hydrogen chloride | Stretching | 2798 |

Once peak intensities in the samples were recorded, the equivalent responses taken from blanks (averaged for the relevant collection session) were subtracted and the resulting values were averaged for each set of samples (i.e. the three repetitions of each sample type were averaged). The resulting averaged peak values for carbon dioxide, water, sulfur dioxide and methane could be translated to quantified masses by reference to mass calibration curves, and in turn the values for masses of gas could be expressed as percentages of the mass of mineral in each sample. Expressing masses of gas relative to the mineral component allowed direct comparison of results across all concentrations.

## 4.3 Results

### 4.3.1 Sensitivity appraisal

The correlation between the amount of *Lycopodium* spores present in a sample and the measured hydrocarbon response during pyrolysis-FTIR analysis is plotted in Figure 4.1. The responses were produced by taking the total area under overlapping absorbance peaks in the 3180 – 2680 $cm^{-1}$ wavenumber region. The data points were used to produce a best-fit trend line shown in Figure 4.1. A quadratic relationship described by the function $A = 2\times10^{-5}m^2 + 0.0011m + 0.0008$ with a coefficient of determination of 0.9301 (95% confidence interval given by the limits $A = 2\times10^{-5}m^2 + 0.0007m - 0.007$ and $A = 2\times10^{-5}m^2 + 0.0016m + 0.009$), where $A$ is the relative absorbance and $m$ is the mass of *Lycopodium* spores, was found to represent all the samples with < 200 µg *Lycopodium* spores.

This modelled the behaviour of the instrument for amounts of *Lycopodium* spores < 200 µg, including the completeness of *Lycopodium* spore conversion to detectable compounds by pyrolysis, the efficiency of pyrolysate delivery to the gas containment cell and its residence time within, and the performance of the beam and detector system. In effect, Figure 4.1 acts as a calibration curve and the strength of any detected absorbance signal area in the hydrocarbon region less than 1 can be referenced with the curve to determine the mass of organic material pyrolysed.

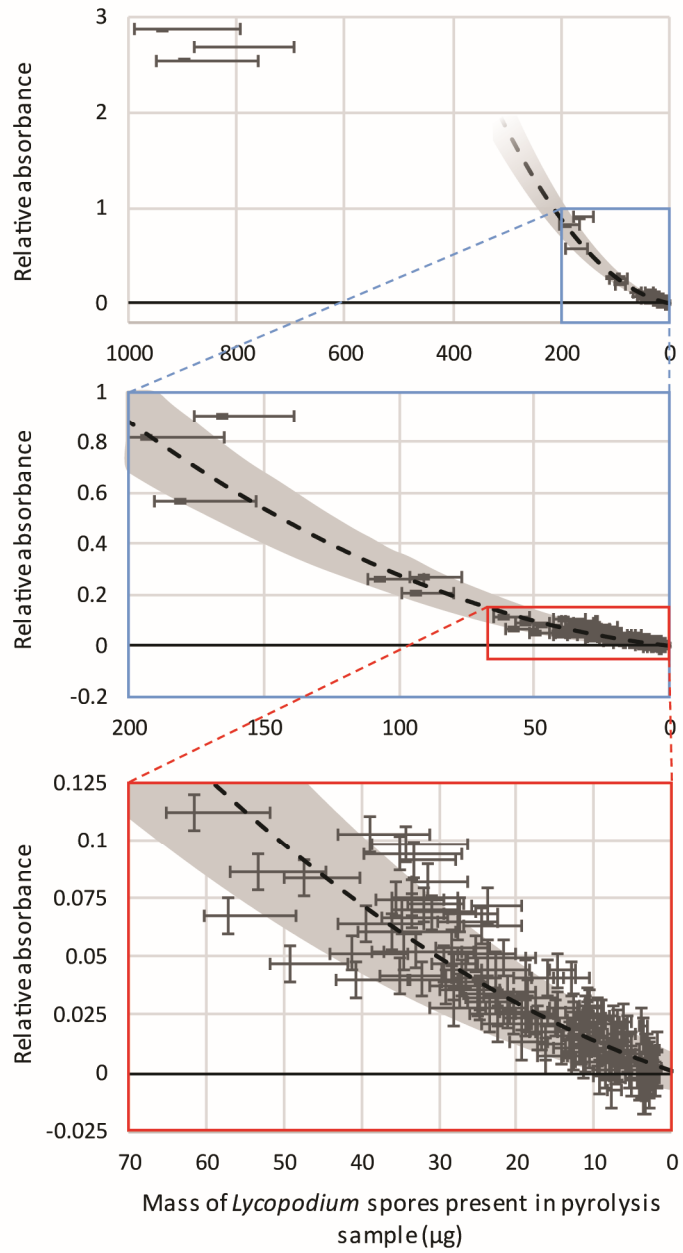



Figure 4.1. Absorbance (measured by taking the total area under the combined peaks) in the hydrocarbon stretching region (3150 – 2740 $cm^{-1}$) plotted as a function of the quantity of *Lycopodium* spores present in the sample. All samples were subjected to 700 °C for 7.2 s before the evolved gases were measured by FTIR. For this study quartz was used to provide an inert substrate. Vertical error bars represent one standard deviation of the data produced by procedural blanks, while horizontal error bars arise from the uncertainty in mass measurements, with additional consideration made for *Lycopodium* spore loss during sample handling (10% of expected mass) on the lower uncertainty boundary. The dashed trend line represents a best-fit quadratic function for data points with *Lycopodium* spore mass < 200 µg, which is numerically represented as $A = 2\times10^{-5}m^2 + 0.0011m + 0.0008$ with a coefficient of determination of 0.9301, where $A$ is the relative absorbance and $m$ is the mass of *Lycopodium* spores (95% confidence bounds are illustrated by they area shaded grey). Three high concentration samples, with *Lycopodium* spore masses > 800 µg, do not adhere to this law and is likely due to saturation effects. It is interesting to note that the vertical intercept of 0.0008 is almost equal to the mean signal given by pure quartz samples of 0.0009 (i.e. when *Lycopodium* spore mass is zero).

It should be noted that the quadratic best-fit function only holds true for amounts of *Lycopodium* spores that are < 200 µg. The three 5% samples, which had *Lycopodium* spore quantities of >200 µg and which did not follow the quadratic best-fit function for lower concentrations most likely reflect saturation effects within the sampling gas cell owing to the large quantity of *Lycopodium* spores analysed. Such saturation effects are relatively unimportant for this study because of the focus on low sensitivity behaviour. In Figure 4.1 it is apparent that the spread of data points lacks a certain degree of closeness to the trend line and this is likely derived from uncertainty in the amount of *Lycopodium* spores present in the sample. *Lycopodium* spores readily become airborne, as a consequence of their evolutionary design. Hence, *Lycopodium* spore losses might be expected during the sequential mixing steps and pyrolysis sample preparation and, unfortunately, such losses could not be recorded easily. As a result detection limits determined by this study were nominal and serve as an upper boundary to the true limits (i.e. they are a worst case scenario).

The results of the sensitivity assessment are plotted in Figure 4.2 where data points represent the probability of detection when an amount of *Lycopodium* spores is present in a given range. It can be seen that the data exhibit relationships where the sensitivity decreases as an increased detection threshold is imposed. The relationships between detection threshold and sensitivity have been identified to resemble cumulative probability functions, and these have been approximated with cumulative logistic distribution functions, given by:

$$S(t) = \frac{1}{1 + e^{s\left(t - t_{1/2}\right)}}$$

Where $S$ is the probability of making a positive organic compound detection (sensitivity), $t$ is the detection threshold, $t_{1/2}$ is the threshold value which gives $S = 0.5$ and $s$ is a scaling parameter. The values for these parameters are listed for the different groupings of *Lycopodium* spore quantities in Table 4.3 and the relationships have been illustrated by solid lines in Figure 4.2.

Table 4.3. Parameters for cumulative logistic probability functions used to model the results of the sensitivity investigation. Using the relationship $S(t) = [1 + e^{s\left(t - t_{1/2}\right)}]^{-1}$, the probability of making a positive organic compound detection (or sensitivity $S$) can be calculated for a given detection threshold $t$, where $t_{1/2}$ is the threshold value which gives $S = 0.5$ and $s$ is a scaling parameter. $n$ is the number of samples used to make each grouping.

| | $n$ | $t_{1/2}$ | $s$ | $R^2$ |
|---|---|---|---|---|
| $m$ >= 25 | 39 | - | - | - |
| 25 > $m$ >= 15 | 29 | 4.44 | 0.85 | 0.47 |
| 15 > $m$ >= 10 | 23 | 2.52 | 1.13 | 0.85 |
| 10 > $m$ >= 5 | 29 | 1.13 | 1.14 | 0.83 |
| 5 > $m$ >= 1 | 30 | -0.15 | 1.35 | 0.91 |

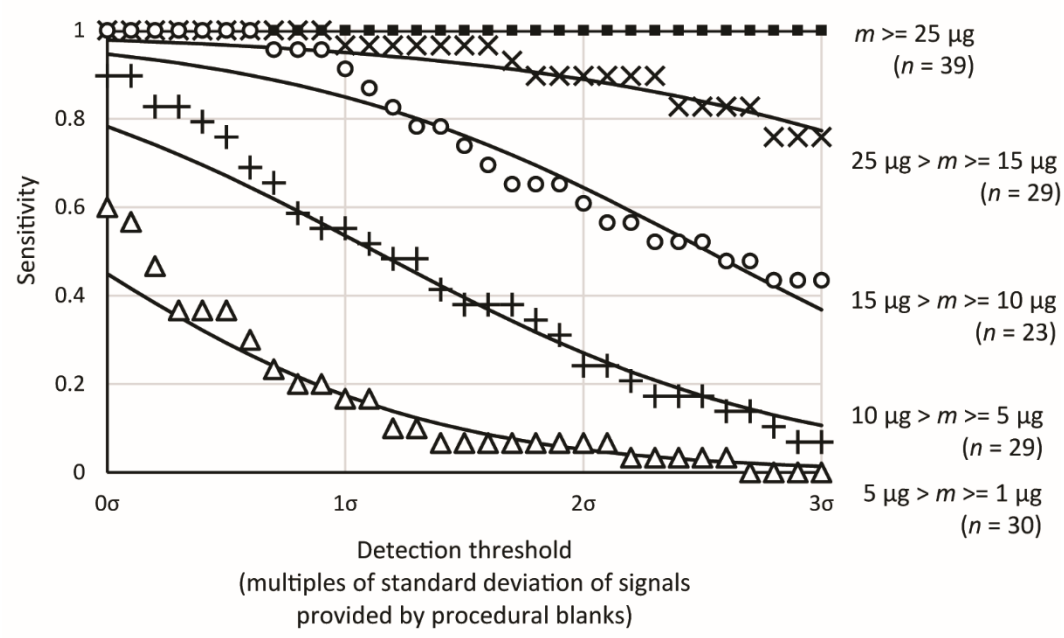



Figure 4.2. For a chosen detection threshold, there is a probability that pyrolysis-FTIR will make a detection given *Lycopodium* spores are present in sufficient quantities. This figure shows how this probability (sensitivity) varies as a function of the chosen detection limit (multiples of the standard deviation obtained from responses in blanks) for a range of concentrations of *Lycopodium* spores-quartz mixture. The solid lines represent best-fit cumulative probability functions, which have be superimposed upon data points calculated from measurements.

If a limit of 2σ is considered significant and set as a requirement for detected signals, then the data suggests that only amounts of *Lycopodium* spores > 25 µg will guarantee detection and the probability of detecting an amount of *Lycopodium* spores < 5 µg is ≈ 5%.

The specificity was also investigated. Figure 4.3 shows the probability of a pyrolysis-FTIR analysis that would not produce a false positive as the required detection threshold was increased. The measured results were modelled with a cumulative logistic distribution as was done with the sensitivity data, with the parameters $s = -4.73$ and $t_{1/2} = 0.33$ (plotted as a solid line in Figure 4.3 and had a coefficient of determination of 0.97). The results showed that the likelihood of a false detection was virtually zero if a detection limit of > 1σ was imposed. Reconciling this finding with the results of the sensitivity assessment, the probabilities of detection at 1σ for 15 mg samples containing *Lycopodium* spores are ≈ 17% for amounts 1 µg ≤ *m* but < 5 µg, ≈ 56% for amounts 5 µg ≤ *m* but < 10 µg, ≈ 86% for amounts 10 µg ≤ *m* but < 15 µg, ≈ 94% for amounts 15 µg ≤ *m* but < 25 µg, and 100% for amounts *m* ≥ 25 µg.

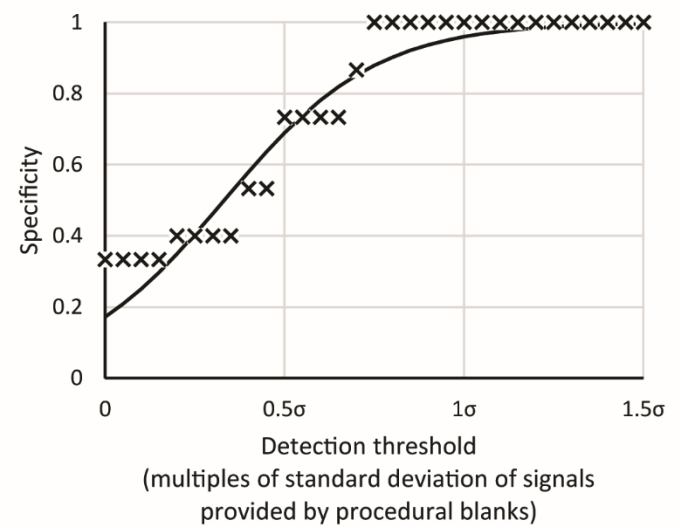



Figure 4.3. Specificity (also known as the true negative rate) of pyrolysis-FTIR organic compound detection as a function of detection threshold. The plot suggests that false positives are unlikely when a detection threshold greater than approximately one standard deviation of the baseline fluctuation is chosen.

### 4.3.2 Mineral matrix effects

A pyrolysis-FTIR spectrum of pure *Lycopodium* spores is shown in Figure 4.4. Representative spectra (formed from the average of three individual samples) of mineral and *Lycopodium* spore mixtures are displayed in Figure 4.5a and Figure 4.5b. These spectra have been colour coded to show where the presence of *Lycopodium* spores in a mineral matrix produces a greater (black) or lesser (red) response for particular gases when compared to an analysis of just the pure mineral. Quantitative data for the responses of carbon dioxide, water, sulfur dioxide and methane are presented in Table 4.4 and Table 4.5 (as percentages of the initial sample mass for pure minerals, and differences owing to *Lycopodium* spores in mixtures as a percentage of the mineral component mass). Table 4.6 lists the relative intensities of absorbance in the wavenumber region associated with hydrocarbons, providing a semi-quantitative record of the organic matter pyrolysis products.

In all cases, the production of hydrocarbons was evident with a few notable exceptions; jarositic clay and the palagonitic tuff appeared to produce no hydrocarbons at the 0.5% concentration at both 700 °C and 1000 °C, and produced no hydrocarbons at the 1.0% concentration at 1000 °C. For jarositic clay and the palagonites the production of hydrocarbons at 700 °C was only tentatively observed.

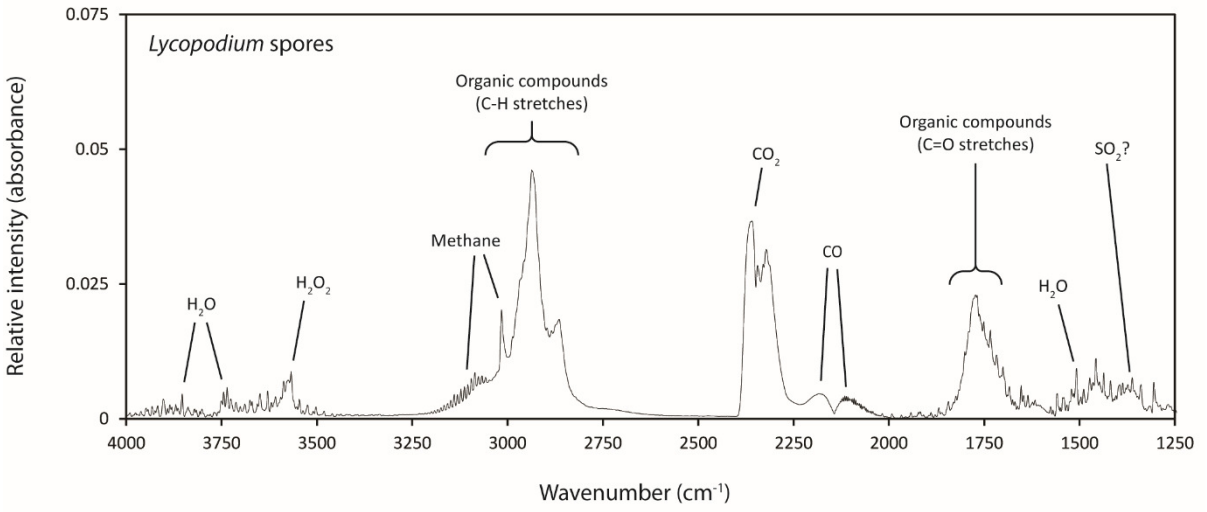



Figure 4.4. Pyrolysis-FTIR spectrum of pure *Lycopodium* spore powder with prominent features of interest labelled (pyrolysed at 750 °C).

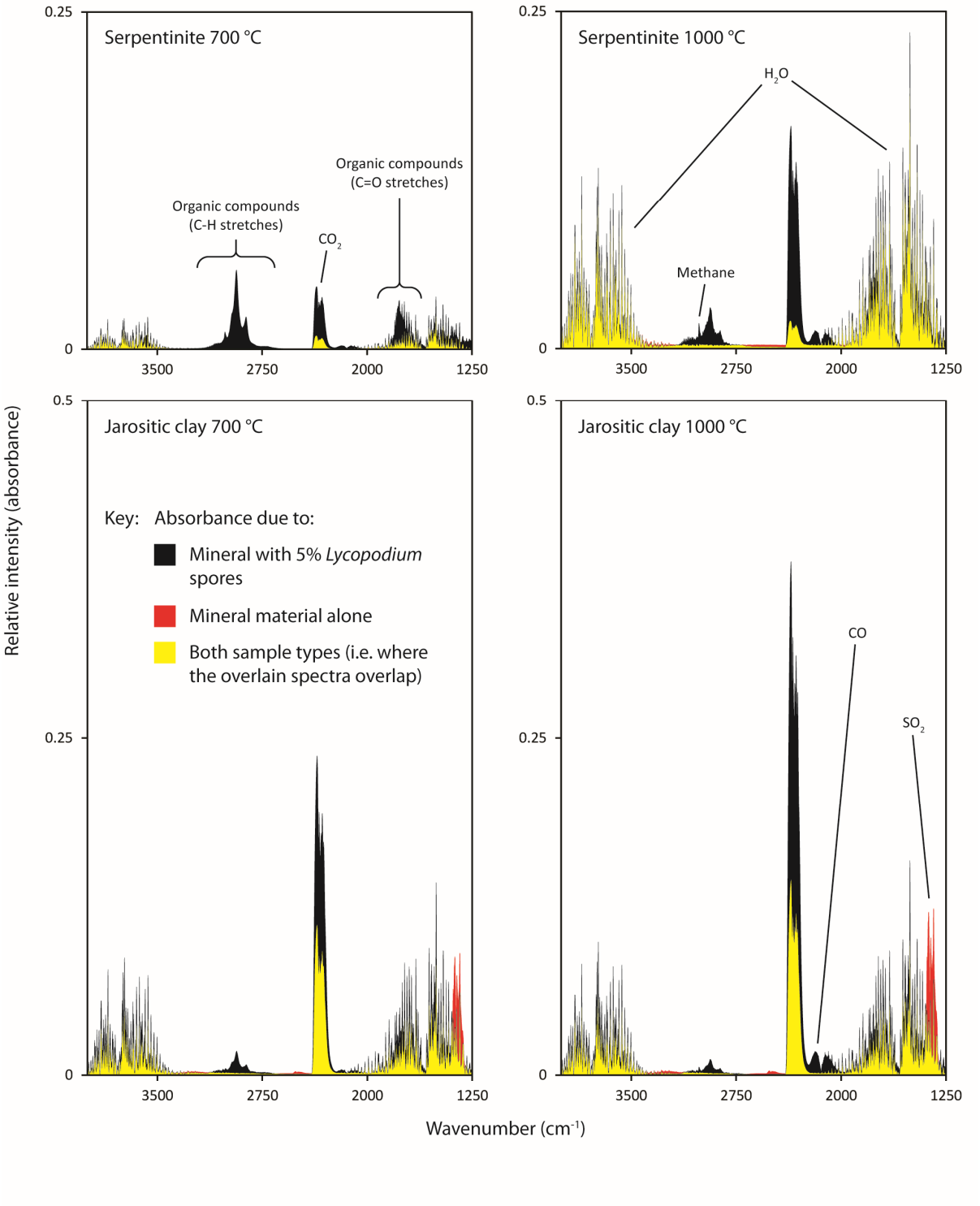



Figure 4.5a. Representative pyrolysis-FTIR results from serpentinite and jarositic clay, where the results of using the unadulterated mineral have been overlain with spectra produced by a mixture containing 5% *Lycopodium* spores. Results have been scaled to represent a scenario where the quantity of mineral is equal in each case. The spectral features which are indicative of different gases are labelled. Colour coding highlights where the presence of *Lycopodium* produces a surplus of a gas (black) or a deficit (red) when compared to the mineral material alone, and where the two spectra overlap (yellow).

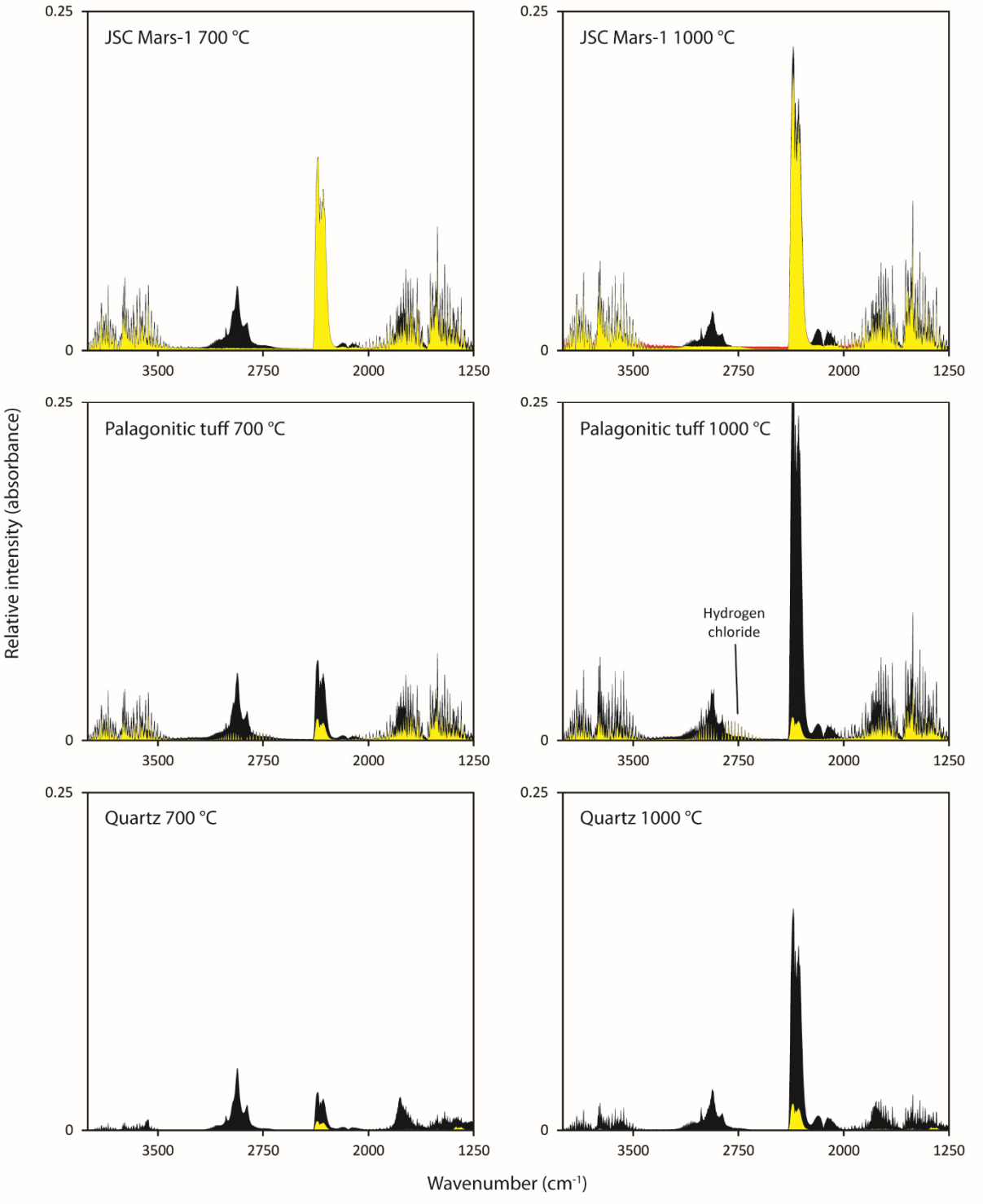



Figure 4.5b. Representative pyrolysis-FTIR results from JSC Mars-1, palagonitic tuff and quartz, where the results of using the unadulterated mineral have been overlain with spectra produced by a mixture containing 5% *Lycopodium* spores. Results have been scaled to represent a scenario where the quantity of mineral is equal in each case. The spectral features which are indicative of different gases are labelled. Colour coding highlights where the presence of *Lycopodium* produces a surplus of a gas (black) or a deficit (red) when compared to the mineral material alone, and where the two spectra overlap (yellow).

Table 4.4. Results from pyrolysis-FTIR survey at 700 °C, showing quantities of gases produced from pure minerals and the differences produced when *Lycopodium* spores are introduced. In bold are the results of the pure mineral forms with gas masses expressed as percentages of the initial sample mass. Listed below are the mass differences between the gases produced by the mineral-*Lycopodium* spore mixtures and the pure mineral form, expressed as percentages of the mass of the mineral component in the sample. Three concentrations (5.0%, 1.0% and 0.5%) of mineral-*Lycopodium* spore mixture were analysed for each mineral.

| | | wt% | | | |
|---|---|---|---|---|---|
| | | $CO_2$ | Water | $SO_2$ | Methane |
| Quartz | | **0.058 ± 0.018** | **0.072 ± 0.015** | **0.043 ± 0.013** | **0.00085 ± 0.00016** |
| | 5.0% | 0.20 ± 0.06 | 0.34 ± 0.09 | 0.00 ± 0.02 | 0.041 ± 0.006 |
| | 1.0% | 0.21 ± 0.06 | 0.16 ± 0.06 | 0.00 ± 0.02 | 0.010 ± 0.003 |
| | 0.5% | 0.16 ± 0.06 | 0.10 ± 0.04 | 0.005 ± 0.019 | 0.0023 ± 0.0008 |
| Serpentinite | | **0.083 ± 0.013** | **1.18 ± 0.15** | **-0.006 ± 0.0009** | **0.0001 ± 0.0002** |
| | 5.0% | 0.35 ± 0.09 | 0.5 ± 0.5 | 0.043 ± 0.006 | 0.048 ± 0.007 |
| | 1.0% | 0.32 ± 0.10 | 0.30 ± 0.4 | 0.0110 ± 0.0019 | 0.0090 ± 0.0011 |
| | 0.5% | 0.22 ± 0.08 | 0.0 ± 0.5 | 0.0055 ± 0.0013 | 0.0040 ± 0.0007 |
| Jarositic clay | | **1.2 ± 0.2** | **4.0 ± 0.6** | **1.4 ± 0.4** | **-0.0022 ± 0.0005** |
| | 5.0% | 1.9 ± 0.6 | 3.2 ± 1.5 | -1.3 ± 0.4 | 0.0047 ± 0.0011 |
| | 1.0% | 1.4 ± 0.6 | 0.7 ± 1.2 | -0.7 ± 0.5 | 0.0006 ± 0.0008 |
| | 0.5% | 0.8 ± 0.6 | 0.5 ± 1.2 | -0.3 ± 0.6 | 0.0006 ± 0.0009 |
| Palagonitic tuff | | **0.14 ± 0.02** | **1.7 ± 0.2** | **0.009 ± 0.002** | **0.004 ± 0.002** |
| | 5.0% | 0.42 ± 0.16 | 1.3 ± 0.9 | 0.042 ± 0.012 | 0.027 ± 0.008 |
| | 1.0% | 0.18 ± 0.08 | 0.5 ± 0.6 | 0.031 ± 0.011 | -0.002 ± 0.003 |
| | 0.5% | 0.22 ± 0.11 | 0.3 ± 0.6 | 0.050 ± 0.014 | -0.003 ± 0.003 |
| JSC Mars-1 | | **1.6 ± 0.3** | **3.0 ± 0.5** | **-0.009 ± 0.003** | **0.0029 ± 0.0007** |
| | 5.0% | 0.0 ± 0.7 | 1.1 ± 1.6 | 0.035 ± 0.012 | 0.045 ± 0.014 |
| | 1.0% | 0.3 ± 0.8 | 0.8 ± 1.5 | 0.005 ± 0.006 | 0.010 ± 0.004 |
| | 0.5% | 0.0 ± 1.0 | 0 ± 2 | -0.003 ± 0.011 | 0.004 ± 0.004 |

Table 4.5. Results from pyrolysis-FTIR survey at 1000 °C, showing quantities of gases produced from pure minerals and the differences produced when *Lycopodium* spores are introduced. In bold are the results of the pure mineral forms with gas masses expressed as percentages of the initial sample mass. Listed below are the mass differences between the gases produced by the mineral-*Lycopodium* spore mixtures and the pure mineral form, expressed as a percentage of the mass of the mineral component in the sample. Three concentrations (5.0%, 1.0% and 0.5%) of mineral-*Lycopodium* spore mixture were analysed for each mineral.

| | | wt% | | | |
|---|---|---|---|---|---|
| | | $CO_2$ | Water | $SO_2$ | Methane |
| Quartz | | **0.18 ± 0.03** | **0.063 ± 0.019** | **0.036 ± 0.014** | **-0.0002 ± 0.0002** |
| | 5.0% | 1.7 ± 0.9 | 1.1 ± 0.3 | 0.00 ± 0.03 | 0.090 ± 0.019 |
| | 1.0% | 0.8 ± 0.2 | 0.38 ± 0.10 | -0.015 ± 0.019 | 0.016 ± 0.003 |
| | 0.5% | 0.45 ± 0.17 | 0.21 ± 0.06 | -0.01 ± 0.02 | 0.008 ± 0.002 |
| Serpentinite | | **0.17 ± 0.03** | **12 ± 2** | **-0.062 ± 0.010** | **-0.0037 ± 0.0011** |
| | 5.0% | 1.8 ± 1.0 | 2 ± 5 | 0.026 ± 0.017 | 0.094 ± 0.018 |
| | 1.0% | 1.0 ± 0.4 | -4 ± 6 | 0.03 ± 0.03 | 0.016 ± 0.004 |
| | 0.5% | 0.41 ± 0.19 | -5 ± 6 | 0.03 ± 0.03 | 0.010 ± 0.004 |
| Jarositic clay | | **1.68 ± 0.17** | **4.8 ± 0.5** | **2.0 ± 0.2** | **-0.0022 ± 0.0004** |
| | 5.0% | 4.3 ± 1.4 | 2.9 ± 1.7 | -2.0 ± 0.2 | 0.023 ± 0.007 |
| | 1.0% | 2.4 ± 1.1 | 0.5 ± 1.4 | -1.2 ± 0.3 | 0.0003 ± 0.0009 |
| | 0.5% | 1.5 ± 0.6 | 0.6 ± 1.2 | -0.1 ± 0.4 | -0.0004 ± 0.0008 |
| Palagonitic tuff | | **0.15 ± 0.05** | **1.7 ± 0.3** | **0.057 ± 0.018** | **0.0008 ± 0.0007** |
| | 5.0% | 3.9 ± 1.6 | 2.7 ± 1.6 | 0.03 ± 0.04 | 0.08 ± 0.03 |
| | 1.0% | 1.5 ± 0.5 | 0.9 ± 1.0 | 0.04 ± 0.05 | 0.004 ± 0.002 |
| | 0.5% | 1.29 ± 0.38 | 0.5 ± 0.8 | 0.07 ± 0.06 | 0.0014 ± 0.0014 |
| JSC Mars-1 | | **2.6 ± 0.6** | **3.5 ± 0.8** | **0.0005 ± 0.0019** | **0.0029 ± 0.0013** |
| | 5.0% | 0.3 ± 1.2 | 1 ± 2 | 0.011 ± 0.009 | 0.07 ± 0.02 |
| | 1.0% | -0.0 ± 1.2 | 0.3 ± 1.7 | -0.010 ± 0.004 | 0.010 ± 0.004 |
| | 0.5% | -0.1 ± 1.6 | 0 ± 2 | -0.011 ± 0.008 | 0.004 ± 0.005 |

Table 4.6. Relative strengths of hydrocarbon responses for different concentrations of *Lycopodium* spore-mineral mixtures and mineral samples free of *Lycopodium* spores (highlighted in bold) from pyrolysis-FTIR analyses. In this case, the response due to hydrocarbons is semi-quantitatively represented by the height of the dominant peak at the 2933 $cm^{-1}$ wavenumber, found in the region strongly associated with the C-H stretches organic compounds. Two temperatures of pyrolysis are compared, 700 °C and 1000 °C.

| | | Relative absorbance | |
|---|---|---|---|
| | | 700 °C | 1000 °C |
| Quartz | | **0.00005 ± 0.00001** | **-0.00009 ± 0.00002** |
| | 5.0% | 0.0448 ± 0.0018 | 0.029 ± 0.004 |
| | 1.0% | 0.0112 ± 0.0017 | 0.0051 ± 0.0003 |
| | 0.5% | 0.0034 ± 0.0003 | 0.00203 ± 0.00019 |
| Serpentinite | | **0.00004 ± 0.00001** | **0.000030 ± 0.000020** |
| | 5.0% | 0.0572 ± 0.0015 | 0.0278 ± 0.0009 |
| | 1.0% | 0.0102 ± 0.0005 | 0.0039 ± 0.0007 |
| | 0.5% | 0.0030 ± 0.0008 | 0.00124 ± 0.00012 |
| Jarositic clay | | **-0.00027 ± 0.00005** | **-0.00059 ± 0.00006** |
| | 5.0% | 0.0162 ± 0.0009 | 0.0107 ± 0.0009 |
| | 1.0% | 0.00011 ± 0.00004 | -0.000056 ± 0.000010 |
| | 0.5% | -0.00015 ± 0.00007 | -0.00026 ± 0.00003 |
| Palagonitic tuff | | **0.00023 ± 0.00008** | **-0.000066 ± 0.000024** |
| | 5.0% | 0.048 ± 0.004 | 0.0326 ± 0.0017 |
| | 1.0% | 0.00316 ± 0.00003 | 0.00080 ± 0.00006 |
| | 0.5% | 0.00097 ± 0.00004 | 0.00006 ± 0.00003 |
| JSC Mars-1 | | **0.00026 ± 0.00004** | **0.00001 ± 0.00007** |
| | 5.0% | 0.045 ± 0.003 | 0.027 ± 0.003 |
| | 1.0% | 0.0033 ± 0.0003 | 0.001630 ± 0.000014 |
| | 0.5% | 0.00131 ± 0.00016 | 0.00071 ± 0.00008 |

In the following discussion the term 'mixtures' refers to the mineral in question where some quantity of *Lycopodium* spores have been added.

#### *4.3.2.1 Lycopodium spores (no minerals)*

The pure *Lycopodium* spores could be seen to produce a range of gases (Figure 4.4). A significant amount of organic compounds were produced and was evidenced by the strong, broad, overlapping C-H stretching features at 2863 $cm^{-1}$ and 2937 $cm^{-1}$, the methane peak at 3015 $cm^{-1}$ and the strong broad carbonyl group feature centred at 1776 $cm^{-1}$. Water and carbon dioxide were also produced, mainly as products of combustion although some water was inherent in the natural constitution of the spores (up to 15% by weight, according to the manufacturer's description) which will be liberated by pyrolysis. Production of carbon monoxide was further evidence of combustion and the presence of hydrogen peroxide was noted as a potential source of oxidation. *Lycopodium* spores produced a small feature at the region known for sulfur dioxide, but as this region was also shared with features characteristic of a number of organic functional groups (e.g. alkane –C-H bending) and as the other organic features were so dominant it was difficult to ascribe this feature conclusively to sulfur dioxide.

#### *4.3.2.2 Quartz*

Quartz was shown, through pyrolysis of its pure form, to be a good inert substance against which other minerals could be compared. Only small contributions of carbon dioxide (comparable to that present in procedural blanks) and sulfur dioxide (approximately 450 ppm by weight) were measurable following pyrolysis of pure quartz. The carbon dioxide could be attributed to adsorbed species while the sulfur dioxide arose from suspected impurities in the quartz sand. Thus the quartz mixtures can give good insights into the flash pyrolysis breakdown of *Lycopodium* spores when suspended in a mineral matrix where the mineral influence has little or no chemical effect. Quartz mixtures however will still emulate the thermal and physical effects of other mineral matrices, thus offering a better standard material to enable comparisons than using pure *Lycopodium* spores.

For quartz and 5.0 % *Lycopodium* spore mixtures at 700 °C responses were highly comparable to those for the pure *Lycopodium* spores and even at the lowest concentration, all the *Lycopodium* spore indicators described in the previous section (and illustrated in Figure 4.4) were present, further confirming quartz as a suitable inert material.

#### *4.3.2.3 Serpentinite*

Pure serpentinite produced significant quantities of water upon pyrolysis. The water contribution was vastly increased at the higher 1000 °C temperature step (shown clearly in Figure 4.5a). The contribution of carbon dioxide was comparable to that seen in the pure quartz samples and thus was not introduced by the addition of serpentinite.

For the serpentine mixtures, methane results were in very close agreement with those seen for the quartz mixtures. For example at 1000 °C, the *Lycopodium* spores in serpentinite produced 0.090 ± 0.019 wt%, 0.016 ± 0.003 wt% and 0.0078 ± 0.0019 wt% methane at 5.0%, 1.0% and 0.5% concentrations of *Lycopodium* spores respectively, while the equivalent quartz mixtures produced 0.090 ± 0.017 wt%, 0.013 ± 0.003 wt% and 0.006 ± 0.003 wt% methane. The relative absorbance strengths in the hydrocarbon region were also concordant with those seen in the quartz mixtures (Table 4.6).

Thus the *Lycopodium* spores did not undergo any additional organic compound degradation relative to that observed in the quartz mixtures and hence the contribution of carbon dioxide from *Lycopodium* spores in serpentinite matches that produced by *Lycopodium* spores in quartz. Any variation in water released from *Lycopodium* spores in the presence of serpentinite was overwhelmed by the substantial signal from water released from serpentinite itself.

#### *4.3.2.4 Jarositic clay*

Pure jarositic clay showed a substantial release of carbon dioxide, water and sulfur dioxide at both temperatures, with the 700 °C step producing these gases at approximately 70 - 80% of the quantities produced at 1000 °C. The jarositic clay response was dramatically different to the serpentinite response,

where the pyrolysis of the latter at 700 °C only liberated approximately 10% of the water produced at 1000 °C. It was apparent that water was more readily released from the jarositic clay when subjected to pyrolysis-FTIR analysis. Weathered materials such as jarositic clay contain significant amounts of water and produce stronger water signals at lower temperatures than materials which are predominantly formed by the products of hydrothermal metamorphism represented by serpentinites.

When *Lycopodium* spores were introduced, a sharp drop in the sulfur dioxide signal was evident, and the reduced response corresponded to the quantity of *Lycopodium* spores present. Simultaneously, there was a sharp increase in the responses of water and carbon dioxide, and a reduction in hydrocarbon responses. It was clear that sulfur dioxide, produced from the sulphate content of the jarositic clay, was assisting the combustion of *Lycopodium* spore pyrolysis products by acting as a source of oxygen gas. The issue of sulphate compounds hindering the thermally-assisted detection of organic matter on Mars has been recently highlighted (Lewis et al. 2015). The production of sulfuric acid also presents another destruction mechanism for hydrocarbons, however the spectral features of sulfuric acid vapour (Hintze et al. 2003) were not readily discernible in the spectra of pure jarositic clay as they coexist in regions obscured by the rotational-vibrational fringes of water.

At lower concentrations of *Lycopodium* spores in jarositic clay, both 0.5% and 1.0%, the hydrocarbon signal could be seen to disappear entirely for both 700 °C and 1000 °C temperature steps. However, the strength of carbon dioxide, water and sulfur dioxide signals relay information on the quantity of *Lycopodium* spores initially present. It could be observed that at *Lycopodium* spore concentrations of 0.5% and 1.0% the extent to which the 1352 $cm^{-1}$ sulfur dioxide peak diminished related to the quantity of spores present. The sulfur dioxide signal from the 0.5% *Lycopodium* spores in jarositic clay appeared to be slightly lower than for pure jarositic clay (although the decrease did not exceed the margins of error). The sulfur dioxide signal was measurably diminished (approximately 40% and 60% of the pure jarositic clay sulfur dioxide signal at 700 °C and 1000 °C respectively) when the *Lycopodium* spore concentration was increased to 1.0%. For

the 5.0% *Lycopodium* spores in jarositic clay, both 700 °C and 1000 °C results showed that the sulfur dioxide peak was lost, suggesting that the entire budget of sulfur dioxide had been exhausted before the complete oxidative destruction of *Lycopodium* spore pyrolysis products could occur.

#### *4.3.2.5 Palagonitic tuff*

Pure palagonitic tuff produced similar quantities of water at both 700 °C and 1000 °C, suggesting the form of hydration was different to that for pure serpentinite which generated more water at 1000 °C than it did at 700 °C. At 700 °C the carbon dioxide produced from palagonitic tuff was higher than observed for pure quartz at the same temperature. However, the carbon dioxide signal in pure palagonitic tuff at 1000 °C was comparable with that observed for pure quartz. The release of carbon dioxide at the lower temperature (700 °C) was probably related to the liberation of adsorbed gas. The ability of palagonite to readily adsorb carbon dioxide has been recognised previously in Mars related studies (Zent, Fanale and Postawko 1987).

Considering gases which are attributed to the presence of added *Lycopodium* spores, the palagonitic tuff mixtures produced only slightly increased amounts of carbon dioxide and water than seen for the equivalent quartz mixtures at 700 °C. The quantities of carbon dioxide and water produced by the palagonitic tuff mixtures were significantly greater than the quartz mixtures at 1000 °C. This suggested that a mechanism was present at 1000 °C that was not substantial in its effects at 700°C and may be related to pre-existing natural weathering products in the palagonite (Eggleton, Foudoulis and Varkevisser 1987) which were accessed by pyrolysis at high temperatures.

The hydrogen chloride, peaks observed in the pure palagonitic tuff, were diminished following the addition of *Lycopodium* spores (Table 4.7). Aside from the 5.0% samples and 1000 °C temperature experiment, it was evident that the more *Lycopodium* spores present, the greater the reduction in the hydrogen chloride signal. Thermally assisted chlorination of *Lycopodium* spore organic matter is a plausible explanation for the features observed. It should be noted that proposals of organic matter chlorination during thermal

extraction of Mars samples is currently attributed to perchlorate minerals (Glavin and others 2013) but now palagonite may also be recognised as a contributor to chlorination reactions.

Table 4.7. Relative absorbance responses for hydrogen chloride produced from the pure palagonitic tuff and palagonitic tuff mixtures with *Lycopodium* spores.

| *Lycopodium* spore concentration | 700 °C | 1000 °C |
|---|---|---|
| 0.0% | 0.00581 ± 0.00010 | 0.0140 ± 0.0002 |
| 5.0% | 0.0027 ± 0.0003 | 0.0109 ± 0.0004 |
| 1.0% | 0.0033 ± 0.0003 | 0.0098 ± 0.0003 |
| 0.5% | 0.0040 ± 0.0005 | 0.0107 ± 0.0011 |

#### *4.3.2.6 JSC Mars-1*

Figure 4.5b shows that pure JSC Mars-1 acted as a source of carbon dioxide and water and that the production of these gases increased with temperature. In mixtures of *Lycopodium* spores and JSC Mars-1 the detected levels of organic compounds, methane and carbon monoxide were comparable with levels for the same pyrolysis products in the quartz mixture experiments (see Figure 4.5b), suggesting that *Lycopodium* spores were undergoing the same degradation processes in both mineral matrices (i.e. JSC Mars-1 had no chemical influence on hydrocarbon degradation during pyrolysis-FTIR analyses). But unlike the case for quartz, the introduction of *Lycopodium* spores to JSC Mars-1 did not result in an increase in water and carbon dioxide at either 700 °C or 1000 °C. As a palagonitic tuff, JSC Mars-1 is a basaltic material that is highly susceptible to weathering by water and carbon dioxide mixtures (Eggleton and others 1987). Such weathering-type processes may be initiated and accelerated during thermal processing in the presence of water and carbon dioxide leading to the reaction of these gases with the palagonitic minerals and their loss from the gas phase pyrolysis products, at least at 700 °C.

## 4.4 Discussion

For the assessment of past habitability reflected by a sample a pyrolysis-FTIR method that provides the greatest sensitivity and the most diagnostic information is desired. A range of pyrolysis methods can be

chosen but for the temperatures examined in this study the highest temperature (1000 °C) produces the greatest response while a multistep approach is most diagnostic and during operation a choice must be made on the priorities for acquisition of either information type (Gordon and Sephton 2016b).

For the detection of an organic matter-containing sample on Mars, a pyrolysis-FTIR procedure that has the best possible sensitivity is preferred. A range of pyrolysis temperatures are available but for the temperatures examined in this study the lowest temperature (700 °C) produces the greatest organic matter response (Table 6). However, pyrolysis-FTIR analysis at 1000 °C is more sensitive to the common simple organic degradation products, namely methane, carbon dioxide and water.

Figure 4.1 and the results of the sensitivity and specificity assessments convey that the instrument in its current form only guarantees detection of total organic contents greater than 15 μg, and for a typical pyrolysis-FTIR sample mass of 10 mg, this equates to 1.5 parts per thousand, a value significantly higher than required for effective triage on Mars. For instance, MSL was tasked with finding organic matter in rocks at a few ppb (Mahaffy and others 2012). MSL uses approximately 0.078 $cm^3$ of powdered sample in its pyrolysis quartz cup when conducting evolved gas analysis (Mahaffy and others 2012). Taking a plausible density of 3 $g/cm^3$ for a serpentinite, and using MSL equivalent sample sizes for the pyrolysis-FTIR system, a detection limit of around 65 ppm is indicated for pyrolysis-FTIR. Extending this reasoning to the lower quantities of organic matter assessed which did not completely guarantee detection, pyrolysis-FTIR has a ≈ 89% probability of identifying Mars samples with organic matter in the 64 to 43 ppm range, ≈ 56% in the 43 to 22 ppm range and ≈ 17% in the 21 to 4 ppm range.

The juxtaposition of organic matter and minerals during pyrolysis leads the transformation (e.g. chlorination) and destruction (e.g. combustion) of organic matter thereby hindering its direct detection. Again, the choice of temperature plays an important role in limiting the obfuscating effects of minerals when attempting to detect organic signals. The lower pyrolysis temperatures promote fewer mineral induced reactions that the higher pyrolysis temperatures.

Mineral effects are inevitably dependent on the mineral present during pyrolysis and analytical windows can be found where organic detection becomes possible. In the case of palagonitic tuff, where significantly less hydrogen chloride is produced at 700 °C than at 1000 °C, the detection of hydrocarbons is possible at the 1.0% concentration for the lower temperature. The results from jarositic clay shows that sulfate bearing minerals pose a significant threat to the detection of organic compounds by thermal extraction methods, undermining the relatively good preservation potential associated with sulfates. In the case of serpentinite, the mineral poses no real threat to the detection of organic material by thermal extraction methods, other than by masking the water signal produced by combusted hydrocarbons. Regions on Mars defined by relative abundances of hydrated minerals, like serpentinites, present the best locations for MSR sample acquisition.

Even for minerals that induce complete combustion of any organic matter present, the amount and temperature of release for carbon dioxide provides important information (Sephton et al. 2014). Carbon dioxide is readily detectable by FTIR and can be recognised at a few ppm or less for pyrolysis-FTIR. Thus any Mars rock sample subjected to pyrolysis-FTIR that produces a strong carbon dioxide signal in a temperature range consistent with organic matter combustion and with no obvious mineral sources of this gas could be considered high priority for biosignature detection and selected for return to Earth.

## 4.5 Conclusions

Pyrolysis-FTIR is an information dense method for Mars sample triage. At the limit where a pyrolysis-FTIR instrument is unlikely to produce false positives, organic compounds could be detected directly in quantities on the order of tens of parts per million. In common with other thermal extraction based methods, organic compounds are susceptible to mineral effects during pyrolysis-FTIR. Inevitably the particular type of mineral matrix determines whether organic compound transformation takes place. Chlorine and sulfur bearing minerals pose a threat to organic pyrolysis products, although the recognition of degradation products provides another avenue for detection. The iron sulphate jarosite which is present

on Mars leads to the oxidation of organic products during pyrolysis. Palagonite is also common on the red planet and can be added to the list of minerals which chlorinate organic compounds during thermal extraction. Selection of pyrolysis temperature is an important aspect where lower temperatures limit the release of potential destructive agents from the host mineral matrix while also conserving the range of organic compound products.

# Chapter 5 Pyrolysis-FTIR survey of an acid stream ecosystem and its implications for sample triage during Mars Sample Return

Peter R. Gordon, Mark A. Sephton

*In preparation for publication.*

## Abstract

Pyrolysis-FTIR can be employed as a triage instrument for Mars Sample Return. The technique can thermally dissociate minerals and organic matter and determine the past habitability of the depositional environment and the presence of organic matter that may suggest past habitation. The Theiikian of Mars represents an attractive target for life search missions and the acquisition of samples for return to Earth. The acidic and increasingly dry Theiikian may have been habitable and followed a lengthy neutral and wet period in Mars history during which life could have originated and proliferated to achieve relatively abundant levels of biomass and a wide distribution. The sulphate minerals produced in the Theiikian are also known to be good preservers of organic matter. We have used pyrolysis-FTIR and a sample set from an acidic sulphate stream which contained a thriving ecosystem to test the triage concept. Pyrolysis-FTIR identifies those samples with the greatest probability of habitability and habitation and our data interpretation methods provide a mechanism to rank samples and identify those that should take the highest priority for return to Earth.

## 5.1 Introduction

Attempts to discover whether life exists or has previously existed on Mars have not yet been conclusive. To seek greater certainty when reading the rock record of habitability and habitation on Mars, mission concepts are being proposed that involve the return of samples to Earth. Once on the Earth, samples of Mars can be distributed to multiple laboratories that host the most powerful analytical techniques available. The probability of successfully obtaining conclusive evidence of past or present life on Mars is inevitably influenced by the choice of sample to be returned to Earth. Consequently, attention is now being directed towards methods that triage the range of possible sampling opportunities on Mars to effectively select a few highest-priority samples.

Environments on Mars known to be historically wet are the primary locations for life searches. Wet environments may still be found on present day Mars. Recurring slope lineae, an observed phenomenon on Mars, are possibly a result of water flows (Ojha et al. 2015). Fluvial environments may have persisted beyond the loss of majority surface water. Subsurface water reservoirs may have produced outflows in the late Hesperian (Rodríguez et al. 2010) and in the Amazonian (Fassett et al. 2010) and evidence for vast present day subsurface reservoirs has been presented (Bramson et al. 2015). Yet the evidence for wet conditions on Mars is overwhelmingly present in rocks that represent the early history of the red planet.

If life emerged on Mars, then this event most likely occurred in the Phyllosian era when wet and neutral conditions were prevalent and conditions were most similar to those on the present day Earth. It is reasonable to consider that any Phyllosian life would have persisted for the remainder of the Era and experienced the transition to the Theiikian Era when wet and neutral settings were replaced with wet and acidic environments. It is also logical to assume that by the beginning of the Theiikian any life that originated in the Phyllosian would have evolved and proliferated to achieve the greatest possible abundance of biomass and widest distribution. The Early Theiikian biomass would have been available for preservation in the Martian rock record. The acidic conditions in the Theiikian led to the widespread deposition of

sulphate minerals. Sulfate-rich environments are known to sustain life and offer high potential for organic matter (Farmer and Des Marais 1999)

Developing triage methods for use on Mars is hindered by the lack of readily accessible Mars samples. No samples have been returned from Mars by space missions and meteorites from Mars are precious and present in only small amounts. Testing of Mars triage methods must therefore rely on the use of analogue sites and samples. Mineralogical samples such as the glassy volcanic ash JSC Mars-1 allow the testing of equipment destined for use on the basalt-rich Mars surface. Astrobiology studies seek out Mars-like conditions such as dry areas such as the Atacama Desert or cold environments such as the Antarctic dry valleys. Yet, the analogues most relevant to the early Theiikian are those in highly acidic settings such as Rio Tinto, Spain.

One instrument that has been proposed for triage on Mars is pyrolysis-FTIR (Sephton et al. 2013). Pyrolysis-FTIR offers the features that make it suitable for triage, namely its relatively simple operation, its limited demand for resources and its production of richly diagnostic information. During pyrolysis-FTIR samples are rapidly heated (up to 20,000 °C $s^{-1}$) to produce volatiles that are subsequently detected and characterised by infrared spectroscopy. Pyrolysis-FTIR has been demonstrated to provide diagnostic information on the mineralogy of samples and therefore past habitability (Gordon and Sephton 2016b). Pyrolysis-FTIR has also been utilized to provide insights into the probability of the presence of biosignatures (Gordon and Sephton 2016a).

In this paper we apply pyrolysis-FTIR to a Mars analogue sample set. Ferrous sulfate-rich streams are found on the southern coast of the UK where oxidation of sedimentary pyrite produces acidic waters. The sulphate-rich stream supports a vibrant ecosystem of acid-tolerant species and provides an effective analogue for the Theiikian of Mars. We use the sulphate ecosystem samples and pyrolysis-FTIR to emulation the sample triage and selection process as could be operated on Mars. Our findings suggest an effective method for choosing those samples which would provide the highest possibility of success when returned to earth for life detection analyses.

## 5.2 Methods

### 5.2.1 Sample selection

Samples were obtained from two acidic, ferrous sulfate-rich streams located in Dorset, Southern England; one flowing and one dry. The collected sample set is listed in Table 5.1 and lists data on mineral characterisation obtained by X-ray diffraction (XRD) and the maximum potential gas products each sample can produce from mineral sources based on stoichiometry. The majority of samples collected came from the flowing stream, which was located at St. Oswald's Bay, while the dry stream was to the east of St Oswald's Bay, in a small cove known as Stair Hole. Oxidation of pyrite, abundant in the Wealden Beds from which the St. Oswald's Bay stream flows, gives the water an acidity of pH 3.5 and jarosite depositions accrue as result of ferrous sulfate-rich waters. The dry stream at Stair Hole was less acidic, with a pH level of 5. Lateral variations across the steam section are significant. Where water volumes and/or pH increase, jarosite is converted to goethite and where the stream is relatively dry a jarosite-containing quartz sand occurs. The goethite is covered by a purple microbial mat and the deepest parts of the stream contain acidophilic algae. Stream samples were obtained as cores before being freeze died and crushed in preparation for analysis. Before pyrolysis-FTIR analysis the samples were characterised through X-ray diffraction and lipid analysis.

### 5.2.2 Attenuated total reflectance-FTIR

All sulfate stream samples were analysed using a Thermo Nicolet 5700 FT-IR spectrometer fitted with an attenuated total reflectance (ATR) Thermo Orbit accessory. Powdered samples were pressed against the diamond ATR crystal and spectra collected using a method aggregating 128 sample scans over 150 second period at a resolution of 4 $cm^{-1}$, from which a background scan (i.e. a spectrum taken of the crystal platform with no sample present) was subtracted. Resulting spectra were then processed using an automatic baseline correction method provided by the Thermo Scientific OMNIC Software Suite which attempts to account for the effects of optical depths varying as a function of wavelength.

Table 5.1. Samples from flowing and dry acidic, ferrous sulfate-rich streams.

Key: Q – Quartz – $SiO_2$ I – Illite – $(K,H_3O)(Al,Mg,Fe)_2(Si,Al)_4O_{10}[(OH)_2,(H_2O)]$
G – Goethite – α-FeO(OH) J – Jarosite – $KFe^{3+}{}_3(OH)_6(SO_4)_2$
M – Microcline – $K(AlSi_3O_8)$ K – Kaolinite – $Al_2Si_2O_5(OH)_4$

W – Water S – Sulfur dioxide

| Sample | Code | XRD data | cm from west bank | cm from centre | pH | Max potential gas products (by stoichiometry) |
|---|---|---|---|---|---|---|
| *Flowing stream* | | | | | | |
| Bank sediment (W) | FlowBS1 | Q:69.4, G:0, J:0.5, I:20.6, K:8.4, M:1.1 | 0 | -225 | 5 | W:2.3, S:0.1 |
| | FlowBS2 | Q:64, G:0, J:8.5, I:12, K:15.2, M:0.3 | 30 | -195 | 4.5 | W:3.9, S:2.2 |
| Matt over goethite | FlowMG1a | Q:63.8, G:25.9, J:10.3, I:0, K:0, M:0 | 85 | -140 | 4 | W:3.7, S:2.6 |
| | FlowMG1b | Q:23.5, G:71.7, J:4.8, I:0, K:0, M:0 | | | | W:7.8, S:1.2 |
| | FlowMG1c | Q:88.9, G:0, J:4.6, I:0, K:4.1, M:2.4 | | | | W:1.1, S:1.2 |
| | FlowMG2a | Q:39.5, G:59, J:0, I:0, K:1.4, M:0 | 150 | -75 | 5.5 | W:6.2, S:0.0 |
| | FlowMG2b | Q:52.5, G:47.5, J:0, I:0, K:0, M:0 | | | | W:4.8, S:0.0 |
| | FlowMG2c | Q:89.4, G:0, J:6.4, I:0, K:3, M:1.1 | | | | W:1.2, S:1.6 |
| Wood over goethite | FlowWG1a | Q:54.6, G:45.4, J:0, I:0, K:0, M:0 | 190 | -35 | 4.5 | W:4.6, S:0.0 |
| | FlowWG1b | Q:79.7, G:0, J:7, I:13.3, K:0, M:0 | | | | W:1.4, S:1.8 |
| Matt over jarosite | FlowMJ1a | Q:56.2, G:18.9, J:1.6, I:18.1, K:4.1, M:1.2 | 225 | 0 | 4 | W:3.6, S:0.4 |
| | FlowMJ1b | Q:98.8, G:0, J:0, I:0, K:0, M:0 | | | | W:0.0, S:0.0 |
| | FlowMJ1c | Q:73.9, G:0, J:26.1, I:0, K:0, M:0 | | | | W:2.8, S:6.7 |
| Wood over jarosite | FlowWJ1a | Q:64.9, G:0, J:27, I:0, K:8.1, M:0 | 260 | 35 | 5 | W:4.2, S:6.9 |
| | FlowWJ1b | Q:63.2, G:0, J:27.5, I:0, K:9.3, M:0 | | | | W:4.4, S:7.0 |
| Bank sediment (E) | FlowBS3 | Q:72, G:0, J:1.2, I:14.8, K:10.7, M:1.4 | 325 | 100 | 4 | W:2.5, S:0.3 |
| Quartz sand | FlowQ1 | Q:87.4, G:0, J:0.5, I:6.9, K:3.4, M:1.8 | 380 | 155 | 4 | W:0.9, S:0.1 |
| *Dry stream* | DryMJ1a | Q:40.3, G:18, J:5.5, I:25.3, K:10.9, M:0 | | | 5 | W:5.3, S:1.4 |
| | DryMJ1b | Q:43.1, G:37.7, J:19.2, I:0, K:0, M:0 | | | | W:5.9, S:4.9 |

Spectral features arising from hydroxyl, water of hydration, carbonates, sulfates and organic compounds were identified in the ATR-FTIR spectra using the same criteria described in Gordon and Sephton (2016b).

### 5.2.3 Pyrolysis-FTIR

Each pyrolysis sample was prepared by adding a quantity (in the range 4 – 23 mg) of the chosen sample type to a quartz tube with the powder being held in place by quartz wool plugs at both ends. Mass measurements were taken, on a scale accurate to 0.1 mg, during the sample preparation steps so that the mass of powdered sample could be ascertained.

Pyrolysis was achieved using a CDS Analytical Pyroprobe 5200. The pyroprobe is a length of metal rod housing a platinum coil heating element at one end. The quartz tube containing the sample is loaded into the platinum coil before the probe is inserted into a gas tight CDS Analytical Brill Cell, which provides interfacing with the FTIR spectrometer (ZnSe windows at two ends of the cell permit an infrared beam to traverse the intermediate cell volume). Pyrolysis is achieved when the coil is heated at a controlled rate of 20 °C $ms^{-1}$ and then held at the desired temperature for 7.2 s. Gas products liberated from the solid sample are contained within the helium atmosphere of the Brill Cell. A controlled helium flow is used to purge the cell of contaminants and spent pyrolysis products between analyses.

FTIR analysis was conducted using a Thermo Scientific Nicolet 5700 FTIR spectrometer. Before pyrolysis, a background scan is taken with the probe loaded in the previously purged cell. The sample spectrum is taken immediately after the probe has finished firing. Background and sample spectra are composed of 32 scans taken over 19.5 s at a resolution of 4 $cm^{-1}$. To account for background artefacts introduced by the experimental process, blanks were prepared in the same manner as geological samples. Before each collection session, three procedural blanks were analysed at each of the temperature modes used for analysis. For each sample spectrum obtained, an average of the appropriate procedural blank spectra was subtracted.

Measurements of spectral features were taken and recorded; a peak located at 2349 $cm^{-1}$ corresponding to the anti-symmetric stretch in carbon dioxide, one at 3853 $cm^{-1}$ arising from a stretching mode of water, one at 1352 $cm^{-1}$ corresponding to the sulfur dioxide anti-symmetric stretching mode, one at 3016 $cm^{-1}$ corresponding to the methane anti-symmetric stretching mode and the height of a peak at 2933 $cm^{-1}$. Organic compounds, depending on the molecular composition and structure, typically produce features in broad spectral window corresponding to the C-H stretch; for comparison with a previous sensitivity assessment (Gordon & Sephton 2016a) the region (3150 – 2740 $cm^{-1}$) was chosen to account for organic compounds. The mass of methane, water, carbon dioxide and sulfur dioxide products were determined through reference to mass calibration curves. Spectrometer operation and data processing were both achieved by using the Thermo Scientific OMNIC Software Suite.

### 5.2.4 Triage operation

To discriminate between samples and reveal that of highest scientific value a triage methodology was developed. To simulate a triage operation in situ, samples were surveyed and promoted through the triage phases based on their reposes to pyrolysis-FTIR.

#### *5.2.4.1 Triage phase one (the habitability assessment phase) using single-step pyrolysis-FTIR (1000 °C)*

All samples are first subjected to a single-step 1000 °C pyrolysis-FTIR analysis. This mode was identified in previous work as a high sensitivity method for detecting geological habitability indicators (Gordon and Sephton 2016b). Certain minerals indicative of past habitability, such as certain serpentinites and carbonates, only release their identifying gases at high temperatures. At high temperatures, organic compounds are more prone to complete thermal dissociation and consolidate into the methane signal. Organic compounds also undergo more aggressive combustion at higher temperatures owing to the greater energy input and interaction with oxidants (from the mineral matrix) than at lower temperatures. However, combusted organic compounds are revealed through the simultaneous release of combustion products

(carbon dioxide and water). Thus the 1000 °C single-step acts as the triage 'catch all' phase, providing good general purpose sensitivity but lacking more detailed diagnostic potential.

#### *5.2.4.2 Triage phase two (the habitation assessment phase) using single-step pyrolysis-FTIR (700 °C)*

The highest ranking sample types of the habitability assessment (single-step 1000 °C) phase are then passed to a round of single-step 700 °C pyrolysis-FTIR analyses. This temperature avoids the extensive organic compound thermal dissociation of the higher 1000 °C step and is more sensitive to detection and identification of complex organic compounds. Although during an actual triage operation only the highest ranking samples would go forward to the habitation (single-step 700 °C) assessment, in this study all samples were analysed at both 700 °C and 1000 °C to test the efficacy of the triage methodology.

#### *5.2.4.3 Triage phase three (the diagnostic phase) using multi-step pyrolysis-FTIR (500 °C, 750 °C and 1000 °C)*

The highest ranking sample types of the 'catch all' phase are then passed to a round of multi-step pyrolysis-FTIR analysis (successive analysis steps performed a given specimen at 500 °C, 750 °C and 1000 °C). This form of pyrolysis-FTIR provides additional diagnostic information over single-step analysis. The characteristic decomposition temperatures of and the ratio of gases released at the different temperature steps are characteristic for each mineral phase (Gordon and Sephton 2016b). Comparing these with pre-existing reference spectra can help identify the material type in situ. Although during an actual triage operation only the highest ranking samples from single-step analysis would be used further for multi-step analysis, in this study a number of low priority samples were also processed in the multi-step phase test the accuracy of the triage methodology.

### 5.2.5 Classifying and ranking sample potential

In order to discover the samples which should be processed further following single-step analyses, a scoring logic was applied to the pyrolysis-FTIR outcomes. This process is illustrated in Figure 5.1 and detailed as follows:

Three hierarchical tiers of assessment were used to construct a score code for each sample. Each element of the code is determined by the confidence of the FTIR signals representing that tier:

- Confirmed – signal over double the associated uncertainty.
- Tentative – signal greater than the associated uncertainty, but weaker than double
- None – signal less than uncertainty.

Tier 1 – Organic compound response. This is the highest priority tier with complex organic compounds being preferred over methane responses.

A. Confirmed organic compounds or methane signal.

B. Tentative organic compounds or methane signal.

C. No organic compounds or methane detected.

Tier 2 – Simultaneous water and carbon dioxide response. Individually these gases serve as habitability indicators however a simultaneous release introduces the possibility of combusted hydrocarbons. With carbon dioxide and water having other possible non-organic sources an additional criterion is set to add significance to scoring outcomes: both carbon dioxide and water contents must exceed 2% of the initial sample weight to be considered a strong signal.

1. Confirmed and strong (above 2% of sample mass) water and carbon dioxide signals.
2. Tentative or confirmed but low (equal or less than 2% of sample mass) water and carbon dioxide signals.
3. No simultaneous release of water and carbon dioxide.

Tier 3 – Sulfur dioxide response. As sulfates have been recognised for aiding the preservation of biomarkers, samples presenting sulfur dioxide are desirable. In addition, sulfur dioxide has been seen to assist the combustion of organic compounds, thus when a sulfur signal is present it is likely that any accompanying

hydrocarbon signal represents a minimum for the organic richness of the original sample and any evidence of combustion is given additional weight.

i. Confirmed sulfur dioxide signal.

ii. Tentative sulfur dioxide signal.

iii. No sulfur dioxide.

So for example, a sample scoring A.1.i would be the highest priority sample and C.3.iii the lowest. Two samples which are assigned the same code can be ranked against each other through comparing quantities of confirmed gases in the highest priority tier.

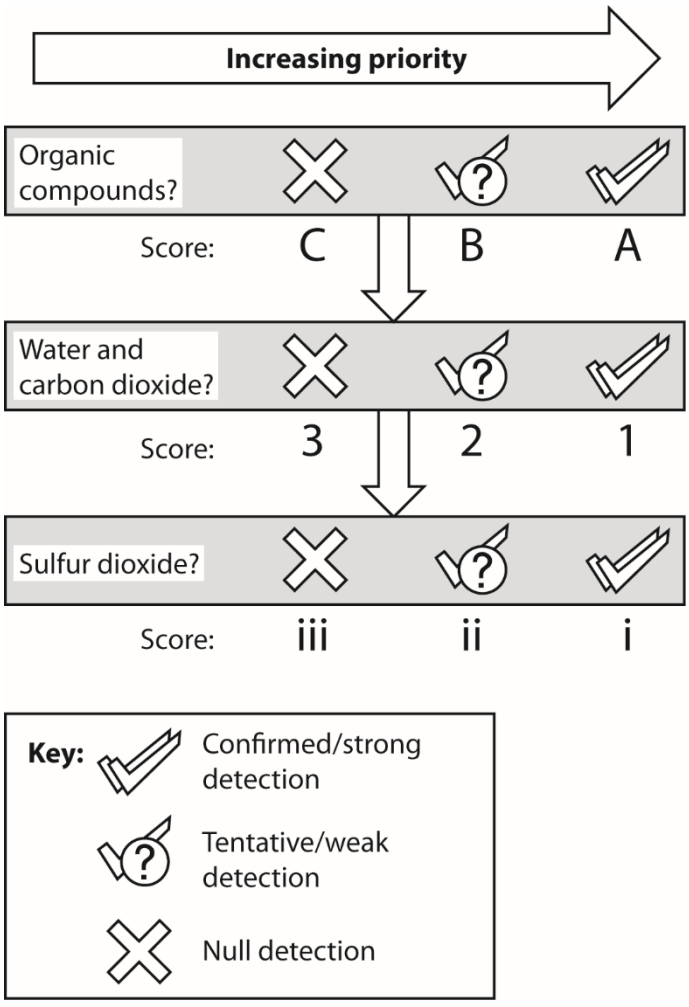



Figure 5.1. Logic for scoring samples for the purpose of ranking them.

## 5.3 Results

### 5.3.1 Attenuated total reflectance-FTIR

The results from ATR-FTIR analysis are presented in Table 5.2. A broad peak for water of hydration was observed for all samples and was detected in weak form for two samples: FlowMJ1b and FlowQ1 while it was detected strongly in all other samples. Hydroxyl peaks were observed strongly for FlowBS1, FlowBS2, FlowWJ1b, FlowBS3 and DryMJ1a and were observed weakly for FlowMG1c, FlowWG1a, FlowWG1b, FlowMJ1a, FlowMJ1b and FlowQ1. Some samples exhibited a broad peak around 1400 $cm^{-1}$, which is characteristic of carbonates, yet cannot be conclusively assigned as the other characteristic carbonate peaks at 890–800 $cm^{-1}$ and 760–670 $cm^{-1}$ were not clearly identifiable. A feature representing sulfates could be identified in all samples in the region of 1090 $cm^{-1}$. In FlowBS1, FlowMG2a FlowMG2b, FlowWG1b, FlowMJ1a, FlowMJ1b and FlowQ1 this only came in the form of a small shoulder which was insufficient to conclusively determine the presence of sulfates. Sulfates could be determined weakly in FlowWG1a and FlowBS3 and strongly in all other samples. Organic compounds were indicated by broad features arising from C-H stretching in the 3050–2650 $cm^{-1}$ region and were observed strongly in FlowMG1a, FlowMG2a, FlowWG1a, FlowMJ1a and DryMJ1a and weakly in FlowBS1, FlowBS2, FlowMG1b, FlowMG2b, FlowWG1b, FlowWJ1b and DryMJ1b. A small sharp peak at 3020 $cm^{-1}$ representing C-H stretching was observed in FlowMG1b, FlowMG2b, FlowWG1a, FlowWJ1b, DryMJ1a and DryMJ1b spectra.

### 5.3.2 Single-step pyrolysis-FTIR (1000 °C)

Results for the first triage phase (1000 °C single-step pyrolysis-FTIR) are presented in Table 5.3. Hydrocarbon responses were confirmed in FlowMG1a, DryMJ1a, FlowMJ1a, FlowWG1a, FlowMG2a and FlowMG2b and detected tentatively in FlowMG1b, FlowWJ1a, FlowMJ1c, FlowBS2, DryMJ1b, DryMJ1b, FlowWJ1b and FlowBS1. Methane responses were confirmed in FlowMG1a, DryMJ1a, FlowMJ1a and FlowMG2a and detected tentatively in FlowWG1a, FlowMG2b, FlowBS2, FlowWG1b and FlowBS1. All confirmed hydrocarbon signals were accompanied by a methane signal and the strength

Table 5.2. ATR results. Solid squares represent strong identification while an empty square represents a relatively weak signal. A question mark is used to denote samples which exhibit a spectral feature in the characteristic region yet cannot be conclusively assigned: a broad peak around 1400 $cm^{-1}$ in the case of carbonates and a shoulder at around 1090 $cm^{-1}$ in the case of sulfates.

| Sample | Code | Hydroxyl | Water of hydration / adsorbed water | Carbonate ion | Sulfate ion | Organic compounds |
|---|---|---|---|---|---|---|
| *Flowing stream* | | | | | | |
| Bank sediment (W) | FlowBS1 | ■ | ■ | | ? | □ |
| | FlowBS2 | ■ | ■ | | ■ | □ |
| Matt over goethite | FlowMG1a | | ■ | ? | ■ | ■ |
| | FlowMG1b | | ■ | | ■ | □ |
| | FlowMG1c | □ | ■ | | ■ | |
| | FlowMG2a | | ■ | ? | ? | □ |
| | FlowMG2b | | ■ | | ? | □ |
| | FlowMG2c | | ■ | | ■ | |
| Wood over goethite | FlowWG1a | □ | ■ | ? | □ | ■ |
| | FlowWG1b | □ | ■ | | ? | □ |
| Matt over jarosite | FlowMJ1a | □ | ■ | ? | ? | ■ |
| | FlowMJ1b | □ | □ | | ? | |
| | FlowMJ1c | | ■ | | ■ | |
| Wood over jarosite | FlowWJ1a | | ■ | | ■ | |
| | FlowWJ1b | ■ | ■ | | ■ | □ |
| Bank sediment (E) | FlowBS3 | ■ | ■ | | □ | |
| Quartz sand | FlowQ1 | □ | □ | | ? | |
| *Dry stream* | DryMJ1a | ■ | ■ | ? | ■ | ■ |
| | DryMJ1b | | ■ | | ■ | □ |

of methane responses tended to correlate with the hydrocarbon response. Only one sample, FlowWG1b, produced a methane peak where there was no measurable broad hydrocarbon feature. Water responses were confirmed for all samples. The most significant water response was observed for FlowMG1a (7.3% of the initial sample mass). Carbon dioxide responses were confirmed for all samples. Sulfur dioxide signals were absent in only three samples, namely FlowMG2a, FlowMG2b and FlowMJ1b. Sulfur dioxide signals for the remaining samples were all significant.

The samples in Table 5.3 were ranked by their scores following the 1000 °C phase. Within each scoring grouping, ranking was determined by the signal strengths of the highest order confirmed gas. In practice,

Table 5.3. 1000 °C pyrolysis-FTIR analysis. C – Confirmed detection (signal over double the associated uncertainty), T – tentative detection (signal greater than the associated uncertainty, but weaker than double), N – null detection (signal less than uncertainty). Uncertainties reported are two standard deviations of the mean calculated from procedural blanks.

| Sample | Hydrocarbon absorbance | | wt% Methane | | Water | | Carbon Dioxide | | Sulfur Dioxide | | Score |
|---|---|---|---|---|---|---|---|---|---|---|---|
| | ± 0.02 | | ± 0.009 | | ± 0.16 | | ± 0.05 | | ± 0.04 | | |
| FlowMG1a | 1.29 | C | 1.202 | C | 7.30 | C | 7.57 | C | 0.35 | C | A.1.ii |
| DryMJ1a | 0.14 | C | 0.120 | C | 6.57 | C | 8.81 | C | 0.17 | C | A.1.ii |
| FlowMJ1a | 0.07 | C | 0.024 | C | 4.67 | C | 11.44 | C | 0.54 | C | A.1.ii |
| FlowWG1a | 0.05 | C | 0.009 | T | 4.11 | C | 8.04 | C | 0.26 | C | A.1.ii |
| FlowMG2a | 0.12 | C | 0.087 | C | 6.86 | C | 13.99 | C | 0.03 | N | A.1.iii |
| FlowMG2b | 0.04 | C | 0.016 | T | 3.77 | C | 4.59 | C | -0.01 | N | A.1.iii |
| FlowMG1b | 0.02 | T | -0.004 | N | 5.39 | C | 7.59 | C | 4.34 | C | B.1.i |
| FlowWJ1a | 0.02 | T | 0.006 | N | 4.16 | C | 4.29 | C | 5.74 | C | B.1.i |
| FlowMJ1c | 0.03 | T | 0.002 | N | 2.92 | C | 3.08 | C | 3.09 | C | B.1.i |
| FlowBS2 | 0.03 | T | 0.017 | T | 3.95 | C | 2.90 | C | 1.51 | C | B.1.i |
| DryMJ1b | 0.03 | T | -0.013 | N | 4.77 | C | 2.57 | C | 3.85 | C | B.1.i |
| FlowWJ1b | 0.03 | T | -0.007 | N | 4.08 | C | 1.57 | C | 4.47 | C | B.2.i |
| FlowWG1b | 0.00 | N | 0.017 | T | 0.82 | C | 0.88 | C | 1.10 | C | B.2.i |
| FlowBS1 | 0.02 | T | 0.017 | T | 2.30 | C | 1.11 | C | 0.14 | C | B.2.ii |
| FlowMG2c | 0.01 | N | -0.004 | N | 1.52 | C | 0.98 | C | 1.48 | C | C.2.i |
| FlowBS3 | 0.00 | N | 0.003 | N | 2.29 | C | 0.75 | C | 0.31 | C | C.2.ii |
| FlowMG1c | 0.01 | N | -0.005 | N | 1.30 | C | 0.69 | C | 0.08 | C | C.2.ii |
| FlowQ1 | 0.00 | N | 0.008 | N | 1.09 | C | 0.54 | C | 0.13 | C | C.2.ii |
| FlowMJ1b | 0.00 | N | 0.005 | N | 0.46 | C | 0.43 | C | 0.03 | N | C.2.iii |

this stage could allow a number of samples to be disregarded for further analysis. For the sake of this study, all samples were passed forward to phase two to reveal the robustness of the triage concept.

### 5.3.3 Single-step pyrolysis-FTIR (700 °C)

Results from the second triage phase (700 °C single-step pyrolysis-FTIR) are presented in Table 5.4. Hydrocarbon responses were confirmed in FlowMG1a, FlowMJ1a, DryMJ1a, FlowWG1a, FlowMG2a, FlowMG2b, FlowBS2, FlowMJ1c and FlowBS1 and detected tentatively in FlowMG1b, FlowWJ1a, DryMJ1b, FlowWJ1b, FlowMG2c, FlowQ1 and FlowWG1b. Methane responses were only tentative observed in DryMJ1a, FlowMG2a and FlowMG2b; the remaining samples had no measurable methane peak. Water and carbon dioxide were confirmed to be produced for all samples. Sulfur dioxide could not be detected from the pyrolysis of FlowMG2a, FlowMG2b, FlowWG1b and FlowMJ1b but was tentatively detected in FlowQ1 and confirmed for all other samples.

The scoring of samples following the 700 °C phase was largely unchanged from the scoring in the 1000 °C phase, except for a few notable exceptions.

- FlowMJ1a became a higher priority sample than DryMJ1a owing to a stronger hydrocarbon response being revealed.
- FlowBS2, FlowMJ1c and FlowBS1 were all promoted from 'B type' samples to 'A type' samples, as the presence of hydrocarbons could be confirmed.
- FlowMG2c, FlowMJ1b and FlowQ1 were both promoted from 'C type' samples to 'B type' samples, because hydrocarbons were now tentatively detected.
- Considering just the results of the 700 °C step alone, FlowWG1b would be scored as a 'iii type' sample, because the sulfur dioxide signal was no longer present. However, as information of the previous triage step can be utilised, FlowWG1b ultimately retains a score of B.2.i. This was the only case where a sulfur signal, previously detected at 1000 °C was not detected at 700 °C.

Table 5.4. 700 °C single-step analysis. C – Confirmed detection (signal over double the associated uncertainty), T – tentative detection (signal greater than the associated uncertainty, but weaker than double), N – null detection (signal less than uncertainty). Uncertainties reported are two standard deviations of the mean calculated from procedural blanks. Scores based of 700 °C step results alone are displayed in grey, with final scores (i.e. scores after the 700 °C step after considering the results of the 1000 °C step) are in black.

| Sample | Hydrocarbon absorbance | | wt% Methane | | Water | | Carbon Dioxide | | Sulfur Dioxide | | Score | |
|---|---|---|---|---|---|---|---|---|---|---|---|---|
| | ± 0.014 | | ± 0.03 | | ± 0.03 | | ± 0.07 | | ± 0.06 | | | |
| FlowMG1a | 2.477 | C | 0.13 | C | 7.85 | C | 6.03 | C | 0.30 | C | A.1.ii | A.1.ii |
| FlowMJ1a | 0.311 | C | 0.03 | N | 4.57 | C | 7.01 | C | 0.64 | C | A.1.ii | A.1.ii |
| DryMJ1a | 0.263 | C | 0.05 | T | 6.09 | C | 5.32 | C | 0.19 | C | A.1.ii | A.1.ii |
| FlowWG1a | 0.172 | C | 0.02 | N | 4.64 | C | 6.89 | C | 0.24 | C | A.1.ii | A.1.ii |
| FlowMG2a | 0.194 | C | 0.06 | T | 6.95 | C | 8.23 | C | 0.04 | N | A.1.iii | A.1.iii |
| FlowMG2b | 0.082 | C | 0.04 | T | 4.63 | C | 4.32 | C | -0.01 | N | A.1.iii | A.1.iii |
| FlowBS2 | 0.079 | C | 0.01 | N | 3.60 | C | 1.22 | C | 1.89 | C | A.2.i | A.2.i |
| FlowMJ1c | 0.075 | C | 0.00 | N | 3.52 | C | 1.47 | C | 3.14 | C | A.2.i | A.2.i |
| FlowBS1 | 0.075 | C | 0.01 | N | 2.34 | C | 0.49 | C | 0.16 | C | A.2.ii | A.2.ii |
| FlowMG1b | 0.022 | T | -0.01 | N | 5.73 | C | 5.95 | C | 4.50 | C | B.1.i | B.1.i |
| FlowWJ1a | 0.026 | T | -0.01 | N | 4.13 | C | 2.79 | C | 4.57 | C | B.1.i | B.1.i |
| DryMJ1b | 0.024 | T | -0.01 | N | 5.47 | C | 2.28 | C | 3.23 | C | B.1.i | B.1.i |
| FlowWJ1b | 0.020 | T | -0.02 | N | 4.59 | C | 1.38 | C | 2.48 | C | B.2.i | B.2.i |
| FlowMG2c | 0.026 | T | 0.00 | N | 1.56 | C | 0.66 | C | 1.23 | C | B.2.i | B.2.i |
| FlowWG1b | 0.019 | T | 0.00 | N | 0.73 | C | 0.35 | C | 0.03 | N | B.2.iii | B.2.i |
| FlowQ1 | 0.023 | T | 0.01 | N | 0.71 | C | 0.18 | C | 0.08 | T | B.2.ii | B.2.ii |
| FlowMJ1b | 0.016 | T | 0.01 | N | 0.48 | C | 0.34 | C | 0.05 | N | B.2.iii | B.2.iii |
| FlowBS3 | 0.008 | N | 0.00 | N | 1.91 | C | 0.32 | C | 0.33 | C | C.2.ii | C.2.ii |
| FlowMG1c | 0.010 | N | 0.00 | N | 1.19 | C | 0.43 | C | 0.89 | C | C.2.ii | C.2.ii |

From these results the highest priority samples that were selected for improved characterisation by multi-step pyrolysis-FTIR were FlowMG1a, FlowMJ1a, DryMJ1a, FlowWG1a, FlowWG1a, FlowMG2b and FlowMG2b. The low priority samples chosen to test the robustness of the triage concept were FlowMJ1b (the lowest ranked sample) and FlowMG1c (a sample located from the same core as the highest priority sample and a low priority sample observed to produce all gases except hydrocarbons).

### 5.3.4 Multi-step pyrolysis-FTIR

The results from second triage phase (multi-step pyrolysis-FTIR) are presented in Table 5.5. Hydrocarbons were confirmed for all high priority samples at the 500 °C step but were absent from the 750 °C and

1000 °C steps, except for a tentative detection in FlowMG1a at 700 °C. For the low priority comparison samples,

Table 5.5. Multi-step analysis, performed on the six highest priority samples identified through the preceding 'habitation sensitivity' triage phase (Table 5.4). Results are ordered by the total response of hydrocarbons for each sample across all three temperature steps. Two low priority samples, FlowMJ1b and FlowMG1c are included for comparison.

| | Sample | Hydrocarbon absorbance | | %wt | | | | | | | |
|---|---|---|---|---|---|---|---|---|---|---|---|
| | | | | Methane | | Water | | Carbon Dioxide | | Sulfur Dioxide | |
| 500 °C | FlowMG1a | 3.022 | ± 0.013 | 0.03 | ± 0.02 | 6.90 | ± 0.09 | 3.59 | ± 0.05 | 0.07 | ± 0.03 |
| | DryMJ1a | 0.363 | | 0.03 | | 4.49 | | 3.26 | | 0.13 | |
| | FlowMG2a | 0.303 | | 0.00 | | 7.04 | | 6.68 | | 0.07 | |
| | FlowWG1a | 0.075 | | 0.01 | | 4.28 | | 3.94 | | 0.29 | |
| | FlowMJ1a | 0.059 | | 0.00 | | 1.63 | | 1.39 | | 0.24 | |
| | FlowMG2b | 0.035 | | 0.00 | | 3.83 | | 2.41 | | 0.00 | |
| | FlowMJ1b | 0.024 | | -0.01 | | 0.43 | | 0.33 | | 0.07 | |
| | FlowMG1c | 0.006 | | 0.00 | | 1.01 | | 0.30 | | 0.13 | |
| 750 °C | FlowMG1a | 0.05 | ± 0.03 | 0.11 | ± 0.02 | 1.24 | ± 0.11 | 3.86 | ± 0.03 | 0.34 | ± 0.03 |
| | DryMJ1a | -0.01 | | 0.04 | | 2.13 | | 4.38 | | 0.23 | |
| | FlowMG2a | 0.01 | | 0.02 | | 1.10 | | 5.72 | | 0.25 | |
| | FlowWG1a | 0.00 | | 0.01 | | 0.90 | | 4.12 | | 0.49 | |
| | FlowMJ1a | 0.01 | | 0.01 | | 0.29 | | 1.29 | | 0.15 | |
| | FlowMG2b | 0.00 | | 0.01 | | 0.60 | | 2.51 | | 0.14 | |
| | FlowMJ1b | 0.01 | | 0.01 | | 0.71 | | 0.49 | | 0.06 | |
| | FlowMG1c | 0.01 | | 0.00 | | 0.37 | | 0.30 | | 0.71 | |
| 1000 °C | FlowMG1a | 0.005 | ± 0.016 | 0.01 | ± 0.03 | 0.25 | ± 0.18 | 3.42 | ± 0.09 | 0.29 | ± 0.02 |
| | DryMJ1a | 0.014 | | 0.02 | | 0.43 | | 2.75 | | 0.38 | |
| | FlowMG2a | 0.014 | | 0.02 | | 0.19 | | 4.89 | | 0.40 | |
| | FlowWG1a | 0.009 | | 0.01 | | 0.10 | | 1.10 | | 0.65 | |
| | FlowMJ1a | 0.003 | | 0.00 | | 0.08 | | 0.75 | | 0.15 | |
| | FlowMG2b | 0.011 | | 0.01 | | -0.06 | | 0.57 | | 0.21 | |
| | FlowMJ1b | -0.014 | | 0.00 | | 0.11 | | 0.44 | | 0.05 | |
| | FlowMG1c | -0.002 | | 0.00 | | 0.08 | | 0.04 | | 0.17 | |

hydrocarbon signals were absent in all analyses except for FlowMJ1b, where a hydrocarbon absorbance was tentatively observed. Multi-step repeat experiments show a significant variability in hydrocarbon signal for repeat sample runs. Methane is mostly undetected in all samples, across all temperature steps, the exceptions being: FlowMG1a tentatively at 500 °C and confirmed at 750 °C; DryMJ1a tentatively at 500 °C and 750 °C; and FlowMG2a tentatively at 750 °C. Water was confirmed for all high priority samples at 500 °C and 750 °C. For all these samples quantities of water were on the order of 5 times greater at the lower of these two temperature steps, except for DryMJ1a, which had only about twice as much water at 500 °C than 750 °C. Water could only be confirmed for one high priority sample at the 1000 °C step, namely DryMJ1a. However, FlowMG1a and FlowMG2a had tentative releases. The low priority samples both produced confirmed water signals at 500 °C and 750 °C but no water responses at 1000 °C. Carbon dioxide was confirmed in all cases, except for FlowMG1c at 1000 °C. Sulfur dioxide could be detected in all samples at each temperature step. The majority of sulfur dioxide was observed at 750 °C in each sample with the exception of FlowMJ1a and FlowMG2b where the main releases were at 500 °C and 1000 °C respectfully. In FlowMG2a, FlowMG2b and FlowWG1a no mineral source of sulfur was indicated by XRD results, thus the sulfur dioxide observed here is likely biogenically sourced. Following multi-step pyrolysis-FTIR FlowMG1a remained the highest priority sample.

## 5.4 Discussion

### 5.4.1 Attenuated total reflectance-FTIR

ATR results are used only as supporting data and would not be expected to be employed during sample triage on Mars Sample Return. The presence of water in all samples is perhaps expected considering their origin from a stream environment. The samples exhibiting hydroxyl peaks in ATR-FTIR correlate with samples revealed to have high quantities of kaolinite by XRD results, which has 4 hydroxyl components in its structure (Giese and Datta 1973). Stronger hydroxyl signals tended to be observed in samples taken from near the edges of the flowing stream. Thus hydroxyl peaks being absent from a number of samples

(FlowMG1a, FlowMG1b, FlowMG2a, FlowMG2b, FlowMG2c, FlowMJ1c, FlowWJ1a and DryMJ1b), found generally in the middle of the stream suggesting that ATR results are reflecting clay mineral chemistry and the various depositional settings. All samples exhibiting the broad 1400 $cm^{-1}$ peak were also identified to have hydrocarbon because alkanes, alcohols and amides can have strong peaks in this region. There are a number of samples which were shown in the XRD results to not have sulfates however ATR-FTIR can identify features that may indicate sulfate bonds; one example is FlowMG2a (a microbial matt sample). FlowMG2a has a clear shoulder around 1090 $cm^{-1}$ which is where a prominent sulfate peak occurs. It could be the case that sulfur compounds are present in non-crystalline forms within the biomass component of some samples.

### 5.4.2 Triage phase one (the habitability assessment phase) using single-step pyrolysis-FTIR (1000 °C)

FlowWG1a appears to shows a hydrocarbon signal at 1000 °C but hydrogen chloride peaks appear in the same region and the assignment is uncertain. There is an apparent correlation between the strength of the hydrocarbon signal and the water signal. The weakest water response at 0.46 %wt came from FlowMJ1b, the interior of the hard, sandy nodule, which has likely been isolated from aqueous processes for some time. FlowWG1b produced slightly less water than would be expected from the XRD results and similar reasoning applies for sulfur dioxide from this sample. The XRD data does not reveal any mineralogical sources in any of the samples that should produce carbon dioxide under pyrolysis. Thus it can be inferred that significant carbon dioxide signals are the by products from organic compound destruction. For low level responses adsorbed species may make a contribution. Yet some samples produce no organic compound signals where the carbon dioxide signal is too significant to be attributed entirely to adsorbed species (e.g. FlowMG2c, approx. 1%wt carbon dioxide), thus the carbon dioxide signal can act as non-specific indicator for the presence of organic compounds in samples.

Particular attention should be paid to cases where organic compound signals are absent, the carbon dioxide signal is high and there is evidence of sulfates because of the ability of sulfates to produce oxygen during thermal decomposition which can then combust organic matter (Lewis et al. 2015). The most shallow and middle depth samples from the least acidic core of the stream bed produced no sulfur dioxide and samples from the edges of the stream produced relatively low levels of sulfur dioxide indicating the influence of the sulphate rich flowing water in sulphate mineral production. FlowMG2a has the strongest carbon dioxide signal of all samples, lacks a sulfur dioxide response and has a hydrocarbon response. These data are consistent with an enhancement of carbon dioxide and diminished hydrocarbon response when organic matter is pyrolysed in the presence of sulfates (Lewis et al. 2015). Sulfates facilitate combustion of organic matter and should organic matter be adequately abundant, the signal for sulfur dioxide can be expunged. For this sample, XRD results do not conclusively present a mineral source for sulfur dioxide but the ATR-FTIR data hint at a possible sulfur feature.

Samples with higher scores generally have higher carbon dioxide-to-water mass ratios.

As shown in Gordon and Sephton (2016b) the presence of water, carbon dioxide and sulfur dioxide in pyrolysis-FTIR results can indicate habitable environments. Single-step 1000 °C pyrolysis-FTIR data were employed for habitability assessment. During single-step 1000 °C pyrolysis-FTIR FlowWG1b and FlowMJ1b were revealed as the least likely samples to have undergone significant alteration by water (water levels are 0.82 %wt and 0.46 %wt respectively). Most other samples produced water >1%, thus can be suspected to contain hydrated mineral phases and are good candidates for habitable environments. Gordon and Sephton (2016b) (Földvári 2011) demonstrated that hydrated minerals generally produce water in amounts greater than 5% of mineral weight. Carbon dioxide being observed for all samples suggests that carbonates are present in each sample. No samples are found to be dominated by carbonates. The strongest carbon dioxide signal arises from FlowMG2a which produces 14% carbon dioxide (pure carbonates produce carbon dioxide in amounts >20% of their weight). A number of samples produce significant sulfur dioxide

signals (>1%) and thus can be assumed to contain sulfates. Methane production was confirmed for number of samples: FlowMG1a (1.202%), DryMJ1a (0.120%), FlowMG2a (0.024%) and FlowMG2a (0.087%). These samples were all obtained from the top of the respective cores. Concurrent release of water and carbon dioxide can result from the combustion of hydrocarbons. Significant concurrent releases (both water and carbon dioxide >2% initial sample mass) were observed for FlowMG1a, DryMJ1a, FlowMJ1a, FlowWG1a, FlowMG2a, FlowMG2b, FlowMG1b, FlowWJ1a, FlowMJ1c, FlowBS2 and DryMJ1b. These signals are generally stronger at the top of the cores. Strong concurrent releases are not observed on the banks of the stream.

### 5.4.3 Triage phase two (the habitation assessment phase) using single-step pyrolysis-FTIR (700 °C)

When compared to the 1000 °C single-step pyrolysis-FTIR phase, 700 °C pyrolysis-FTIR produces stronger hydrocarbon signals across all samples tested. As a consequence, three samples which were previously tentatively believed to have produced hydrocarbons are confirmed to produce hydrocarbons at the higher temperature (FlowBS2, FlowMJ1c and FlowBS1). Four samples were promoted from being understood to produce no hydrocarbons to tentatively producing them (FlowMG2c, FlowQ1, FlowMJ1b and FlowWG1b), although FlowWG1b tentatively produced methane at 1000 °C so its score is unchanged. These results reinforce the choice of using 700 °C as a more diagnostic temperature for detecting organic compounds than 1000 °C. Across the entire sample set, methane signals are less intense following 700 °C single-step pyrolysis-FTIR than at 1000 °C single-step pyrolysis where almost complete conversion of all organic matter to a single analyte at the higher temperature facilitates detection.

Generally water quantities are observed to be similar between pyrolysis-FTIR analyses at 700 °C and 1000 °C suggesting that the sources of water are probably the combustion of organic compounds, low energy bound mineral water (water of hydration and crystallisation, associated with weathered material) and adsorbed water. Of the samples with strong hydroxyl responses from ATR-FTIR, only FlowBS1 did

not produce more water at 1000 °C than at 700 °C (FlowBS2, FlowWJ1b, FlowBS3 and DryMJ1a all produced more water at 1000 °C). Generally the quantity of carbon dioxide produced is lower at 700 °C than at 1000 °C. The reason for lower levels of carbon dioxide at 700 °C than at 1000 °C is because at 1000 °C the extent of hydrocarbon combustion is greater. Any mineral source of carbon dioxide can be eliminated by the XRD and ATR-FTIR results (alternately high temperature carbon dioxide can be interpreted as an indication of calcium carbonate). Sulfur dioxide quantities are generally comparable between the single-step 700 °C and 1000 °C pyrolysis-FTIR modes. For FlowWG1b, the signal seen at 1000 °C disappears when subjected to 700 °C and FlowQ1 signal (confirmed at 1000 °C) was demoted to tentative.

The drop in sulfur dioxide in FlowWG1b when pyrolysed at a lower temperature indicates either:

- The mineral source of sulfur dioxide in FlowWG1b differs from that in other samples (that do not see a drop in sulfur dioxide across the different temperature modes). According to XRD data, jarosite was the only sulfate source in any of the samples. ATR-FTIR data shows little difference in the position of the sulfate peaks, confirming that sulfate components are comparable amongst samples.
- The hydrocarbons present in FlowWG1b being more conducive to the sulfur dioxide destruction pathway at 700 °C than at 1000 °C. Though if this were the case, an increase in carbon dioxide and water should be expected in the 700 °C mode when compare to 1000 °C mode; the inverse of this is observed.

### 5.4.4 Triage phase three (the diagnostic phase) using multi-step pyrolysis-FTIR (500 °C, 750 °C and 1000 °C)

FlowMG1a produced a strong signal at multi-step 500 °C than at single-step 700 °C (the supposed high sensitivity temperature for hydrocarbon responses) hinting that the optimal temperature may be a function of the nature of organic matter. Interesting to note is the pattern of methane in FlowMG1a (which is also

observed in the repeat experiments) where methane can only be confirmed at 750 °C. This likely results from the 500 °C step not being able to liberate all organic matter and that remaining is more exposed to thermal dissociation by the higher energy being delivered at 750 °C. Also, XRD data shows that there is a portion of the mineral component that is jarosite. A jarositic clay processed by a previous multi-step pyrolysis-FTIR study (Gordon and Sephton 2016b) was observed to release the bulk of its sulfur dioxide at the 750 °C step. These results show that DryMJ1a, in terms of its form of hydration, differs from the other samples. FlowMG2a releases the most carbon dioxide and sulfur dioxide induced destruction of hydrocarbons can be a reason for elevated carbon dioxide signals. If sulfur dioxide destruction was the reason for the significant carbon dioxide peak in FlowMG2a, we should expect FlowMG1a to have an even greater carbon dioxide peak owing to the same sulfur dioxide-organic matter destruction mechanism. The greater carbon dioxide signal from FlowMG2a could be due to the nature of the organic content. FlowMG1a and FlowMG2a are both microbial matt samples, but had visually different qualities when collected and could contain different organic assemblages. It could be that the organism remnants in FlowMG2a were more readily destroyed by thermal effects at 500 °C than those in FlowMG1a. Organisms with increased resilience to thermal dissociation can be indicative of greater macromolecular complexity. Thus the hydrocarbon signal should remain higher priority in the assessment of scientific potential than the carbon dioxide signal.

The three most organic rich samples being processed by multi-step pyrolysis-FTIR (FlowMG1a, DryMJ1a and FlowMG2a) produce similar quantities of carbon dioxide across all temperature steps. The three other high priority samples see a reduction at 1000 °C to approximately half (FlowMJ1a) or a quarter (FlowWG1a and FlowMG2a) of their levels at 750 °C. FlowMG1c at multi-step 1000 °C is only time in the study that carbon dioxide was not detected, showing that pyrolysis-FTIR is sensitive to carbon dioxide from organic sources. FlowMG1c, which has been demonstrated to be the 'leanest' organic content sample of the collection, gives the best picture of true sulfur dioxide levels (i.e. not influenced by interaction with organic compounds). The jarosite releases sulfur dioxide at all temperatures, but the maximum release occurs at

750 °C, with the bulk of hydrocarbons being released at 500 °C. Multi-step pyrolysis-FTIR has the capability of isolating the release of gases from different sources with different decomposition temperatures, preventing secondary reactions that may otherwise obscure scientific information.

During multi-step pyrolysis-FTIR the majority of minerals released the bulk of their total water products at the 500 °C temperature step, making weathered rock and clays a most likely source. FlowMG1a, DryMJ1a, FlowMG2a and FlowWG1a still produced significant quantities of carbon dioxide at 1000 °C (>1 %wt). High temperature carbon dioxide release is a signature of certain carbonates (e.g. calcium carbonate), however XRD does not reveal any carbonates and – being an acidic environment – carbonates are unlikely to form through passive chemistry. However ankerite, a calcium bearing carbonate, has been observed to be precipitated by microbes in acidic environments (Fernández-Remolar et al. 2012), which produces carbon dioxide at temperatures >800 °C (Meurant 1967). Non-crystalline carbonates in the biomass would be missed by XRD, but are possible seen in the ATR-FTIR data. The carbon dioxide levels could be explained by the continued combustion of remnant organic compounds, though the expected water signals that should accompany such carbon dioxide levels during combustion are not present (e.g. FlowMG2a with only 0.19 %wt water and 4.89 %wt carbon dioxide).

The strongest sulfur dioxide signal in the samples chosen for multi-step analysis was FlowMG1c (0.71 %wt at 750 °C). The temperature-step release profile is reflective of that seen in a jarositic clay. Generally, the high priority samples produce their strongest sulfur dioxide signal at 1000 °C. Sulfur dioxide evolves from magnesium sulfate in the 750 °C – 1000 °C temperature range (McAdam et al. 2016).

### 5.4.5 Assessment of the triage process

Figure 5.2 illustrates an example application of the triage operation on a subset of the samples used in this study, where resource limitations require that candidate samples are eliminated at each phase. The correctness of the sample ranking process is evident during the very first triage step where the highest priority samples are correctly ranked and the best sample is clearly recognised confirming the utility of pyrolysis-

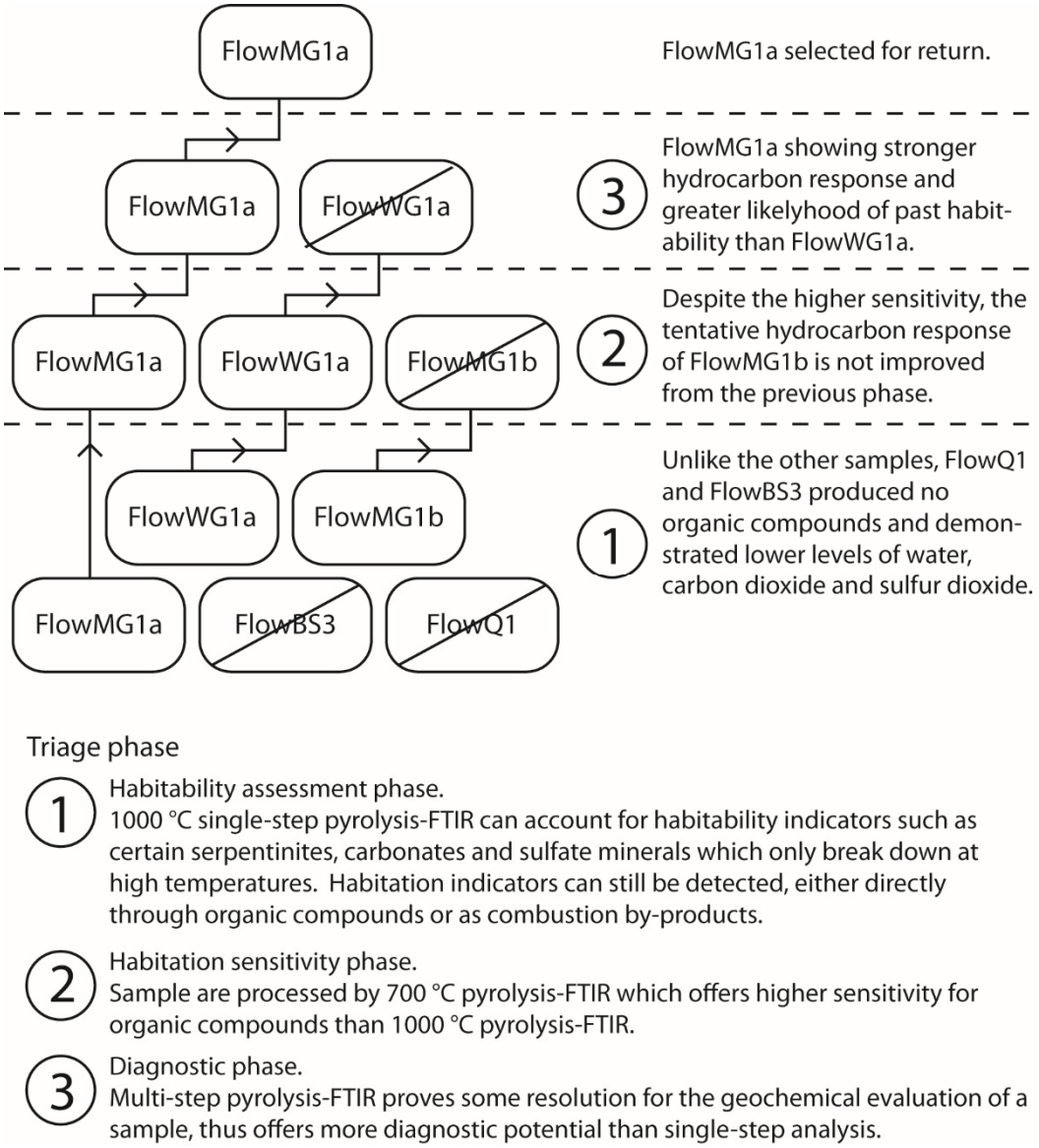



Figure 5.2. Example triage operation.

FTIR. The pyrolysis-FTIR triage process clearly identifies FlowMG1a to be the highest priority sample and assigns FlowBS3 and FlowMG1c to be the lowest priority samples. The pyrolysis-FTIR triage process is clearly correctly recognising the highest priority samples based in field observations of this active iron sulphate-rich acid stream ecosystem. Notably, the scoring system has prioritised the four microbial matt samples where FlowMG2a, DryMJ1a, FlowMG2a and FlowMJ1a routinely occupy four of the five highest positions. The next group of samples favoured by the scoring system are those with mineral components relatively high in goethite, namely FlowMG1b, FlowMG2b and FlowWG1a. The identification of the

goethite as high priorities is in accord with recently published data that reveal that goethite minerals derived from the humidity assisted decomposition of jarosite display high a preservation potential for organic records (Lewis et al. 2016).

The pyrolysis-FTIR triage process also provides refinements to prioritisations during the second stage of triage. For example, FlowMJ1b is the lowest ranked sample at 1000 °C, partly a result of having no detectable hydrocarbon signal, yet is then revealed to have an unconfirmed hydrocarbon signal during the high sensitivity 700 °C phase. In a Mars context, this would justify characterisation by multi-step analysis, through which we get an even stronger hydrocarbon signal in the 500 °C step. Failing to notice samples with appreciable organic matter content (like FlowMJ1b) is not acceptable for any Mars sample triage process, thus it is notable that the pyrolysis-FTIR triage process will detect such samples through the initial identification of simultaneously released water and carbon dioxide at the 1000 °C step and then identify organic matter through subsequent high sensitivity steps.

## 5.5 Conclusions

Due to the payload quantity restrictions imposed on vehicles returning from Mars to Earth, samples surveyed in situ by a caching rover must be categorised and ranked for the purpose of sample prioritisation for Mars Sample Return.

The quantitative chemical information produced by pyrolysis-FTIR is adequate to effectively rank candidate samples based on criteria relevant to the search for life on Mars: the habitability of the sample environment, the presence of organic compound biosignatures and the preservation potential of the sample for biosignatures.

The pyrolysis-FTIR triage operation is benefitted by a phased approach, which offers efficiency and additional layers of information.

# Chapter 6 Design considerations for a future Mars mission pyrolysis-FTIR spectrometer system

## 6.1 Introduction

With the concept of using pyrolysis-FTIR as a triage instrument to assess past habitability and past or present habitation of samples during Mars Sample Return now demonstrated, it is appropriate to consider how the bench top laboratory instrument could be adapted and improved for space flight missions.

## 6.2 Sampling gas cell design

### 6.2.1 Multi-pass cell

One of the issues that may be experienced when operating FTIR instruments is the current relatively insensitive nature of the technique. Yet sensitivity can be improved by optimising the cell design to improve the signal for a given quota of analytes. Modifications of cell design in this fashion could combine the benefits of FTIR with sensitivities approaching those achieved by GC-MS systems. In this project, signals were measured from absorbance spectra, which are produced from transmittance spectra.

Transmittance given by Beer-Lambert law (Braslavsky 2007):

$$T = \frac{I}{I_0} = e^{-\sigma N l} \tag{6.1}$$

Where $N$ is the particle number density, $l$ is the beam path length through the absorbing species, $\sigma$ is the absorption cross section of the molecular species, $I_0$ is the source intensity and $I$ is the transmitted intensity.

The factors influencing signal strength that can be controlled by cell design are the path length of the beam through the sample gas and the number density of target analytes in the sample gas.

In atmospheric sampling increasing the path length can be achieved simply by increasing the length of the sampling cell. Doing so increases the volume of gas being sampled but the number density of analytes remains constant. In pyrolysis-FTIR the number density of analytes in the beam will diminish with increasing the cell volume (as the number of analytes from a given solid sample is restricted to the amount the delivery mechanism can provide).

A multi-pass cell (i.e. a cell which reflects the sampling beam through its internal volume multiple times) provides a solution for increasing sensitivity by increasing the path length without changing volume thus without changing the number density of analytes. However, the following considerations must be made for multi-pass cells:

- Each reflection event attenuates the incident beam, thus noise contributions extrinsic to the source beam (e.g. thermal noise at the detector) become a larger factor in the final signal.
- The optical complexity increases with more beam passes through the cell, which does not favour polychromatic methods such as FTIR. Imperfect beam collimation is an inevitability, and any optical distortions (such as diffraction, refraction, beam spreading, scattering etc.), which are mostly frequency dependent, are going to worsen as the beam length and number of reflections is increased. Consistency and reliability is key on space missions.
- Reflection surfaces can be sensitive to thermal and mechanical influences. The temperature gradients faced on a space mission can be severe, and Pyrolysis-FTIR currently uses a heated cell to prevent condensation of pyrolysis products (at 250 °C). The material properties of a multiple-reflection configuration must accommodate for the thermal and mechanical requirements of a Mars mission.

While smaller cell volumes are desired (they require less energy to regulate their temperature, have lower surface area for condensation and use less gas to purge) it is unlikely that the restrictive size of the Brill cell will allow for easy adaptation to a multi-pass cell. However, off-the-shelf multi-pass cells exist for FTIR with chambers as small as 200 cc and are advertised as being workable at temperatures of 190 °C and in unstable conditions[4].

[4] http://www.mksinst.com/docs/UR/onlinemultigas2030ds.pdf

The following investigation was conducted to compare various cell designs, primarily to see how multi-reflection design would affect detection sensitivities for a pyrolysis-FTIR instrument. The following adaptations of the Beer-Lambert law are original to this investigation.

Considering the Beer-Lambert law from above for the case of a single-pass cell (like the Brill cell) the path length through the pyrolysis products is simply the cell length. Adjusting Equation (6.1) for a multi-reflection cell, where the total distance traversed through the pyrolysis products is the length of the cell multiplied by the number of passes of the beam, and accounting for the beam being diminished at each reflection event gives:

$$T_n = \frac{I}{I_0} = R^n e^{-\sigma N l_c (n+1)} \tag{6.2}$$

Where $n$ is the number of reflections, $R$ is the reflection co-efficient of the reflecting material and $l_c$ is the length of cell (and distance between the parallel reflecting surfaces).

In the event of collecting sample data, the transmission $T_n$ will arise from the absorption of sample and background molecules ($N_S + N_B$). To isolate the absorption of the sample molecules, the transmission of the sample analysis is divided by that of the background.

$$T_{S\&B} = R^n e^{-\sigma (N_S + N_B) l_c (n+1)} \tag{6.3}$$

$$T_B = R^n e^{-\sigma N_B l_c (n+1)} \tag{6.4}$$

$$T_S = \frac{T_{S\&B}}{T_B} = e^{-\sigma N_S l_c (n+1)} \tag{6.5}$$

In a transmittance spectrum, the strength of an absorption signal is given by $1 - T_S$ (i.e. the more prevalent the absorption by a molecular species, the lower $T_S$ will be, thus the signal $1 - T_S$ will be greater).

The validity of any signal is judged by the signal-to-noise ratio. This can be written:

$$\text{SNR} = \frac{1 - T_S}{T_{\text{RMS}}} \tag{6.6}$$

Where $T_{\text{RMS}}$ is the root-mean-square value of baseline transmission values, which arises from the noise in the detected intensity:

$$T_{\text{RMS}} = \frac{I_{RMS}}{I} = \frac{I_{RMS}}{I_0 R^n} \tag{6.7}$$

Where $I_{\text{RMS}}$ root-mean-square value of baseline fluctuations in the light intensity. While in practice the factors which influence the noise in the light signal can be complex and varying, this argument considers this noise value to be constant and extrinsic to the beam conditions (which is generally true for factors such as thermal noise at the detector).

Using Equations (6.5) & (6.7), the relationship for signal-to-noise ratio in a multi-pass cell becomes:

$$\text{SNR} = R^n \frac{I_0}{I_{\text{RMS}}} \left(1 - e^{-\sigma N_S l_c (n+1)}\right) \tag{6.8}$$

If a desired signal-to-noise ratio value is set, we can rearrange to give a relationship for the number density of sample analytes needed to meet the chosen signal-to-noise ratio for the number of reflections in a multi-pass cell.

$$N_S = -\frac{1}{\sigma l_c (n+1)} \ln\left(1 - \frac{1}{R^n} \frac{I_{\text{RMS}}}{I_0} \text{SNR}\right) \tag{6.9}$$

For the single pass Brill cell, Equation (6.7) shows a value for the $\frac{I_{\text{RMS}}}{I_0}$ term can be obtained simply by measuring the $T_{\text{RMS}}$ in a spectrum and taking the inverse (as $n = 0$, $R^n = 1$). If the cell design is the only thing that changes (i.e. source and detector are the same) the same $\frac{I_{\text{RMS}}}{I_0}$ value can be used to calculate estimates for the lower sensitivity limits of difference chemical species in difference cell designs.

Accurate data for absorption cross-section for different gas species is not readily available. However, the high-resolution transmission molecular absorption database (HITRAN) (Rothman et al. 2013) contains

the line strengths and other spectroscopic parameters of various molecular energy level transitions for a number of molecules and their isotopologues.

The line strength $S$ is the energy of a molecular energy transition and is the integration of the absorption cross-section $\sigma_v$ across a line (Bernath 2015).

$$S = \int \sigma_v \, dv \tag{6.10}$$

Where the value of $\sigma_v$ is governed by a normalised line-shape function $f(v - v_0)$ centred on the spatial frequency of the absorption line, $v_0$.

$$\sigma_v = S \, f(v - v_0) \tag{6.11}$$

For molecules in the gas phase, broadening of spectral lines is dominated by pressure broadening so a Lorentz profile is assumed for the line-shape function (Peach 1981, Rothman et al. 1998). HITRAN output includes data for the air-broadening of molecules, which is used for the half-width at half-maximum (HWHM), $\gamma$, in the line-shape function:

$$f(v - v_0) = L(v, v_0, \gamma) = \frac{1}{\pi} \frac{\gamma}{(v - v_0)^2 + \gamma^2} \tag{6.12}$$

Lines tend to be grouped into bands, which means that their broadened profiles are overlapping. Thus it is necessary to sum the contribution of every line $l$ in a band to get accurate absorption cross-section values:

$$\sigma_v = \sum_l S_l \, \frac{1}{\pi} \frac{\gamma_l}{(v - v_{0_l})^2 + {\gamma_l}^2} \tag{6.13}$$

A computer program was written to calculate absorption cross-sections from HITRAN line-strength data; the code can be viewed in Appendix C.1 and has been made available on an online repository[5]. Data sets

[5] https://github.com/petegordondev/JavaHitranCalc

of line strengths for the primary isotopologues of the gases used in this project (and other Mars relevant gases) were produced from the HITRAN 2004 dataset using the JavaHAWKS program (Rothman et al. 2004) for the 600 – 4000 $cm^{-1}$ spectral range. A temperature of 293 K was chosen with all available energy level transitions included.

This program was inspired by a previously written FORTRAN program[6] but implements an improved method (the mathematical approach was altered to omit an integration step which was computationally taxing). Calculating cross-sections in high detail from a large number of energy transitions requires significant time on a modestly powered computer, especially for the wide spectral range used by the pyrolysis-FTIR instrument. The program overcomes this by first analysing all line strengths across a spectral region at a low resolution, then identifies the location of spectral features and then reprocesses the local region of each feature in fine detail, thus useful high detail cross-section data can be calculated in a few minutes for wide spectral ranges. The program also gives the user the option of calculating over all spectral lines in the selected range, should that be preferred. The validity of the spectra output by the program was confirmed by comparison with images of cross-section data produced by the Pacific Northwest National Laboratory (PNNL) hosted by the University of Washington Virtual Planetary Laboratory (VPL)[7], an example of such a comparison is shown in **Error! Reference source not found.**.

**Error! Reference source not found.** lists the absorption cross-sections, calculated by the program written for this project, for spectral features used in the measurement of gas quantities in pyrolysis-FTIR spectra.

[6] http://home.pcisys.net/~bestwork.1/CalcAbs/CalcAbsHitran.html
[7] http://depts.washington.edu/naivpl/content/molecular-database

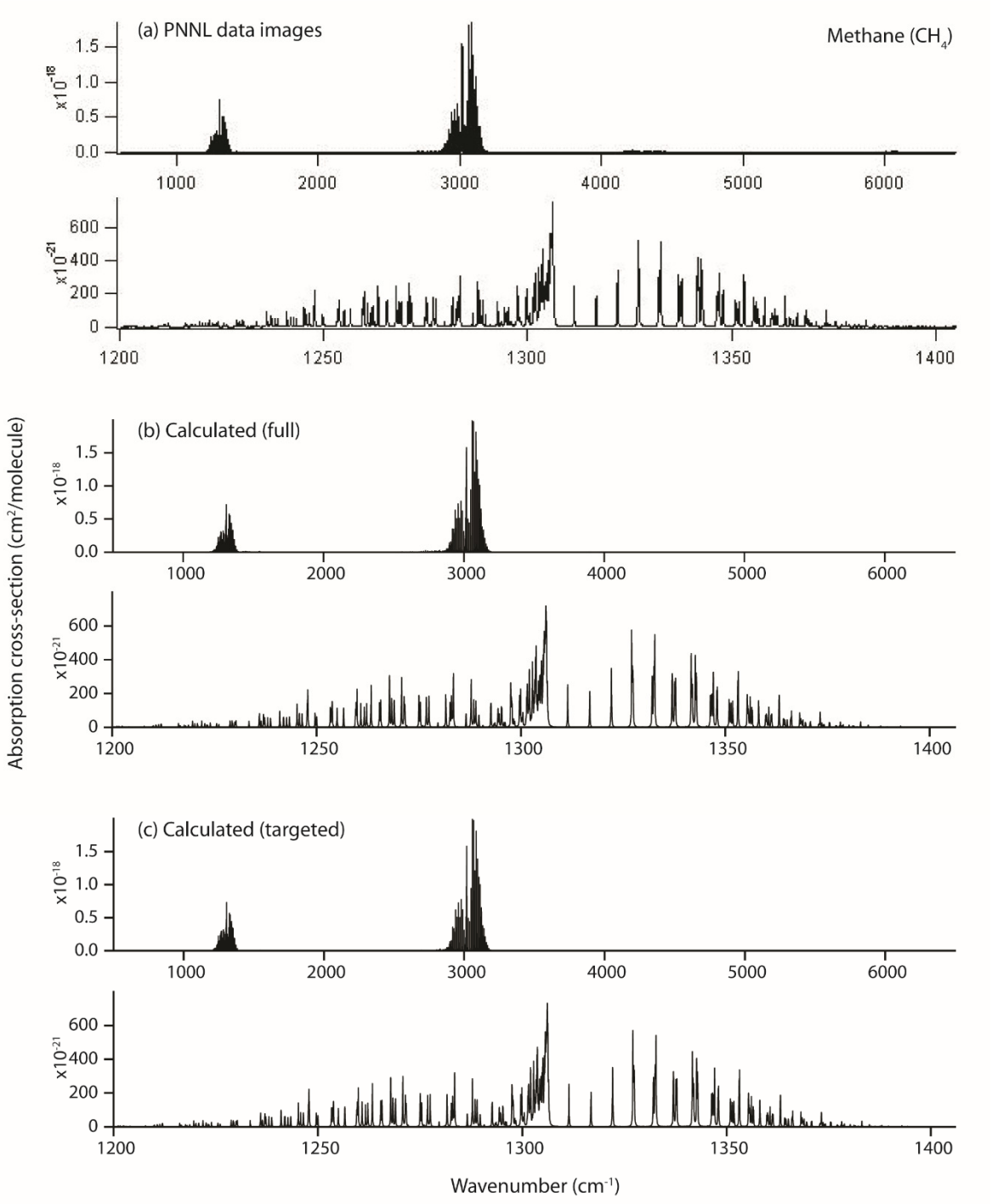



Figure 6.1. Comparison of absorption cross-section data sets for methane, demonstrating the success of the program written for this project (through the close resemblance of output to PNNL data). (a) These are images available on the VPL Molecular Spectroscopic Database made of PNNL data, which is not freely available. (b) and (c) are the resulting cross-section values calculated by the program written for this project, where the former calculated each value over the full specified frequency range at high resolution, while the latter only calculated at high resolution in regions where peaks had been identified by a low resolution calculation, saving significant computational time. Note the strong resemblance of calculated values to the PNNL images. (b) and (c) were only calculated in the 4000 $cm^{-1}$ to 600 $cm^{-1}$, hence the feature at 4200 $cm^{-1}$ in the first PNNL image is missing.

Table 6.1. Cross-section data for molecules commonly measured in the project and other Mars relevant molecules.

| Species | Vibrational mode | Wavenumber ($cm^{-1}$) | Cross-section ($cm^2$/molecule) |
|---|---|---|---|
| Carbon Dioxide ($CO_2$) | Antisymmetric stretch | 2361 | $1.57 \times 10^{-17}$ |
| Water ($H_2O$) | Stretch | 3854 | $6.59 \times 10^{-19}$ |
| Sulfur Dioxide ($SO_2$) | Antisymmetric stretch | 1361 | $1.10 \times 10^{-18}$ |
| Methane ($CH_4$) | Antisymmetric stretch | 3018 | $1.53 \times 10^{-18}$ |
| Acetylene ($C_2H_2$) | CH bend | 729 | $1.02 \times 10^{-17}$ |
| Ethylene ($C_2H_4$) | $CH_2$ wag | 949 | $1.60 \times 10^{-18}$ |
| Nitrous oxide ($N_2O$) | Antisymmetric stretch | 2237 | $4.30 \times 10^{-18}$ |
| Ammonia ($NH_3$) | Symmetric deformation | 967 | $2.24 \times 10_{-18}$ |
| Hydrogen cyanide (HCN) | Bend | 712 | $2.87 \times 10^{-18}$ |
| Methyl chloride ($CH_3Cl$) | CCl stretch | 733 | $1.59 \times 10^{-19}$ |
| Hydrogen chloride (HCl) | Stretch | 2963 | $2.35 \times 10^{-18}$ |
| Ethane ($C_2H_6$) | $CH_3$ stretch | 2987 | $1.54 \times 10^{-18}$ |
| Methanol ($CH_3OH$) | CO stretch | 1033 | $1.11 \times 10^{-18}$ |
| Formaldehyde ($H_2CO$) | $CH_2$ stretch | 2798 | $9.65 \times 10^{-19}$ |

Table 6.2 lists sensitivity limits calculated for a number of different cell designs: the single-pass Brill cell used currently in lab, the Brill cell modified to include a number of reflections (the number of reflections adopted from another FTIR cell design, the MKS MultiGas™ 2030) and three off-the-shelf multi-pass gas cells: an ultra-compact cell designed for tuned lasers with comparable volume to the Brill cell (the Sentinel Photonics DMPC03), a large volume cell for atmospheric sampling (the Specac Tornado™) and a multi-pass cell designed for FTIR (the MKS MultiGas™ 2030). These values were calculated by adopting a reflection co-efficient of 97.5%, a desired signal-to-noise ratio of 10 and a measured value of intrinsic noise in the lab bench pyrolysis-FTIR instrument.

The results show that in all cases, a reflection design improves upon the single-pass Brill cell. Despite having a vastly longer path length than the rival designs, we see that the Specac Tornado has the lowest increase in sensitivity of the multi-pass designs, due to its much larger volume being inappropriate for pyrolysis sample sizes. The Sentinel Photonics cell loses out due to the high number of reflections. These results show the MKS MultiGas 2030 to be the better cell-design, despite having a larger volume than the Brill cell.

Table 6.2. Sensitivity limits calculated for a number of different cell designs: the single-pass Brill cell used currently in lab, the Brill cell modified to include a number of reflections (the number of reflections adopted from a comparable design) and three off-the-shelf multi-pass gas cells: an ultra-compact cell (designed for tuned lasers) with comparable volume to the Brill cell, a large volume cell for atmospheric sampling and a multi-pass cell designed for FTIR. Concentrations values displayed are mass fractions of a representative sample mass (based on sample quantities processed by MSL). These values were calculated by adopting a reflection co-efficient of 97.5%, a desired signal-to-noise ratio of 10 and a measured value for intrinsic noise in the lab bench pyrolysis-FTIR instrument.

| Species | Brill Cell (Single-pass) | Brill Cell (Multi-pass) | Sentinel Photonics DMPC03 | Specac Tornado™ | MKS MultiGas™ 2030 |
|---|---|---|---|---|---|
| Carbon Dioxide ($CO_2$) | 150 ppb | 11 ppb | 18 ppb | 51 ppb | 10 ppb |
| Water ($H_2O$) | 1.5 ppm | 110 ppb | 170 ppb | 500 ppb | 94 ppb |
| Sulfur Dioxide ($SO_2$) | 3.1 ppm | 230 ppb | 360 ppb | 1.1 ppm | 200 ppb |
| Methane ($CH_4$) | 560 ppb | 42 ppb | 65 ppb | 190 ppb | 36 ppb |
| Acetylene ($C_2H_2$) | 140 ppb | 10 ppb | 16 ppb | 46 ppb | 8.8 ppb |
| Ethylene ($C_2H_4$) | 940 ppb | 70 ppb | 110 ppb | 320 ppb | 60 ppb |
| Nitrous oxide ($N_2O$) | 550 ppb | 41 ppb | 64 ppb | 190 ppb | 35 ppb |
| Ammonia ($NH_3$) | 410 ppb | 30 ppb | 47 ppb | 140 ppb | 26 ppb |
| Hydrogen cyanide (HCN) | 500 ppb | 38 ppb | 59 ppb | 170 ppb | 32 ppb |
| Methyl chloride ($CH_3Cl$) | 17 ppm | 1.3 ppm | 2 ppm | 5.8 ppm | 1.1 ppm |
| Hydrogen chloride (HCl) | 830 ppb | 62 ppb | 97 ppb | 280 ppb | 53 ppb |
| Ethane ($C_2H_6$) | 1 ppm | 78 ppb | 120 ppb | 350 ppb | 67 ppb |
| Methanol ($CH_3OH$) | 1.5 ppm | 120 ppb | 180 ppb | 520 ppb | 99 ppb |
| Formaldehyde ($H_2CO$) | 1.7 ppm | 120 ppb | 190 ppb | 560 ppb | 110 ppb |
| **Improvement factor** | | **13** | **9** | **3** | **16** |
| **No. of reflections** | **0** | **23** | **106** | **31** | **23*** |
| **Length (cm)** | **2** | **2** | **3.5** | **25** | **21.6** |
| **Volume ($cm^3$)** | **21.5** | **21.5** | **32** | **1330** | **200** |

*Estimated based on other advertised parameters

It should be noted that these values are 'best case' estimates; factors that influence the signal-to-noise ratio – like variability in the chemical background – have been overlooked and will raise sensitivity limit values in practice. The reflection coefficient and intensity variables required in Equation (6.9) are in reality functions of wavelength, but approximating these to constants for the entire spectral range was deemed satisfactory to produce results which act as a guideline. An important assumption was that pyrolysis products would diffuse evenly in all cases; the ability to successfully deliver sample gases to the sampling volume should be ensured before adopting a multi-cell design.

The equations and methods developed here should be used to guide the design choices, when choosing reflection material, cell dimensions and optical design.

### 6.2.2 Cell windows

Gases produced by thermal evolution techniques are susceptible to secondary reactions which adds to the challenge of interpreting results. All measures should be taken in instrument design to restrict uncontrolled secondary reactions to those between the pyrolysis products themselves.

It became apparent that the potassium bromide (KBr) windows used in the early phases of the project were unsuitable. It was suspected that water and sulfur dioxide reactions were responsible for corrosion on the window surfaces and introduced volatility in the background conditions. KBr is highly water soluble and hydroscopic, and sulfur dioxide can react with water to produce sulfuric acid which can the react with the KBr window (Volz 1979).

These were replaced with zinc selenide (ZnSe) windows, which were not susceptible to water interaction thus acids are unlikely to form directly on the surface, although if acids were to form in the atmosphere of the cell ZnSe would still be sensitive to this.

It is clear that the final choice of window material for the final instrument will require careful consideration. The transmission efficiency, spectral range, refractive index, material properties and chemical properties must be considered.

Mini-TES uses a cadmium telluride (CdTe) window for the interface between the interferometer and external environment (Christensen et al. 2003). CdTe suffers less from thermal expansion and is significantly stronger than KBr (previously used in the Brill cell windows) however it is more than twice as dense[8]. Its optical window of 0.9 - 30.0 μ would be sufficient for the 600 - 4000 $cm^{-1}$ range currently used

[8] http://www.makeitfrom.com/compare-materials/?A=Cadmium-Telluride-CdTe&B=Potassium-Bromide-KBr

on our FTIR instrument, however KBr has shown better transmission at these wavelengths (~60%[9] for CdTe as opposed to ~90%[10] for KBr). Note that CdTe is toxic, so it is not suitable for general lab investigations.

## 6.3 Interferometer type

The Michelson–Morley interferometer used in the lab-bench pyrolysis-FTIR has been designed for stable, level conditions – not the violent inertial trial of space flight and the unsteady platform of a mobile rover. Moving mirror requires precision and regular motion, although the motion can be tracked with a reference laser. Moving part interferometers have been used on rover missions before: Mini-TES on the MER rovers used Michelson–Morley interferometers, although there may be more suitable alternatives. A suitably chosen interferometer could allow multiple purpose use, such as remote sensing like on Mini-TES or solid state FTIR analysis.

### 6.3.1 Rotating refractor

An FTIR instrument concept developed by NASA's Jet Propulsion Laboratory employs a rotating refractor interferometer design rather than a Michelson–Morley style, to eliminate the need for a reference laser and overcome the mechanical instability of a linearly moving mirror (Anderson et al. 2005). This interferometer was commercially available and initially designed for rugged applications such as deployment on military aircraft, making it ideal for space missions. It is compact, lightweight and can achieve resolutions of 8 – 1 $cm^{-1}$ (Wadsworth and Dybwad 2002). For comparison, measurements in the project were generally taken with a resolution of 4 $cm^{-1}$. Called a 'Turbo FT' interferometer, this rotary refractor type designed by Designs & Prototypes is displayed in Figure 6.2.

[9] http://www.globalopticsuk.com/cadmium-telleride.htm
[10] http://www.globalopticsuk.com/potassium-bromide.htm

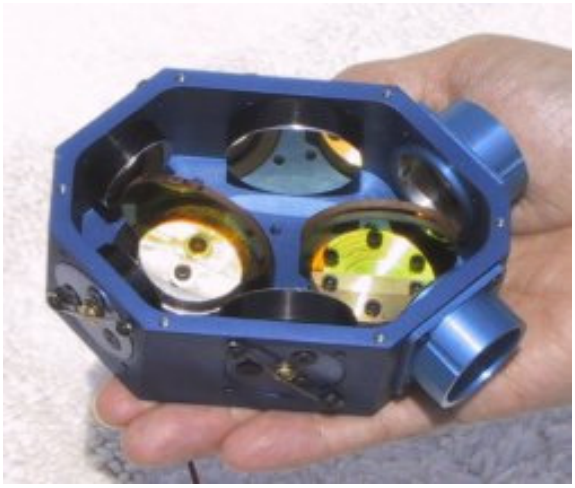


Figure 6.2 - The Designs & Prototypes 'Turbo FT' rotary refractor interferometer adopted by the JPL FTIR. The 'space frame' housing boasts excellent mechanical and thermal stability and weighs just over 0.55 kg (Wadsworth and Dybwad 2002, Mahaffy et al. 2009).

### 6.3.2 Non-moving parts spectrometry

There are numerous designs of interferometer that eliminate the need for the moving mirror or rotary refractor. This would be beneficial as high speed, high precision moving parts are a potential point of failure which in the case of an FTIR instrument would be fatal to operation.

Non-moving parts interferometers can achieve interferograms utilizing birefringence (Huang and Wang 2012, Harvey and Fletcher-Holmes 2004), wave-front division (Möller 1995, Hashimoto and Kawata 1992, Okamoto, Kawata and Minami 1984) or spectrograms through dispersion like OMEGA (Bibring et al. 2004). However, these techniques can be less resource efficient: source light is discarded post-collimation in the case of some designs: the wave division and stepped mirror technique described in Möller (1995) requires that only the zero-order light resulting from diffraction patterns reaches the detector, and techniques without moving parts can require larger detector arrays, which are more costly to cool and require larger spatial dimensions. Thus these instruments cannot be 'throughput matched', which is "when the detector is exactly filled by the image of the source while the beam passes through the interferometer with the maximum allowed throughput" (Griffiths and De Haseth 2007), which is required for optimal sensitivity.

### 6.3.3 Tuned laser

One potential solution to the relatively low sensitivities of FTIR systems is the inclusion of tuneable laser spectrometer. Tuneable laser spectrometers achieve higher sensitivities by concentrating on a single absorption line in the absorption spectrum of a target analyte. Tunable laser spectrometers can measure many of the gases encountered during pyrolysis-FTIR but at the parts per billion level. A tuneable laser spectrometer system is ideally suited to the Martian environment and is already operating on Mars as part of the Sample Analysis on Mars instrument on MSL (Mahaffy et al. 2012). The increased sensitivity for a selected number of key compounds with diagnostic qualities such as methane would be of great benefit for triage during a Mars Sample Return mission.

## 6.4 Mitigating consumables

A MSL caching rover could require a mission lifespan of at least 500 sols in which it should traverse 20 km, all while analysing enough samples to produce a cache of between 19 and 37 rock cores from geologically distinct locations (Mattingly and May 2011). Thus we must consider the capability of instruments to remain operable over the required mission time frame and process adequate volumes of samples. A caching rover may also be tasked with secondary scientific objectives which increases the required quota of analyses (Pratt et al. 2009).

Reliance on non-replenishable physical consumables puts an obvious limit on the total number of analyses. The Mars Exploration Rover Mission (MER) rovers were designed to last for only 90 sols and to travel 600 m (Crisp et al. 2003). Multiple extensions of MER can be accredited to the permissive design of the rovers, with instruments relying mainly on electrical power. Eradicating physical consumables also saves on spatial and weight requirements, although the resource costs of any compensating technology has to be accounted for.

Currently our lab based instrument utilises three physical consumables in its fundamental mode of operation: helium purge gas, nitrogen coolant and quartz pyrolysis boats.

### 6.4.1 Purge gas for sampling cell

On Earth, the purge gas primary function is to limit oxidation during pyrolysis. Mars however has a relatively oxygen poor atmosphere, thus use of Martian atmosphere could be considered as a replacement or alleviation mechanism for a purge gas reservoir.

Carbon dioxide makes up >95% of the atmosphere. At Earth pressures this would cause significant obfuscation of the useful carbon dioxide signal from pyrolysis products, but the Mars atmosphere is significantly sparser thus the background carbon dioxide presents less of a problem. For a cell the same volume as that used in the lab bench pyrolysis-FTIR instrument, the cell would contain approximately 400 µg of carbon dioxide when filled with Martian atmosphere, which would result in the intensity that reaches the detector (at 2364 $cm^{-1}$) being diminished by 30% in the current system. This would mean a decreased signal-to-noise ratio for carbon dioxide signals, but the following should be considered:

- Carbon dioxide signals are the strongest of all the gases utilised in pyrolysis-FTIR, thus a hit in sensitivity can often be afforded.
- Carbon dioxide quantities from the Martian atmosphere could be well accounted for in the background spectra, thus have little influence on variability in the sample signal.
- Carbon dioxide produces well constrained spectral features thus the lower signal-to-noise will impact few other gases, importantly none of the other gases observed in this project.

However, introducing an unaltered Martian atmosphere will bring approximately 0.6 µg of oxygen into the cell. This cannot be accounted for in the background spectra as oxygen is not infrared active. However, should Martian atmosphere be used in the instrument, it will be filtered and treated by processes which could include an oxygen scrubber. Vacuum pumps could be used on the gas cell prior to background collection and sampling to reduce the levels of carbon dioxide and oxygen in the cell. Vacuum pumps have been utilised successfully on MSL gas chamber instruments.

The other main Martian atmosphere gases, argon and nitrogen, are not IR active, and have insignificant chemical influence.

If use of the abundant external atmosphere is possible, the volume of the gas chamber becomes less of a restrictive consideration. A larger gas chamber (which may be required for a multi-pass cell) would require greater volumes of purge gas per analysis, which is undesirable when relying on an on-board helium reservoir.

Designing mechanisms for introducing Martian atmosphere to the pyrolysis-FTIR gas train brings the added scientific capability of atmospheric sampling.

The boiling temperatures of different compounds in the solid will vary depending on the gas used for the cell atmosphere, with a vacuum chamber having the lowest boiling points. The lower pressure of a near vacuum will also reduce the rate of secondary reactions.

### 6.4.2 Detector cooling

The lab bench pyrolysis-FTIR analyses were conducted using a liquid nitrogen cooled MCT/A detector. Liquid nitrogen is 80% as heavy as water thus is inappropriate for inclusion on a rover with long life requirements.

Mini-TES mass and spatial requirements mandated the use of uncooled detectors (Silverman et al. 2006) and uncooled DTGS detectors sufficiently met the sensitivity requirements (Christensen et al. 2003), though admittedly the sensitivity requirements of remote sensing and pyrolysis-FTIR are different. Cooled MCT/A detectors offer sensitivity gains over the uncooled DTGS option available on the lab bench instrument, thus their inclusion is desired.

Active, electronic Sterling cycle coolers can offer an alternative cooling solution. A Ricor K508 rotary Stirling cryocooler was used on MSL to cool the CheMin CCD to 173 K (Johnson, Lysek and Morookian

2014). This is still much higher than the 77 K of liquid nitrogen, however may still provide adequate sensitivity.

### 6.4.3 Pyrolysis solution

The lab bench pyrolysis-FTIR applies thermal energy to the rock samples by means of a heated platinum coil. For this, the powdered samples need to be housed in small quartz tubes, or boats, and plugged at both ends by small amounts of quartz wool. This solution is not feasible for Mars operation for the following reasons:

- Loading samples and sealing powder in place would require complex mechanical manipulation.
- The platinum coil, into which the quartz tubes are loaded, can be easily damaged by rough handling. Misshaping the coil can invalidate the temperature calibration or cause a damaging short circuit.
- Quartz tubes are difficult to clean. In some cases, a combination of solvent baths, acid baths, sonication, scraping and blow torch application have not been enough to clean a tube.

The pyrolysis cups used on MSL offer a more robust solution which also analyse a larger sample quantity, which benefits sensitivity. However, these cups were not designed for flash heating and only have a limited number of uses.

The pyrolysis mechanism presents itself as the most likely limiting factor in producing the most robust, high sample capacity instrument possible. It is likely that a bespoke engineering solution will be required.

## 6.5 Volatiles trap & atmospheric sampling

A trap for volatiles was included on board the MSL SAM instrument to trap hydrocarbon compounds released from heated solid samples (Mahaffy et al. 2012). A similar trap could be added to the gas stream of the pyrolysis-FTIR instrument (downstream from the sample gas cell) to collect analytes over successive

analyses: this would result in higher sensitivity for an aggregate of samples (compared to the sensitivity of individual sample analyses). The trap would have to be desorbed back to the gas cell at appropriate intervals to maintain geographic relevance of any positive results.

However, as traps are lightweight and compact, multiple traps could be used for different purposes. For example, a trap to collect an aggregation of hydrocarbons from the most recent subset of samples (as described above) and a trap to accumulate and retain all volatiles exhausted from all samples. A trap could also be included on the atmospheric inlet, to both filter Martian atmosphere for utility (i.e. purging the sampling cell), and to accumulate atmospheric volatiles for higher sensitivity atmospheric measurements.

The efficacy of trapping materials are commonly understood through 'breakthrough volumes', the volume of gas required to push a compound through 1 gram of an adsorbing material (Dettmer and Engewald 2002). For the following investigations terrestrially applicable breakthrough volumes[11] were converted to molar quantities so that they could be applied in the Martian context.

Should volatile trap be in place on a pyrolysis-FTIR instrument and should a solid sample produce volatiles, the volatiles will be captured by the trap and held until the breakthrough volume is reached. The carrier gas in this case will be the cell atmosphere during the pyrolysis-FTIR analysis and any subsequent purge gas, thus a breakthrough volume will eventually be reached after successive analyses. The minimum concentration is given by the number of analyses that can occur before the minimum detectable number of analytes (detectable by the FTIR measurement apparatus) begin to be lost from the trap.

The minimum detectable number of analytes were calculated in Section 6.2.1 for individual solid samples (of quantities equivalent to those processed on MSL). Using these values, Table 6.4 lists possible sensitivity limits for successive solid sample analyses with the addition of an MSL equivalent volatiles trap, maintained

[11] http://www.sisweb.com/index/referenc/resins.htm

Table 6.4. Possible sensitivity limits for solid sample analyses with the addition of an MSL equivalent volatiles trap. Concentration values are mass fractions while the numbers in bold are the number of repeat analyses after which volatiles are lost from the trap (from which the minimum detectable concentration arises). These calculation assumed a carrier gas volume equivalent to three times the sampling cell volume is used in each analysis. Methane values for the Specac Tornado cannot be quoted as the large volume of the cell means that the breakthrough volume for methane is exceeded in just one analysis procedure.

| Species | Brill Cell (Single-pass) | | Specac Tornado™ | | MKS MultiGas™ 2030 | |
|---|---|---|---|---|---|---|
| Methane ($CH_4$) | 19 ppb | 30 | N/A | | 12 ppb | 3 |
| Ethane ($C_2H_6$) | 2.5 ppb | 412 | 59 ppb | 6 | 1.5 ppb | 44 |
| Methanol ($CH_3OH$) | 0.6 ppb | 2609 | 12 ppb | 42 | 0.4 ppb | 280 |

at 0 °C, to three designs of gas cell: the Brill cell used in this project, a FTIR multi-pass cell designed for atmospheric sampling (Specac Tornado) and a low volume multi-pass cell designed for FTIR (MKS MultiGas 2030). Concentration values are mass fractions while the numbers in bold are the number of repeat analyses after which volatiles are lost from the trap. These calculations assumed a carrier gas volume equivalent to three times the sampling cell volume is used in each analysis of ambient Martian atmospheric pressure. Methane values for the Specac Tornado cannot be quoted as the large volume of the cell means that the breakthrough volume for methane is exceeded in just one analysis procedure.

Table 6.3 uses breakthrough volumes and the pyrolysis-FTIR minimum sensitivity limits (as calculated in Section 6.2.1) to estimate lower detection limits for molar concentrations of organic compounds in the Martian atmosphere. These have been calculated for the same three designs of gas cell included in the pyrolysis-FTIR investigation above. The values in bold represent the improved limits when a volatile trap

Table 6.3. Lower detection limits for molar concentrations of example organic compounds in the Martian atmosphere. These have been calculated for three designs of gas cell: the Brill cell used in this project, a FTIR multi-pass cell designed for atmospheric sampling (Specac Tornado) and a low volume multi-pass cell designed for FTIR (MKS MultiGas 2030). The values in bold represent the improved limits when a volatile trap (of similar design to that used for MSL) is utilised, maintained at 0 °C. Volumes are listed for the amount of Martian atmosphere that needs to be sampled to achieve the limits in bold.

| Species | Volume (L) | Brill Cell (Single-pass) | | Specac Tornado™ | | MKS MultiGas™ 2030 | |
|---|---|---|---|---|---|---|---|
| Methane ($CH_4$) | 2 | 1100 ppm | **12 ppm** | 5.8 ppm | **3.9 ppm** | 7.3 ppm | **750 ppb** |
| Ethane ($C_2H_6$) | 27 | 1100 ppm | **850 ppb** | 5.8 ppm | **290 ppb** | 7.3 ppm | **55 ppb** |
| Methanol ($CH_3OH$) | 170 | 1500 ppm | **190 ppb** | 8 ppm | **63 ppb** | 10 ppm | **12 ppb** |

(of similar design to that used for MSL) is utilised, maintained at 0 °C. Volumes are listed for the amount of Martian atmosphere required to be sampled to achieve the limits in bold.

Calculations could only be done for methane, ethane and methanol as only these gases had the associated HITRAN data (for calculating absorption cross-sections) in addition to published break through volumes for each of the trapping materials used in the MSL trap. Note that data on Carbosieve G (one of the materials used on MSL) was not available, so this investigation substituted this for a comparable material, Carbosieve SIII.

In all cases the addition of a trap offers gains in sensitivity. Due to the nature of trapping material, the factor of sensitivity improvement would be even greater for compounds of increasing size, and this is demonstrated in these results. For heavier compounds, the sampling volumes required to achieve detection at the sensitivity limit (for both solid and atmospheric analysis) are unfeasible, but demonstrate how effectively the trap can retain compounds.

For atmospheric sampling (without a trap) it is interesting to note that the smaller volume MKS MultiGas™ 2030 offers comparable sensitivities to the large volume Specac Tornado for each compound. However, because of the smaller sampling volume, the MKS MultiGas™ 2030 makes greater gains in sensitivity than the Specac Tornado due to the addition of a trap.

If available, the maximum abundances of volatiles that can be held by a trap could be used to calculate even better sensitivity limits for a design where saturation is achieved by bypassing the breakthrough volume by thermally desorbing a primary trap onto a secondary trap. However, saturation data of trapping materials is not readily available for even the most common volatiles. Helmig and Vierling (1995) have calculated saturation quantities of different trapping materials for water, but as these materials have a low propensity for water, a MSL equivalent trap would not hold enough water to improve upon quantities already detectable in the pyrolysis-FTIR instrument.

A volatiles trap can be a potential source of contamination so the benefits must outweigh the risk of contamination. The potential levels of contamination on MSL were considered too low to obfuscate the Martian chlorobenzene signal (Miller et al. 2015), thus are unlikely to present a problem for pyrolysis-FTIR with its relative lower sensitivity.

## 6.6 Other considerations

### 6.6.1 Sampling time

This project has demonstrated that useful geochemical data can be obtained by pyrolysis-FTIR from a sample in a matter of minutes. Previously, Mars rovers have obtained contact chemical information over much longer time frames (e.g. 2 - 4 hours for trace elements, 8 hours for carbon by the MER rovers (Rieder et al. 2003) and 4 – 6 hours for an EGA-GCMS-TLS sequence on MSL (Mahaffy et al. 2012)). The speed of pyrolysis-FTIR means a higher frequency of samples can be processed than on previous missions. This means higher geochemical resolution across the spatial domain is offered in a given locale.

However, it is highly likely that the speed of the pyrolysis-FTIR will outpace the delivery mechanisms of samples: drilling can take up to 4 hours (depending on sample target rock, drilling mode and environmental conditions) and sieving can take up to an additional hour on MSL (Anderson et al. 2012). While MSL offers a guideline sample delivery timeframe, it is recognised that a caching rover should have a sample acquisition system tailored to its needs, which should consider effective use of the sample turnaround of the triage analysis suite in its design. However, it is unlikely that any feasible sample delivery can match the rates of pyrolysis-FTIR sample turnover, and this means pyrolysis-FTIR is afforded the luxury of extending the sampling time to the time interval between sample deliveries.

Longer sampling times allows for:

- Higher resolution spectra.
- Greater number of co-added interferograms used in the final sample spectrum, enhancing the signal-to-noise ratio.
- The option of slow gradient heating as opposed to flash pyrolysis.
- Greater number of temperature steps in multi-step analysis.
- More assured thermal equilibrium in the sampling cell before measurement, ensuring more consistency between background and sample spectrum conditions.

However, many of these benefits are only possible should the instrument conditions be adequately stable during analyses.

Experience with lab bench version has shown that analytes have a tendency to condense over time, despite the cell walls being heated to 250 °C, though this is suspected to arise from avoidable design flaws. One point of weakness is the long entrance pipe which houses the pyrolysis rod during operation - this part of the cell is not directly heated to the same temperature as the main body of the Brill cell and had the potential to act as a 'cold finger'. Also the pyrolysis rod does not make a neat fit with this housing, thus the gap is partly responsible for weakening the signal by unnecessarily increasing the cell volume thus lowering the number density of analytes in the beam path.

Lab bench experiments, on occasion, exhibited interference fringes within the resulting spectra. Interference fringes can appear when parallel reflection boundaries, which are perpendicular to the beam, cause the beam to partially reflect leading to the reflected component recombining with some new optical path difference, causing destructive interference.

It is possible to use the spacing of fringes to calculate the path length between reflection boundaries. In the case of the lab bench FTIR instrument the 43 $cm^{-1}$ fringe separation means a separation between reflection

boundaries of approximately 0.116 mm. Being much larger than the cell window thickness (4 mm) and the cell path length between windows (20 mm) it is not apparent what two reflection boundaries could be that distance apart.

It was discovered that the length of time following sample loading and sample analysis was correlated with the amplitude of the fringes – shorter intervals between samples loading and spectrum acquisition meant stronger fringes.

### 6.6.2 Resolution

The resolution of a spectrogram is the inverse of the maximum optical path difference (OPD) implemented to create the interference pattern thus, in a Michelson type interferometer, the mirror must move further to obtain higher resolutions. If the mirror moves at a constant speed, acquiring spectra of increasing resolution takes more time. Higher resolutions reveal spectral fine structure, reducing spectral overlap between different gas species, which benefits identification. Higher resolutions also reduce absorbance nonlinearity which can give more accurate quantification.

Jaakkola et al. (1997) demonstrate that high resolution spectra do not offer higher sensitivities than lower resolution measurements (conducted under identical experimental conditions), due to lower signal-to-noise ratios at higher resolutions. The signal-to-noise ratio is largely dependent on optical throughput, which is partially set by resolution; the best sensitivity is given when the instrument is throughput matched. Thus the optimal resolution is set by instrument design and the application specific resolution requirements should inform the optical design.

It should be noted that the resolution used in this project, $4 cm^{-1}$, revealed adequate structure for the purpose of identifying and quantifying gases of interest.

### 6.6.3 Pyrolysis temperature steps

The temperatures quoted in this project should only be considered nominal and applicable to this configuration of pyrolysis, as it is unlikely that the temperatures stated are the actual temperatures in the sample during pyrolysis. This means that an improved pyrolysis-FTIR instrument would have to be reassessed for the optimal temperatures for different types of analyses (i.e. for high mineral sensitivity and organic compound sensitivity).

### 6.6.4 Beyond Mars Sample Return

Use of pyrolysis-FTIR beyond Mars Sample Return is feasible and worthy of consideration due to its relatively light requirement demands and demonstrated analytical power. Following the first manned landing on Mars, adaptation of pyrolysis-FTIR to a hand operated, portable tool could give an astronaut almost real-time geochemical data as they perform exploration. Robotic missions to the moons of the gas giants are hoped to return a wealth of science, of which a pyrolysis-FTIR instrument could be a contributor.

Part of NASA's future roadmap is to capture an asteroid into lunar orbit and have astronauts perform scientific operations in situ (Strange et al. 2013) and pyrolysis-FTIR could be adapted to be operated manually as part of an astronaut's portable toolkit. Near Earth asteroids also present a future ambition of private space enterprise (Lewicki et al. 2013). Initially remote observations would be used to identify asteroids which offer the highest financial return, but subsequently pyrolysis-FTIR could be a helpful tool in prospecting the most effective drilling sites on a more local level.

Design revisions would be required to repurpose pyrolysis-FTIR to the interplanetary environment, however a number of these could be advantageous to the resource limitations of pyrolysis-FTIR: the increased solar flux at the orbital distances of near Earth objects (NEOs) would afford a higher operating power than on Mars (when using solar power as an energy source); passive radiation of heat could assist electronic cryocoolers in keeping the detectors at low temperatures for improved sensitivity and use of the near perfect vacuum of space would eliminate the need for a cell atmosphere or a purge gas.

# Chapter 7 Discussion & Conclusions

This thesis aimed to demonstrate the capability of a pyrolysis-FTIR instrument as a triage instrument for Mars Sample Return and devise recommendations for its future design.

Because the highest priority objective of Mars Sample Return is to find evidence for past or present life on Mars, the thesis project was focused on demonstrating the ability of pyrolysis-FTIR to assess key factors relating to life – regions of habitability, biosignatures and the preservation of biosignatures – from rock samples. With the pyrolysis-FTIR instrument being in a lab bench form, the project also aimed at making considerations for the advancement of the method towards a flight ready instrument.

Thus the key questions addressed by this project were:

i. What diagnostic information can pyrolysis-FTIR offer on mineral samples and, through which, what capacity does pyrolysis-FTIR have to recognise minerals which indicate habitability, habitation and preservation potential for biosignatures?
ii. What are the sensitivity limits for the detection of organic matter by pyrolysis-FTIR?
iii. To what extent does the mineral composition of a sample affect the signal of organic matter contained within, and what are the likely effects to be experienced on Mars?
iv. How could pyrolysis-FTIR be used for effective triage on Mars and how does it perform on 'real world' sample set?
v. What fundamental design improvements need to be made to progress pyrolysis-FTIR towards a viable mission instrument?

To achieve these aims it was important to gain an understanding of space missions so a future instrument could be envisioned. An understanding of the general space mission design process was garnered, while attention was paid to relevant non-similar instruments; Mini-TES for being a successfully deployed in situ Michelson-Morley type FTIR interferometer and the JPL DRIFTS FTIR instrument, for being a prototype FTIR instrument designed for analysing solid rock samples. The SAM instrument on MSL was recognised as a point of reference for the operation and output of a thermal decomposition instrument.

To demonstrate the analytical capability of pyrolysis-FTIR a series of experiments were conducted.

To assess the capability of the instrument to identify regions of past or present habitability from the mineral record, a broad range of terrestrial mineral types were subjected to pyrolysis-FTIR analysis. The mineral set was chosen such that it included mineral types representative of mineralogically defined eras on Mars (the Phyllosian, the Theiikian and the Siderikian), minerals which are indicative of habitable environments, minerals recognised for preservation potential for biosignatures and minerals containing organic compounds. Different modes of pyrolysis-FTIR were used in the aim of assessing their advantages.

Organic compounds can be a biosignature of paramount importance. Thus an investigation was conducted to ascertain the sensitivity limits of the pyrolysis-FTIR instrument for detecting organic compounds. This investigation involved processing samples containing controlled quantities of a complex organic assemblage of biotic origin (*Lycopodium* plant spores). Samples were analysed using a pyrolysis protocol found to maximise the hydrocarbon signal returned by thermal decomposition of *Lycopodium*. Obtaining sets containing high numbers of data allowed a statistical interpretation of the instrument performance.

The use of *Lycopodium* spores was extended to an investigation to answer the question of mineral influences on the organic compounds signal. Different concentrations of *Lycopodium* spores were added to a range of Mars relevant rock types and analysed by pyrolysis-FTIR at the temperature found to be most suited to detection of *Lycopodium* spores and at another temperature designed to maximise the thermal decomposition of minerals.

A field study was conducted using the pyrolysis-FTIR instrument to demonstrate triage operation. Samples were collected from a sulfur rich stream which was recognised to be inhabited. A scoring logic was created to facilitate prioritisation of samples based on pyrolysis-FTIR results.

The habitability investigation demonstrated that important gases, which have been the target of previous and current space missions, are detectable by pyrolysis-FTIR (specifically water, carbon dioxide and sulfur

dioxide) which can lead to the identification of habitable environments. It was learned that, in addition to the presence of these gases alone giving some indication about conditions suitable for life, the temperature they are observed to be liberated from the sample offered another layer of information about the host material. Quantitative analysis by Pyrolysis-FTIR was shown to permit further assessment of the habitability of a region, as quantities of the different gases detected informs on the composition of the rock.

The sensitivity investigation revealed that, in a quantity of sample similar to those processed by MSL, organic compounds could be detected directly in quantities on the order of tens of parts per million at the detection limit where false positives are unlikely.

If was found that the detection of organic matter by pyrolysis-FTIR can be influenced by different mineral types when also present in the sample, similarly to other thermal extraction methods like pyrolysis-GC-MS; the particular type of mineral matrix determines if organic compounds will ultimately present themselves in the pyrolysis products. If available in sufficient quantities, sulfate and chlorine components of rocks can completely obscure the potential organic compound signal however the by-products of the destruction of organic compounds, mainly water and carbon dioxide, can lead to the identification of an organic bearing rock. This could make detection of organic compounds in regions defining the Theiikian era more challenging than finding similar quantities in regions of the Phyllosian. The iron sulphate jarosite has been identified as a mineral which causes oxidation of organic compounds and this mineral has been found on Mars. Palagonite can lead to the chlorination of organic compounds; a problem encountered on Mars by MSL. Palagonite is also found on Mars. The destructive effects of the aforementioned mineral phases on organic compounds can be reduced by using lower pyrolysis temperatures to liberate organic compounds.

Through the sulfate stream field study it was shown that pyrolysis-FTIR provides adequate layers of information to discern between samples and prioritise them when conducting field operations. A phased approach can enhance resource efficiency when a large sampling set is presented. The phased approach is permitted by the flexibility of pyrolysis-FTIR operation. Different modes are possible with the controllable

temperatures of the pyrolysis probe. A low energy cost, rapid, high sensitivity assessment can be used to survey all samples initially, and worthy candidates can be examined in better detail with modes that target particular analytes or modes that offer resolved thermal decomposition steps. A scoring system allows rapid discernment of samples but would benefit from a more robust algorithmic approach.

To demonstrate improvements that could be made to the design of pyrolysis-FTIR, the different components were considered. Through application of the Beer-Lambert law to a multi-pass gas cell, improvements to sensitivity were calculated for a range of possible cell designs. The sensitivity limits achievable by the addition of a volatile trap were calculated also. Arguments were made for other design alterations by analogy with other instruments.

Pyrolysis-FTIR has been demonstrated to have technical viability as a Mars Sample Return triage instrument. In addition to the credence given to the components of pyrolysis-FTIR through involvement on board successful in situ missions, the technical performance parameters described by Wertz and Larson (1999) and outlined in the introduction, have been considered. The resolution of the spectra have been shown to provide unambiguous identifications of target gases. Detection sensitivity has been proven adequate for habitability indicators while sensitivities for organic matter fall short of other analytical methods previously deployed to Mars, specifically GC-MS. Through the numerical analyses conducted, addition of a multi-pass cell and/or a volatile trap have been identified as solutions that offer significant improvements in organic compound detection. The sample turnover of a few minutes far exceeds the sampling rate of other instruments on current rovers thus is ideal for a high frequency sampling rate. The number of uses is heavily depended on final design; consumables used in this project such as coolant and purge gas offer benefits in sensitivity but limit the number of uses. Though analogy to other instruments, arguments have been made for alternative solutions that utilise electrical power instead of physical consumables (a cryocooler for detector cooling and vacuum pumps to purge the cell and achieve an inert cell atmosphere).

Future directions from this work should include the assembly of a breadboard model, containing components based on the recommendations made in this work. I contend that a multi-pass cell is essential to unlock the potential of pyrolysis-FTIR, thus this is the highest priority inclusion of the next pyrolysis-FTIR iteration. As noted in the thesis, a low volume, commercially available multi-pass cell for FTIR is available, although the interfacing with the pyrolysis mechanism may present a configurational challenge.

A breadboard model of carefully selected components would be the appropriate opportunity to conduct a budget analysis. Once the operational costs of the instrument are understood, optimisation of the pyrolysis-FTIR modes can be investigated from a more technical perspective (as opposed to the investigation of different modes from a perspective of science return, as done in this project). This would place the instrument in a position where it could be judged directly against any technical requirements imposed by a mission proposal.

# Bibliography


Allen, C. C., K. M. Jager, R. V. Morris, D. J. Lindstrom, M. M. Lindstrom & J. P. Lockwood. 1998. JSC Mars-1: a martian soil simulant. In *Space 98*, 469-476. ASCE.

Anderson, M. S., J. M. Andringa, R. W. Carlson, P. Conrad, W. Hartford, M. Shafer, A. Soto, A. I. Tsapin, J. P. Dybwad & W. Wadsworth (2005) Fourier transform infrared spectroscopy for Mars science. *Review of Scientific Instruments,* 76**,** 034101.

Anderson, R. C., L. Jandura, A. B. Okon, D. Sunshine, C. Roumeliotis, L. W. Beegle, J. Hurowitz, B. Kennedy, D. Limonadi, S. McCloskey, M. Robinson, C. Seybold & K. Brown (2012) Collecting Samples in Gale Crater, Mars; an Overview of the Mars Science Laboratory Sample Acquisition, Sample Processing and Handling System. *Space Science Reviews,* 170**,** 57-75.

Atreya, S. K., P. R. Mahaffy & A.-S. Wong (2007) Methane and related trace species on Mars: Origin, loss, implications for life, and habitability. *Planetary and Space Science,* 55**,** 358-369.

Aubrey, A., H. J. Cleaves, J. H. Chalmers, A. M. Skelley, R. A. Mathies, F. J. Grunthaner, P. Ehrenfreund & J. L. Bada (2006) Sulfate minerals and organic compounds on Mars. *Geology,* 34**,** 357-360.

Balint, T. (2002) Summary of Russian planetary lander missions. *NASA-JPL Deep Space Mission Architecture Group*.

Bell, J., J. Maki, G. Mehall, M. Ravine, M. Caplinger & M.-Z. Team (2016) Mastcam-Z: Designing a Geologic, Stereoscopic, and Multispectral Pair of Zoom Cameras for the NASA Mars 2020 Rover. *LPI Contributions,* 1980.

Bernath, P. F. 2015. *Spectra of Atoms and Molecules*. Oxford University Press.

Bibring, J.-P., Y. Langevin, J. F. Mustard, F. Poulet, R. Arvidson, A. Gendrin, B. Gondet, N. Mangold, P. Pinet, F. Forget, t. O. team, M. Berthé, J.-P. Bibring, A. Gendrin, C. Gomez, B. Gondet, D. Jouglet, F. Poulet, A. Soufflot, M. Vincendon, M. Combes, P. Drossart, T. Encrenaz, T. Fouchet, R. Merchiorri, G. Belluci, F. Altieri, V. Formisano, F. Capaccioni, P. Cerroni, A. Coradini, S. Fonti, O. Korablev, V. Kottsov, N. Ignatiev, V. Moroz, D. Titov, L. Zasova, D. Loiseau, N. Mangold, P. Pinet, S. Douté, B. Schmitt, C. Sotin, E. Hauber, H. Hoffmann, R. Jaumann, U. Keller, R. Arvidson, J. F. Mustard, T. Duxbury, F. Forget & G. Neukum (2006) Global Mineralogical and Aqueous Mars History Derived from OMEGA/Mars Express Data. *Science,* 312**,** 400-404.

Bibring, J. P., A. Soufflot, M. Berthé, Y. Langevin, B. Gondet, P. Drossart, M. Bouyé, M. Combes, P. Puget & A. Semery. 2004. OMEGA: Observatoire pour la Minéralogie, l'Eau, les Glaces et l'Activité. In *Mars Express: the scientific payload*, 37-49.

Biemann, K., J. Oro, P. Toulmin, L. Orgel, A. Nier, D. Anderson, P. Simmonds, D. Flory, A. Diaz & D. Rushneck (1976) Search for organic and volatile inorganic compounds in two surface samples from the Chryse Planitia region of Mars. *Science,* 194**,** 72-76.

Bramson, A., S. Byrne, S. Sutton, N. Putzig, E. Martellato, G. Cremonese, J. Plaut & J. Holt. 2015. A Study of Martian Mid-Latitude Ice Using Observations and Modeling of Terraced Craters. In *Lunar and Planetary Science Conference*, 1565.

Braslavsky, S. E. (2007) Glossary of terms used in photochemistry, (IUPAC Recommendations 2006). *Pure and Applied Chemistry,* 79**,** 293-465.

Bridges, J. C., D. Catling, J. Saxton, T. Swindle, I. Lyon & M. Grady. 2001. Alteration assemblages in Martian meteorites: Implications for near-surface processes. In *Chronology and evolution of Mars*, 365-392. Springer.

Brownlee, D. E., P. Tsou, J. D. Anderson, M. S. Hanner, R. L. Newburn, Z. Sekanina, B. C. Clark, F. Hörz, M. E. Zolensky, J. Kissel, J. A. M. McDonnell, S. A. Sandford & A. J. Tuzzolino (2003) Stardust: Comet and interstellar dust sample return mission. *Journal of Geophysical Research: Planets (1991–2012),* 108.

Burnett, D., B. Barraclough, R. Bennett, M. Neugebauer, L. Oldham, C. Sasaki, D. Sevilla, N. Smith, E. Stansbery & D. Sweetnam (2003) The Genesis Discovery Mission: return of solar matter to Earth. *Space Science Reviews,* 105**,** 509-534.

Cady, S. L., J. D. Farmer, J. P. Grotzinger, J. W. Schopf & A. Steele (2003) Morphological biosignatures and the search for life on Mars. *Astrobiology,* 3**,** 351-368.

Christensen, P. R., J. L. Bandfield, V. E. Hamilton, S. W. Ruff, G. Mehall, N. Gorelick, K. Bender, K. Murray, H. Kieffer & T. Titus (2001) Mars Global Surveyor Thermal Emission Spectrometer experiment- Investigation description and surface science results. *Journal of Geophysical Research,* 106**,** 23823-23871.

Christensen, P. R., G. L. Mehall, S. H. Silverman, S. Anwar, G. Cannon, N. Gorelick, R. Kheen, T. Tourville, D. Bates, S. Ferry, T. Fortuna, J. Jeffryes, W. O'Donnell, R. Peralta, T. Wolverton, D. Blaney, R. Denise, J. Rademacher, R. V. Morris & S. Squyres (2003) Miniature Thermal Emission Spectrometer for the Mars Exploration Rovers. *Journal of Geophysical Research: Planets,* 108**,** n/a-n/a.

Coates, J. (2000) Interpretation of infrared spectra, a practical approach. *Encyclopedia of analytical chemistry*.

Colthup, N. B. (1950) Spectra-Structure Correlations in the Infra-Red Region. *Journal of the Optical Society of America,* 40**,** 397-400.

Court, R. W. & M. A. Sephton (2009) Investigating the contribution of methane produced by ablating micrometeorites to the atmosphere of Mars. *Earth and Planetary Science Letters,* 288**,** 382-385.

Crisp, J. A., M. Adler, J. R. Matijevic, S. W. Squyres, R. E. Arvidson & D. M. Kass (2003) Mars Exploration Rover mission. *Journal of Geophysical Research: Planets (1991–2012),* 108.

Dettmer, K. & W. Engewald (2002) Adsorbent materials commonly used in air analysis for adsorptive enrichment and thermal desorption of volatile organic compounds. *Analytical and Bioanalytical Chemistry,* 373**,** 490-500.

Edgett, K., M. Ravine, M. Caplinger, F. Ghaemi, J. Schaffner, M. Malin, J. Baker, D. DiBiase, J. Laramee & J. Maki. 2009. The mars science laboratory (MSL) mars hand lens imager (MAHLI) flight instrument. In *Lunar and Planetary Science Conference*, 1197.

Eggleton, R. A., C. Foudoulis & D. Varkevisser (1987) Weathering of basalt: changes in rock chemistry and mineralogy. *Clays and Clay Minerals,* 35**,** 161-169.

Eisberg, R. & R. Resnick. 1985. *Quantum physics*. John Wiley & Sons.

El Goresy, A., P. Gillet, M. Miyahara, E. Ohtani, S. Ozawa, P. Beck & G. Montagnac (2013) Shock-induced deformation of Shergottites: Shock-pressures and perturbations of magmatic ages on Mars. *Geochimica et Cosmochimica Acta,* 101**,** 233-262.

Farmer, J. D. & D. J. Des Marais (1999) Exploring for a record of ancient Martian life. *Journal of Geophysical Research: Planets,* 104**,** 26977-26995.

Fassett, C. I., J. L. Dickson, J. W. Head, J. S. Levy & D. R. Marchant (2010) Supraglacial and proglacial valleys on Amazonian Mars. *Icarus,* 208**,** 86-100.

Fernández-Remolar, D. C., L. J. Preston, M. Sánchez-Román, M. R. M. Izawa, L. Huang, G. Southam, N. R. Banerjee, G. R. Osinski, R. Flemming, D. Gómez-Ortíz, O. Prieto Ballesteros, N. Rodríguez, R. Amils & M. Darby Dyar (2012) Carbonate precipitation under bulk acidic conditions as a potential biosignature for searching life on Mars. *Earth and Planetary Science Letters,* 351–352**,** 13-26.

Fleischer, R. L., P. B. Price, R. M. Walker, M. Maurette & G. Morgan (1967) Tracks of heavy primary cosmic rays in meteorites. *Journal of Geophysical Research,* 72**,** 355-366.

Földvári, M. (2011) Handbook of thermogravimetric system of minerals and its use in geological practice.

Formisano, V., S. Atreya, T. Encrenaz, N. Ignatiev & M. Giuranna (2004) Detection of methane in the atmosphere of Mars. *Science,* 306**,** 1758-1761.

Freissinet, C., D. Glavin, P. Mahaffy, K. Miller, J. Eigenbrode, R. Summons, A. Brunner, A. Buch, C. Szopa & P. Archer (2015) Organic molecules in the sheepbed mudstone, gale crater, mars. *Journal of Geophysical Research: Planets,* 120**,** 495-514.

Gadsden, J. A. 1975. *Infrared Spectra of Minerals and Related Inorganic Compounds*. Butterworths.

Gellert, R., J. Campbell, P. King, L. Leshin, G. Lugmair, J. Spray, S. Squyres & A. Yen (2009) The alpha-particle-x-ray-spectrometer (apxs) for the mars science laboratory (msl) rover mission. *Lunar Planet. Sci. XL. Abstract,* 2364.

Genge, M. J. & M. M. Grady (1999) The fusion crusts of stony meteorites: Implications for the atmospheric reprocessing of extraterrestrial materials. *Meteoritics & Planetary Science,* 34**,** 341-356.

Giese, R. & P. Datta (1973) Hydroxyl orientation in kaolinite, dickite, and nacrite. *American Mineralogist,* 58**,** 471-479.

Glavin, D. P., C. Freissinet, K. E. Miller, J. L. Eigenbrode, A. E. Brunner, A. Buch, B. Sutter, P. D. Archer, S. K. Atreya & W. B. Brinckerhoff (2013) Evidence for perchlorates and the origin of chlorinated hydrocarbons detected by SAM at the Rocknest aeolian deposit in Gale Crater. *Journal of Geophysical Research: Planets,* 118**,** 1955-1973.

Goldstein, A. H. & I. E. Galbally (2007) Known and Unexplored Organic Constituents in the Earth's Atmosphere. *Environmental Science & Technology,* 41**,** 1514-1521.

Gordon, P. R. & M. A. Sephton (2016a) Organic matter detection on Mars by pyrolysis-FTIR: an analysis of sensitivity and mineral matrix effects. *Astrobiology,* submitted.

--- (2016b) Rapid habitability assessment of Mars samples by pyrolysis-FTIR. *Planetary and Space Science,* 121**,** 60-75.

Griffith, D. W. T. (1996) Synthetic Calibration and Quantitative Analysis of Gas-Phase FT-IR Spectra. *Applied Spectroscopy,* 50**,** 59-70.

Griffiths, P. R. & J. A. De Haseth. 2007. *Fourier transform infrared spectrometry*. Hoboken, N.J.: Wiley-Interscience.

Halliday, A. N. (2012) The Origin of the Moon. *Science,* 338**,** 1040-1041.

Hamran, S.-E., H. Amundsen, L. Carter, R. Ghent, J. Kohler, M. Mellon & D. Paige. 2014. The RIMFAX Ground Penetrating Radar on the Mars 2020 Rover. In *AGU Fall Meeting Abstracts*, 3746.

Harvey, A. & D. Fletcher-Holmes (2004) Birefringent Fourier-transform imaging spectrometer. *Optics Express,* 12**,** 5368-5374.

Hashimoto, M. & S. Kawata (1992) Multichannel Fourier-transform infrared spectrometer. *Applied Optics,* 31**,** 6096-6101.

Hedges, J. I. (1977) The association of organic molecules with clay minerals in aqueous solutions. *Geochimica et Cosmochimica Acta,* 41**,** 1119-1123.

Helmig, D. & L. Vierling (1995) Water Adsorption Capacity of the Solid Adsorbents Tenax TA, Tenax GR, Carbotrap, Carbotrap C, Carbosieve SIII, and Carboxen 569 and Water Management Techniques for the Atmospheric Sampling of Volatile Organic Trace Gases. *Analytical Chemistry,* 67**,** 4380-4386.

Hintze, P. E., H. G. Kjaergaard, V. Vaida & J. B. Burkholder (2003) Vibrational and Electronic Spectroscopy of Sulfuric Acid Vapor. *The Journal of Physical Chemistry A,* 107**,** 1112-1118.

Hoffman, J. H., R. C. Chaney & H. Hammack (2008) Phoenix Mars Mission—The Thermal Evolved Gas Analyzer. *Journal of the American Society for Mass Spectrometry,* 19**,** 1377-1383.

Honda, M. & J. R. Arnold (1961) Radioactive species produced by cosmic rays in the Aroos iron meteorite. *Geochimica et Cosmochimica Acta,* 23**,** 219-232.

Huang, C.-Y. & W.-C. Wang. 2012. A fourier transform spectrometer based on birefringent interferometer. In *Optomechatronic Technologies (ISOT), 2012 International Symposium on*, 1-4. IEEE.

Jaakkola, P., J. Tate, M. Paakkunainen, J. Kauppinen & P. Saarinen (1997) Instrumental resolution considerations for Fourier transform infrared gas-phase spectroscopy. *Applied spectroscopy,* 51**,** 1159-1169.

Johnson, D. L., M. J. Lysek & J. M. Morookian. 2014. The Ricor K508 cryocooler operational experience on Mars. In *ADVANCES IN CRYOGENIC ENGINEERING: Transactions of the Cryogenic Engineering Conference-CEC*, 1792-1799. AIP Publishing.

Keller, L. P., S. a. Bajt, G. A. Baratta, J. Borg, J. P. Bradley, D. E. Brownlee, H. Busemann, J. R. Brucato, M. Burchell & L. Colangeli (2006) Infrared spectroscopy of comet 81P/Wild 2 samples returned by Stardust. *Science,* 314**,** 1728-1731.

Klein, H. P., J. Lederberg, A. Rich, N. H. Horowitz, V. I. Oyama & G. V. Levin (1976) The Viking Mission search for life on Mars. *Nature,* 262**,** 24-27.

Landau, L. & E. Lifshitz (1976) Mechanics, vol. 1. *Course of theoretical physics*.

Laul, J., J. Papike & S. Simon. 1982. The lunar regolith-Comparative studies of the Apollo and Luna sites. Chemistry of soils from Apollo 17, Luna 16, 20, and 24. In *Lunar and Planetary Science Conference Proceedings*, 389-407.

Lee, M. R. & P. A. Bland (2004) Mechanisms of weathering of meteorites recovered from hot and cold deserts and the formation of phyllosilicates1. *Geochimica et Cosmochimica Acta,* 68**,** 893-916.

Lewicki, C., P. Diamandis, E. Anderson, C. Voorhees & F. Mycroft (2013) Planetary resources—the asteroid mining company. *New Space,* 1**,** 105-108.

Lewis, J. M., J. Najorka, J. S. Watson & M. A. Sephton (2016) Iron oxides associated with acid waters could host Life's organic remains on Mars. *Geology,* submitted.

Lewis, J. M., J. S. Watson, J. Najorka, D. Luong & M. A. Sephton (2015) Sulfate minerals: a problem for the detection of organic compounds on Mars? *Astrobiology,* 15**,** 247-258.

Mahaffy, P. (2008) Exploration of the Habitability of Mars: Development of Analytical Protocols for Measurement of Organic Carbon on the 2009 Mars Science Laboratory. *Space Science Reviews,* 135**,** 255-268.

Mahaffy, P., M. Cabane, P. Conrad, C. Webster & S. Team. 2009. Sample analysis at Mars (SAM) instrument suite for the 2011 Mars Science Laboratory. In *Lunar and Planetary Institute Science Conference Abstracts*, 1088.

Mahaffy, P., C. Webster, M. Cabane, P. Conrad, P. Coll, S. Atreya, R. Arvey, M. Barciniak, M. Benna, L. Bleacher, W. Brinckerhoff, J. Eigenbrode, D. Carignan, M. Cascia, R. Chalmers, J. Dworkin, T. Errigo, P. Everson, H. Franz, R. Farley, S. Feng, G. Frazier, C. Freissinet, D. Glavin, D. Harpold, D. Hawk, V. Holmes, C. Johnson, A. Jones, P. Jordan, J. Kellogg, J. Lewis, E. Lyness, C. Malespin, D. Martin, J. Maurer, A. McAdam, D. McLennan, T. Nolan, M. Noriega, A. Pavlov, B. Prats, E. Raaen, O. Sheinman, D. Sheppard, J. Smith, J. Stern, F. Tan, M. Trainer, D. Ming, R. Morris, J. Jones, C. Gundersen, A. Steele, J. Wray, O. Botta, L. Leshin, T. Owen, S. Battel, B. Jakosky, H. Manning, S. Squyres, R. Navarro-González, C. McKay, F. Raulin, R. Sternberg, A. Buch, P. Sorensen, R. Kline-Schoder, D. Coscia, C. Szopa, S. Teinturier, C. Baffes, J. Feldman, G. Flesch, S. Forouhar, R. Garcia, D. Keymeulen, S. Woodward, B. Block, K. Arnett, R. Miller, C. Edmonson, S. Gorevan & E. Mumm (2012) The Sample Analysis at Mars Investigation and Instrument Suite. *Space Science Reviews,* 170**,** 401-478.

Mattingly, R. & L. May. 2011. Mars Sample Return as a campaign. In *Aerospace Conference, 2011 IEEE*, 1-13. IEEE.

McAdam, A., C. Knudson, B. Sutter, H. Franz, P. Archer Jr, J. Eigenbrode, D. Ming, R. Morris, J. Hurowitz & P. Mahaffy (2016) Reactions Involving Calcium and Magnesium Sulfates as Potential Sources of Sulfur Dioxide During MSL SAM Evolved Gas Analyses.

McLennan, S. & M. Sephton. 2011. Planning for Mars Sample Return: Results from the MEPAG Mars Sample Return End-to-End International Science Analysis Group (E2E-iSAG). In *AGU Fall Meeting Abstracts*, 04.

McLennan, S., M. Sephton, C. Allen, A. Allwood, R. Barbieri, D. Beaty, P. Boston, M. Carr, M. Grady & J. Grant (2012) Planning for Mars Returned Sample Science: Final Report of the MSR End-to-End International Science Analysis Group (E2E-iSAG). *Astrobiology,* 12**,** 175-230.

Meurant, G. 1967. *Carbonate rocks*. Elsevier Science.

Miller, K. E., B. Kotrc, R. E. Summons, I. Belmahdi, A. Buch, J. L. Eigenbrode, C. Freissinet, D. P. Glavin & C. Szopa (2015) Evaluation of the Tenax trap in the Sample Analysis at Mars instrument suite on the Curiosity rover as a potential hydrocarbon source for chlorinated organics detected in Gale Crater. *Journal of Geophysical Research: Planets,* 120**,** 2015JE004825.

Miller, S. L. (1953) A production of amino acids under possible primitive earth conditions. *Science,* 117**,** 528-529.

Möller, K. D. (1995) Wave-front-dividing array interferometers without moving parts for real-time spectroscopy from the IR to the UV. *Applied Optics,* 34**,** 1493-1501.

Mumma, M. J., G. L. Villanueva, R. E. Novak, T. Hewagama, B. P. Bonev, M. A. DiSanti, A. M. Mandell & M. D. Smith (2009) Strong release of methane on Mars in northern summer 2003. *Science,* 323**,** 1041-1045.

Mustard, J., M. Adler, A. Allwood, D. Bass, D. Beaty, J. Bell, W. Brinckerhoff, M. Carr, D. Des Marais & B. Drake (2013) Report of the Mars 2020 science definition team. *Jet Propulsion Laboratory, California Institute of Technology, Pasadena, CA*.

Newman, E. (1941) Behavior Of Calcium Sulfate At High Temperatures. *J. Res. Natl. Bur. Stand,* 27**,** 191.

Ojha, L., M. B. Wilhelm, S. L. Murchie, A. S. McEwen, J. J. Wray, J. Hanley, M. Masse & M. Chojnacki (2015) Spectral evidence for hydrated salts in recurring slope lineae on Mars. *Nature Geosci,* 8**,** 829-832.

Okamoto, T., S. Kawata & S. Minami (1984) Fourier transform spectrometer with a self-scanning photodiode array. *Applied Optics,* 23**,** 269-273.

Peach, G. (1981) Theory of the pressure broadening and shift of spectral lines. *Advances in Physics,* 30**,** 367-474.

Pratt, L., C. Allen, A. Allwood, A. Anbar, S. Atreya, M. Carr, D. Des Marais, J. Grant, D. Glavin & V. Hamilton (2009) Mars Astrobiology Explorer-Cacher (MAX-C): A Potential Rover Mission for 2018. *White paper submitted to the NASA Planetary Decadal survey* http://mepag. *jpl. nasa. gov/decadal/index. html*.

Quay, P., J. Stutsman, D. Wilbur & A. Snover (1999) The isotopic composition of atmospheric methane. *Global Biogeochemical Cycles,* 13**,** 445-461.

Rieder, R., R. Gellert, J. Brückner, G. Klingelhöfer, G. Dreibus, A. Yen & S. Squyres (2003) The new Athena alpha particle X-ray spectrometer for the Mars Exploration Rovers. *Journal of Geophysical Research: Planets,* 108.

Rodríguez, J. A. P., K. L. Tanaka, D. C. Berman & J. S. Kargel (2010) Late Hesperian plains formation and degradation in a low sedimentation zone of the northern lowlands of Mars. *Icarus,* 210**,** 116-134.

Rothman, L., I. Gordon, Y. Babikov, A. Barbe, D. C. Benner, P. Bernath, M. Birk, L. Bizzocchi, V. Boudon & L. Brown (2013) The HITRAN2012 molecular spectroscopic database. *Journal of Quantitative Spectroscopy and Radiative Transfer,* 130**,** 4-50.

Rothman, L. S., C. Rinsland, A. Goldman, S. Massie, D. Edwards, J. Flaud, A. Perrin, C. Camy-Peyret, V. Dana & J.-Y. Mandin (1998) The HITRAN molecular spectroscopic database and HAWKS (HITRAN atmospheric workstation): 1996 edition. *Journal of Quantitative Spectroscopy and Radiative Transfer,* 60**,** 665-710.

Rothman, L. S., J. Schroeder, K. Tang & J. Manual (2004) JavaHAWKS Manual.

Saladino, R., E. Carota, G. Botta, M. Kapralov, G. N. Timoshenko, A. Y. Rozanov, E. Krasavin & E. Di Mauro (2015) Meteorite-catalyzed syntheses of nucleosides and of other prebiotic compounds

from formamide under proton irradiation. *Proceedings of the National Academy of Sciences,* 112**,** E2746-E2755.

Sandford, S. A., J. Aléon, C. M. D. Alexander, T. Araki, S. a. Bajt, G. A. Baratta, J. Borg, J. P. Bradley, D. E. Brownlee & J. R. Brucato (2006) Organics captured from comet 81P/Wild 2 by the Stardust spacecraft. *Science,* 314**,** 1720-1724.

Schueler, C. F., S. H. Silverman, M. I. Greenfield & P. Christensen. 1997. Advanced planetary thermal spectroscopy. In *Aerospace Conference, 1997. Proceedings., IEEE*, 299-313. IEEE.

Sephton, M. & O. Botta (2008) Extraterrestrial Organic Matter and the Detection of Life. *Space Science Reviews,* 135**,** 25-35.

Sephton, M. A. & J. N. Carter (2015) The chances of detecting life on Mars. *Planetary and Space Science,* 112**,** 15-22.

Sephton, M. A., R. W. Court, J. M. Lewis, M. C. Wright & P. R. Gordon (2013) Selecting samples for Mars sample return: Triage by pyrolysis–FTIR. *Planetary and Space Science,* 78**,** 45-51.

Sephton, M. A., J. M. Lewis, J. S. Watson, W. Montgomery & C. Garnier (2014) Perchlorate-induced combustion of organic matter with variable molecular weights: Implications for Mars missions. *Geophysical Research Letters,* 41**,** 7453-7460.

Silverman, S., R. Peralta, P. Christensen & G. Mehall (2006) Miniature thermal emission spectrometer for the Mars Exploration Rover. *Acta Astronautica,* 59**,** 990-999.

Sims, M. R., C. T. Pillinger, I. P. Wright, G. Morgan, I. J. Praine, G. W. Fraser, D. Pullan, S. Whitehead, J. Dowson, A. A. Wells, L. Richter, H. Kochan, H. Hamacher, A. Griffiths, A. J. Coates, S. C. Peskett, A. Brack, J. Clemmet, R. Slade, N. Phillips, C. Berry, A. Senior, J. C. Zarnecki, M. E. Towner, M. Leese, A. P. Zent, N. Thomas, J.-L. Josset, G. Klingelhoefer, P. van Duijn & G. Sims. 2000. Instrumentation on Beagle 2: the astrobiology lander on ESA's 2003 Mars Express mission. 36-47.

Squyres, S. W. & J. F. Kasting (1994) Early Mars: How Warm and How Wet? *Science,* 265**,** 744-749.

Strange, N., D. Landau, G. Lantoine, T. Lam, M. McGuire, L. Burke, M. Martini & J. Dankanich. 2013. Overview of mission design for NASA asteroid redirect robotic mission concept. In *33rd International Electric Propulsion Conference, The George Washington University, Washington, DC*.

Summers, M. E., B. J. Lieb, E. Chapman & Y. L. Yung (2002) Atmospheric biomarkers of subsurface life on Mars. *Geophysical Research Letters,* 29**,** 2171.

Summons, R., J. Amend, R. Buick, G. Dromart, J. Eigenbrode & A. Knoll (2010) Identification of Biosignature Preservation Windows to Guide MSL Landing Site Selection. *LPI Contributions,* 1538**,** 5256.

Summons, R. E., J. P. Amend, D. Bish, R. Buick, G. D. Cody, D. J. Des Marais, G. Dromart, J. L. Eigenbrode, A. H. Knoll & D. Y. Sumner (2011) Preservation of Martian organic and environmental records: final report of the Mars Biosignature Working Group. *Astrobiology,* 11**,** 157-181.

Villanueva, G. L., M. J. Mumma, R. E. Novak, Y. L. Radeva, H. U. Käufl, A. Smette, A. Tokunaga, A. Khayat, T. Encrenaz & P. Hartogh (2013) A sensitive search for organics (CH4, CH3OH, H2CO, C2H6, C2H2, C2H4), hydroperoxyl (HO2), nitrogen compounds (N2O, NH3, HCN) and chlorine species (HCl, CH3Cl) on Mars using ground-based high-resolution infrared spectroscopy. *Icarus,* 223**,** 11-27.

Vinogradov, A. P. 1971. Preliminary data on lunar ground brought to Earth by automatic probe" Luna-16". In *Lunar and Planetary Science Conference Proceedings*, 1.

Volz, F. E. (1979) Sulfuric acid in KBr pellet spectroscopy. *Applied optics,* 18**,** 2353.

Wadsworth, W. & J.-P. Dybwad (2002) Rugged high-speed rotary imaging Fourier transform spectrometer for industrial use. 83-88.

Wagner, E., R. Dändliker & K. Spenner. 2008. *Sensors, Optical Sensors*. Wiley.

Wagner, I. & H. Musso (1983) New naturally occurring amino acids. *Angewandte Chemie International Edition in English,* 22**,** 816-828.

Webster, C. R., P. R. Mahaffy, S. K. Atreya, G. J. Flesch, M. A. Mischna, P.-Y. Meslin, K. A. Farley, P. G. Conrad, L. E. Christensen, A. A. Pavlov, J. Martín-Torres, M.-P. Zorzano, T. H. McConnochie, T. Owen, J. L. Eigenbrode, D. P. Glavin, A. Steele, C. A. Malespin, P. D. Archer, B. Sutter, P. Coll, C. Freissinet, C. P. McKay, J. E. Moores, S. P. Schwenzer, J. C. Bridges, R. Navarro-Gonzalez, R. Gellert & M. T. Lemmon (2015) Mars methane detection and variability at Gale crater. *Science,* 347**,** 415-417.

Wertz, J. R. & W. J. Larson. 1999. *Space mission analysis and design*. Microcosm.

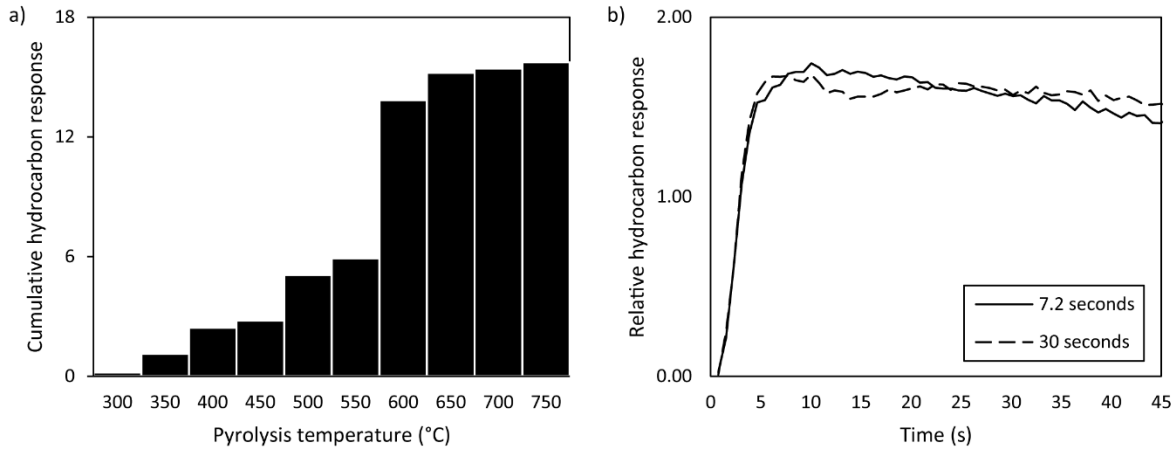
Wilson, E. B., J. C. Decius & P. C. Cross. 2012. *Molecular vibrations: the theory of infrared and Raman vibrational spectra*. Courier Corporation.

Yano, H., T. Kubota, H. Miyamoto, T. Okada, D. Scheeres, Y. Takagi, K. Yoshida, M. Abe, S. Abe & O. Barnouin-Jha (2006) Touchdown of the Hayabusa spacecraft at the Muses Sea on Itokawa. *Science,* 312**,** 1350-1353.

Zent, A. P., F. P. Fanale & S. E. Postawko (1987) Carbon dioxide: Adsorption on palagonite and partitioning in the Martian regolith. *Icarus,* 71**,** 241-249.

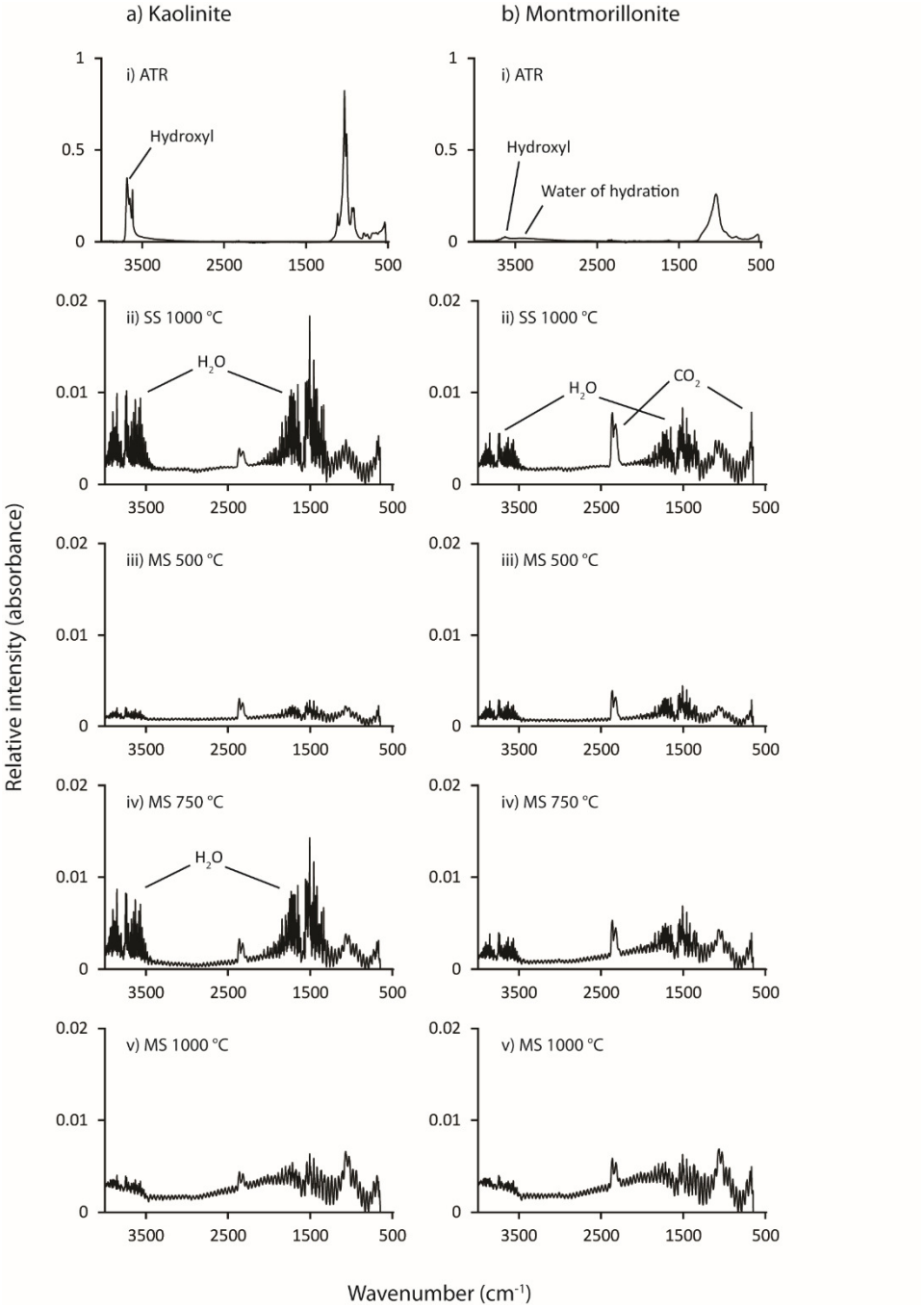
Zettler, L. A. A., M. A. Messerli, A. D. Laatsch, P. J. Smith & M. L. Sogin (2003) From genes to genomes: beyond biodiversity in Spain's Rio Tinto. *The Biological Bulletin,* 204**,** 205-209.

# Appendix A

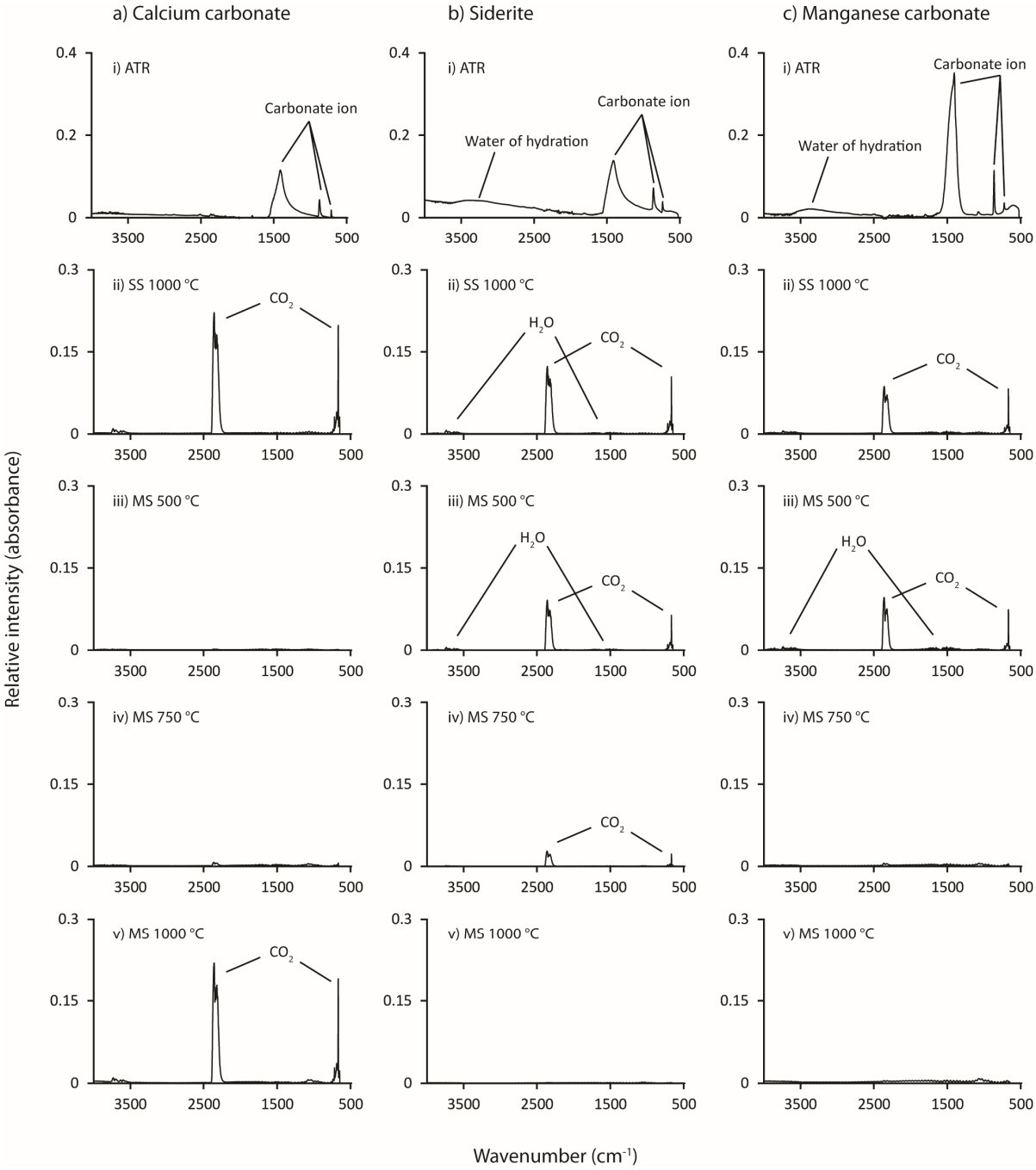



Appendix A.1. Results from preliminary investigations to determine the optimal pyrolysis mode for *Lycopodium* spore sensitivity analysis by pyrolysis-FTIR. Part a) shows the hydrocarbon responses from a single sample of *Lycopodium* spores subjected to successive increasing pyrolysis temperatures (through separate pyrolysis-FTIR measurements). Results are cumulative i.e. each bar represents the response of the temperature being investigated in addition to the total of the responses from all prior temperature steps. This shows the hydrocarbon response begin to plateau around 600 – 750 °C thus a temperature of 700 °C was considered adequate for producing the bulk of hydrocarbon compounds from a sample of *Lycopodium* spores. Part b) shows the hydrocarbon response measured continuously over a 45 s period by FTIR for two different pyrolysis durations (30 s and 7.2 s) at 700 °C (where the probe begins firing at zero seconds). This shows that no additional hydrocarbons are produced after a period of 5 – 10 s, regardless of whether the probe continues to deliver energy to the sample or not thus the probe duration of 7.2 s was chosen for the investigation for its energy efficiency. The hydrocarbon response measured was the total area in the 3150 – 2740 $cm^{-1}$ wavenumber region on the absorbance spectra produced by the pyrolysis-FTIR measurements.

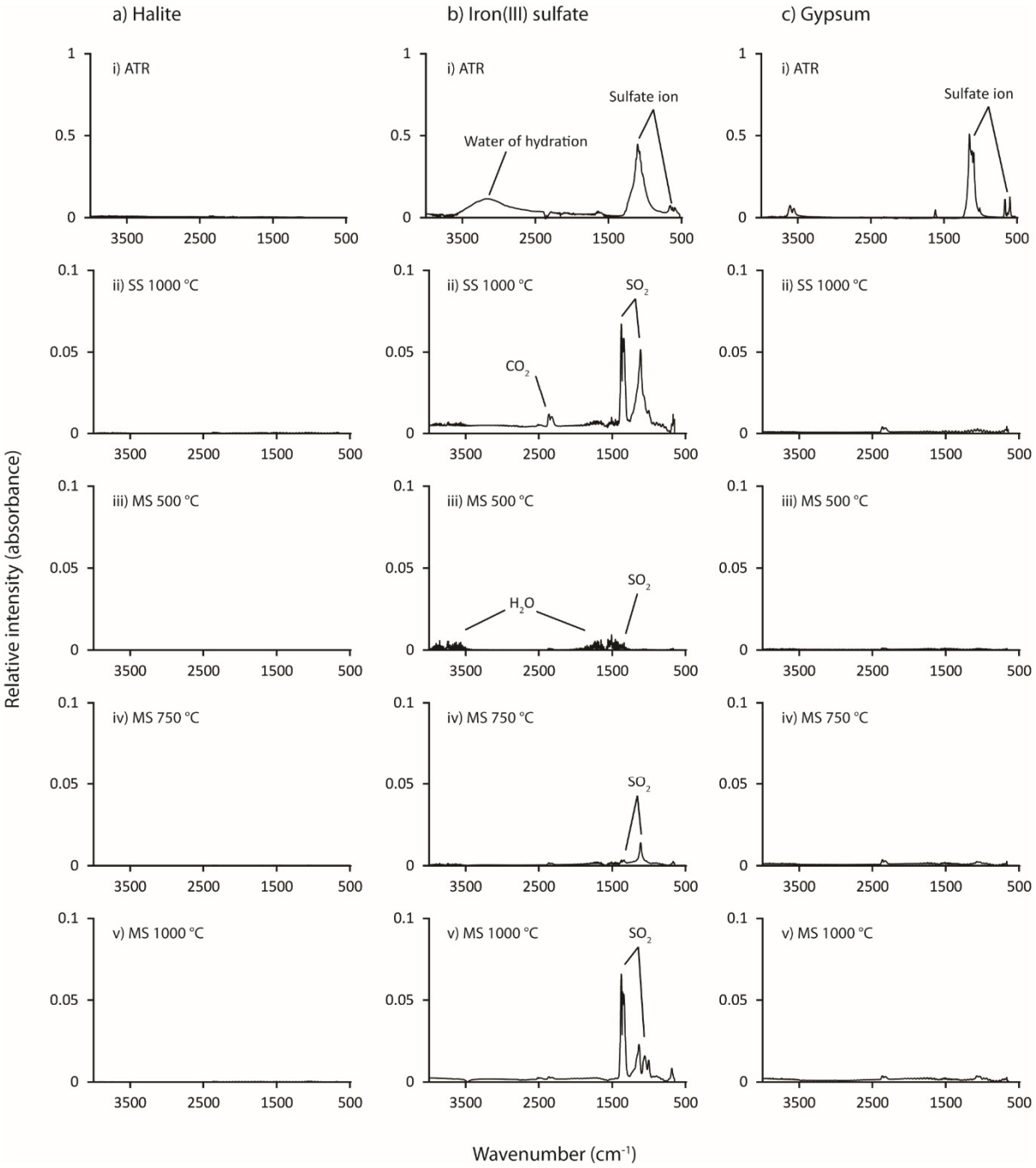
# Appendix B



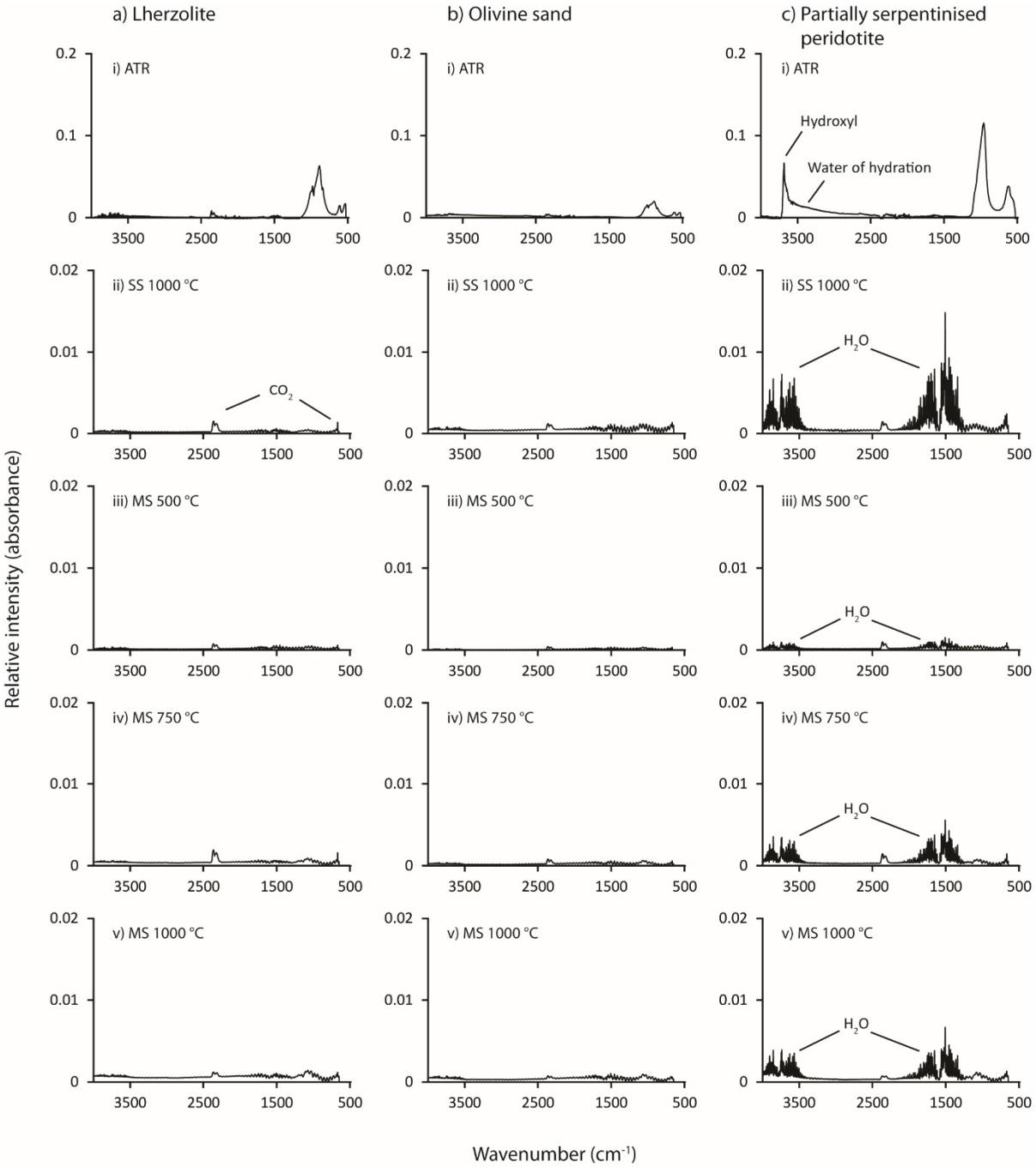

Appendix B.2. Pyrolysis-FTIR spectra for the phyllosilicates surveyed. ATR = attenuated total reflectance, SS = single step pyrolysis-FTIR, MS = multi step pyrolysis-FTIR.



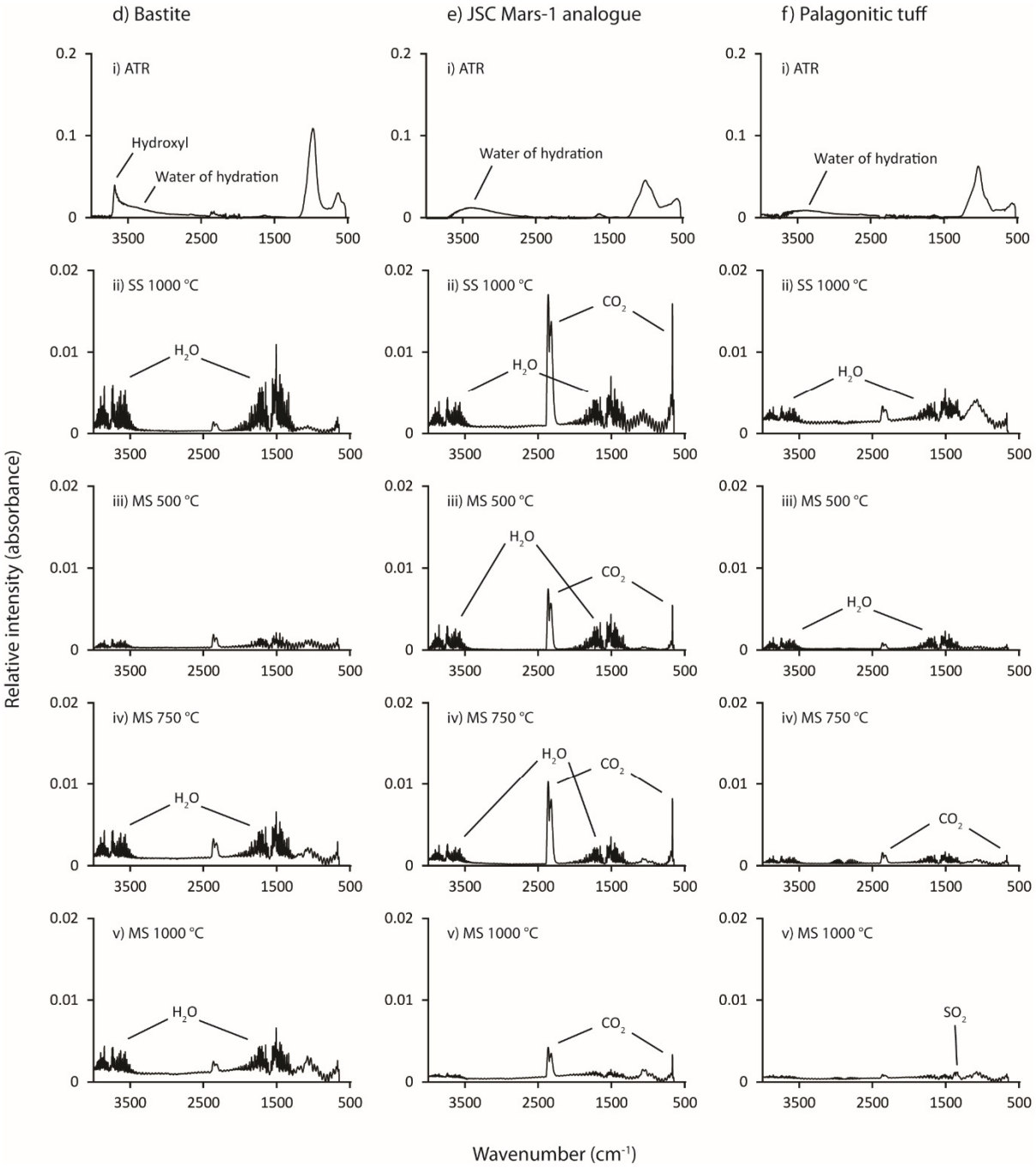

Appendix B.3. Pyrolysis-FTIR spectra for the carbonate minerals surveyed. ATR = attenuated total reflectance, SS = single step pyrolysis-FTIR, MS = multi step pyrolysis-FTIR.



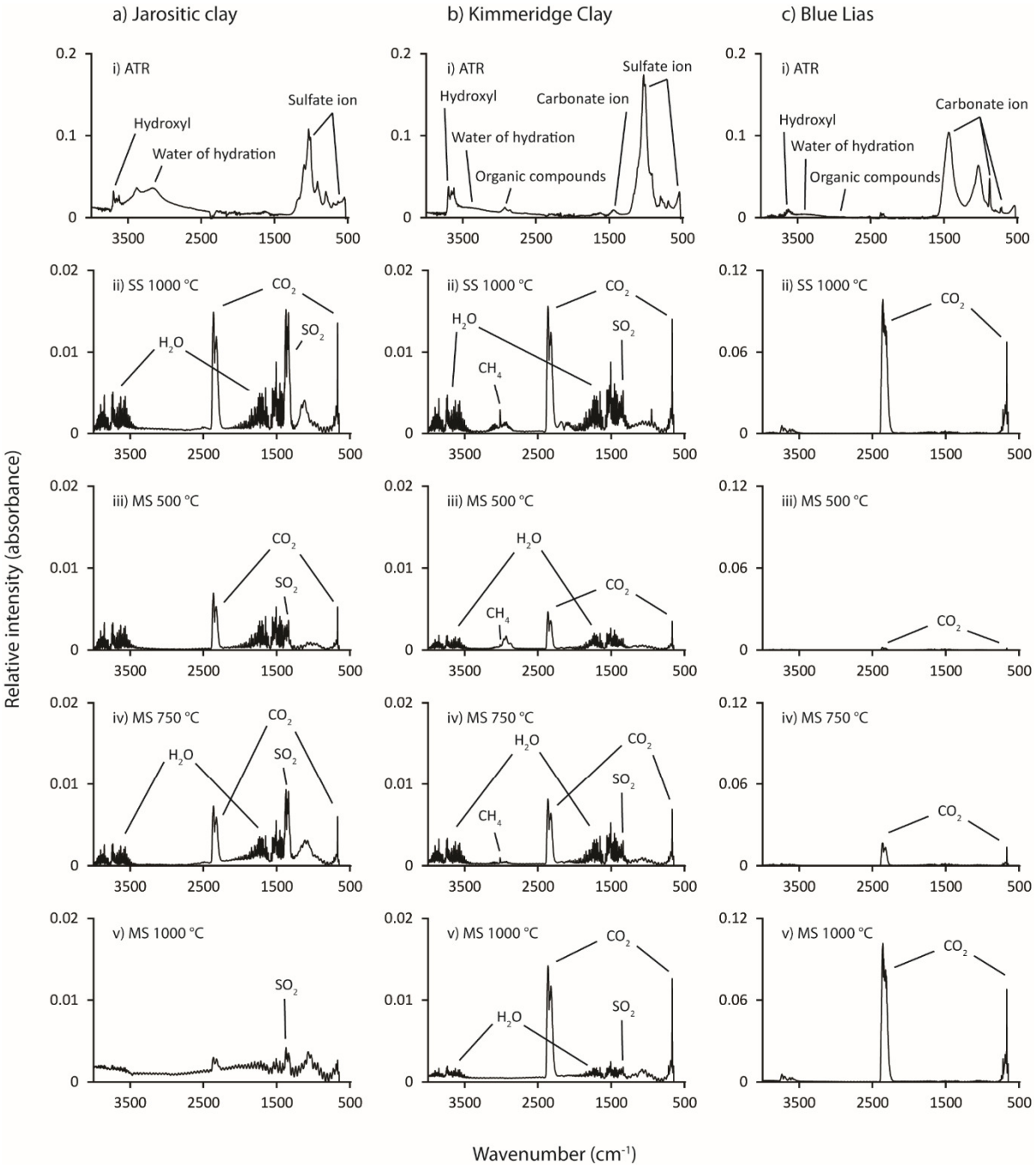

Appendix B.4. Pyrolysis-FTIR spectra for the sulfates and other salts. ATR = attenuated total reflectance, SS = single step pyrolysis-FTIR, MS = multi step pyrolysis-FTIR.




Appendix B.5. Pyrolysis-FTIR spectra for the unaltered and altered igneous materials surveyed. ATR = attenuated total reflectance, SS = single step pyrolysis-FTIR, MS = multi step pyrolysis-FTIR.




Appendix B.4 (cont.). Pyrolysis-FTIR spectra for the unaltered and altered igneous materials surveyed. ATR = attenuated total reflectance, SS = single step pyrolysis-FTIR, MS = multi step pyrolysis-FTIR.




Appendix B.6. Pyrolysis-FTIR spectra for the jarositic clay, and the organic, clay and carbonate rich rocks. ATR = attenuated total reflectance, SS = single step pyrolysis-FTIR, MS = multi step pyrolysis-FTIR.

# Appendix C

Appendix C.1. Java code for processing absorption cross-sections from HITRAN data files. Code is available on the following online repository: https://github.com/petegordondev/JavaHitranCalc/.

```
1    import java.io.*;
2    import java.math.RoundingMode;
3    import java.text.DecimalFormat;
4    import java.util.*;
5
6    public class Main {
7
8        private static File dirIn = new
     File(System.getProperty("user.dir") + "/data/HitranData/");
9        private static File dirOut = new
     File(System.getProperty("user.dir") + "/data/Output/");
10       private static File[] directoryListing = dirIn.listFiles();
11
12       // Values.
13       private static final int RANGE_LO = 600;
14       private static final int RANGE_HI = 4000;
15
16       private static final float RES_COARSE = (float) (100/2);
17
18       private static final float RANGE_RES_FINE = 200;
19       private static final float RES_FINE = (float) (0.03/2);
20
21
22       public static void main(String[] args) {
23           // Process gases.
24           if (directoryListing != null) {
25               for (File child : directoryListing) {
26                   processGas(child);
27               }
28           }
29       }
30
31       private static double lorentz(float nu, float nu0, float gamma){
32           return (1/Math.PI) * gamma/(Math.pow((nu - nu0),2) +
      Math.pow(gamma,2));
33       }
34
35       private static void processGas(File inputFile) {
36
37
38           // Create output file.
39           if(!dirOut.exists()){
40               //noinspection ResultOfMethodCallIgnored
41               dirOut.mkdir();}
42
43           String name = inputFile.getName();
44           int pos = name.lastIndexOf(".");
45           if (pos > 0) {
46               name = name.substring(0, pos);
47           }
48
49           System.out.println("Processing file: " + name);
50
51           File outputFile = new File(dirOut, name + ".csv");
```

```
52
53
54
55          // Load data file.
56          List<LineStrength> hitranData = new
     DataFileHelper(inputFile).read();
57
58
59          System.out.print(name + " has " + hitranData.size() +
    " lines. Would you like to do a full render?: ");
60
61          Scanner scanner = new Scanner(System.in);
62          String userInput = scanner.next();
63
64          boolean fullScan = userInput.equalsIgnoreCase("y") ||
    userInput.equalsIgnoreCase("yes");
65
66          try (Writer writer = new BufferedWriter(new
    OutputStreamWriter(
67                  new FileOutputStream(outputFile), "UTF-8"))) {
68
69
70
71          // Process.
72
73          if (fullScan){
74              // Process all lines.
75
76              System.out.print("\nCalculating over all lines in spectral
    range. This could take some time... ");
77
78              Timer t = new Timer();
79              for (float nu = RANGE_LO; nu <= RANGE_HI; nu += 2 *
RES_FINE) {
80                  double theta = 0;
81                  for (LineStrength aHitranData : hitranData) {
82                      double theta_nu = aHitranData.lineStrength *
    lorentz(nu, aHitranData.waveNumber, aHitranData.airWidth);
83                      theta += theta_nu;
84                  }
85                  writer.write(nu + ", " + theta + "\n");
86              }
87              writer.close();
88              t.end();
89          }
90          else {
91
92              // Get coarse map of features.
93
94              HashMap<Float, Double> coarseMap = new LinkedHashMap<>();
95
96              for (float nu = RANGE_LO; nu <= RANGE_HI; nu += 2 *
    RES_COARSE) {
97                  double theta = 0;
98                  for (LineStrength aHitranData : hitranData) {
99                      double theta_nu = aHitranData.lineStrength *
    lorentz(nu, aHitranData.waveNumber, aHitranData.airWidth);
100                     theta += theta_nu;
101                 }
102                 coarseMap.put(nu, theta);
103             }
```

```
104
105             // Identify feature locations.
106
107             System.out.print("\nFeature locations: ");
108
109             List<Float> mapKeyIndex = new ArrayList<>();
110             List<Float> features = new ArrayList<>();
111             for (Map.Entry<Float, Double> entry :
    coarseMap.entrySet()) {
112                 mapKeyIndex.add(entry.getKey());
113             }
114
115             for (int i = 0; i < mapKeyIndex.size(); i++) {
116
117                 float keyCurr = mapKeyIndex.get(i);
118                 double valCurr = coarseMap.get(keyCurr);
119                 if (i != 0 && i != mapKeyIndex.size() - 1) {
120                     // Check neighbour values.
121                     float keyPrev = mapKeyIndex.get(i - 1);
122                     double valPrev = coarseMap.get(keyPrev);
123                     float keyNext = mapKeyIndex.get(i + 1);
124                     double valNext = coarseMap.get(keyNext);
125
126                     if (valCurr > valPrev && valCurr > valNext) {
127                         // Found a feature so record location.
128                         features.add(keyCurr);
129                     }
130                 }
131             }
132
133             for (int i = 0; i < features.size(); i++) {
134                 System.out.print(features.get(i) + " cm-1");
135                 if (i < features.size() - 1) System.out.print(", ");
136             }
137             System.out.print("\n\n");
138
139             // Render features in detail.
140             // Write to output file.
141
142                 for (Float feature : features) {
143                     Timer t = new Timer();
144                     System.out.print("Rendering " + name + " " +
    feature + " cm-1 feature... ");
145                     for (float nu = feature - RANGE_RES_FINE / 2; nu
    <= feature + RANGE_RES_FINE / 2; nu += 2 * RES_FINE) {
146                         double theta = 0;
147                         for (LineStrength aHitranData : hitranData) {
148                             double theta_nu = aHitranData.lineStrength
    * lorentz(nu, aHitranData.waveNumber, aHitranData.airWidth);
149                             theta += theta_nu;
150                         }
151
152                         writer.write(nu + ", " + theta + "\n");
153                     }
154                     t.end();
155                 }
156                 writer.close();
157                 System.out.print("\n\n");
158
159         }
160         } catch (IOException e) {
```

```
161             e.printStackTrace();
162         }
163     }
164 }
165 
166 class LineStrength {
167     // Represents a HITRAN data point.
168 
169     final float waveNumber;
170     final double lineStrength;
171     final float airWidth;
172 
173     LineStrength(float waveNumber, double lineStrength, float
    airWidth) {
174 
175         this.waveNumber = waveNumber;
176         this.lineStrength = lineStrength;
177         this.airWidth = airWidth;
178     }
179 }
180 
181 class DataFileHelper {
182 
183     private final File file;
184 
185     DataFileHelper(File file) {
186         this.file = file;
187     }
188 
189     List<LineStrength> read(){
190         Timer t = new Timer();
191         List<LineStrength> l = new ArrayList<>();
192         // Read lines from file.
193         System.out.print("Loading HITRAN data from file... ");
194         BufferedReader in = null;
195         try {
196             in = new BufferedReader(new FileReader(file));
197         } catch (FileNotFoundException e) {
198             e.printStackTrace();
199         }
200 
201         String line;
202         try {
203             if (in != null) {
204                 while ((line = in.readLine()) != null) {
205                     // Remove annoying whitespace and null characters
    added by HITRAN.
206                     line = line.replaceAll("\\s+","");
207                     line = line.replaceAll("\\u0000","");
208 
209                     // Parse line for the necessary values.
210                     Scanner scanner = new Scanner(line);
211                     scanner.useDelimiter(",");
212                     scanner.nextInt();
213                     scanner.nextInt();
214                     float waveNumber = scanner.nextFloat();
215                     double lineStrength = scanner.nextDouble();
216                     scanner.nextDouble();
217                     float airWidth = scanner.nextFloat();
218 
```

```
219                     LineStrength values = new LineStrength(waveNumber,
    lineStrength, airWidth);
220
221                     // Add values to ArrayList.
222                     l.add(values);
223                 }
224             }
225         } catch (IOException e) {
226             e.printStackTrace();
227         }
228
229         try {
230             if (in != null) {
231                 in.close();
232             }
233         } catch (IOException e) {
234             e.printStackTrace();
235         }
236
237         t.end();
238
239         return l;
240     }
241 }
242
243 class Timer{
244     private long startTime;
245     Timer() {
246         this.startTime = System.nanoTime();
247     }
248     void end(){
249         long endTime = System.nanoTime();
250         long duration = (endTime - startTime)/1000000;
251         if (duration < 1000){
252             System.out.println("Complete (" + duration + " ms)");
253         } else {
254             DecimalFormat df = new DecimalFormat("#.##");
255             df.setRoundingMode(RoundingMode.CEILING);
256             System.out.println("Complete (" + df.format( (float)
    duration/1000) + " s)");
257         }
258     }
259 }
260
```